

# 博士学位論文

## Motion Planning and Control for Collision Avoidance of Autonomous Vehicles Considering Uncertain Dynamic Urban Environments

国立大学法人東京農工大学大学院  
工学府機械システム工学専攻

章儼  
Yan Zhang

2024 年 2 月

## Abstract

The advent of advanced driver assistance systems (ADAS) and autonomous driving technology has significantly contributed to the global reduction of road traffic accidents. Nonetheless, achieving the ultimate goal of zero traffic accidents remains a challenging endeavor. Despite extensive research efforts by academic institutions and automotive companies, certain areas demand further enhancement. This paper focuses on the persistent issue of traffic accidents in regions with ambiguous traffic regulations, particularly in non-signalized roads and shared spaces. These areas pose unique challenges due to the close proximity of traffic participants and the unpredictable nature of their movements, necessitating a reevaluation and improvement of collision avoidance (CA) strategies.

Firstly, when an automated vehicle needs to avoid multiple obstacles at the same time, consuming travel time and safety assurance of CA need to be carefully considered especially in the case related to unpredictable motion of obstacles. This thesis proposes a feasible solution to this situation by controlling speed and the steering wheel angle. A three-layer control algorithm which contains: (1) behavior re-planning layer, that bases on post-encroachment time (PET) provides a judgment of a function which calculates the possibility of unavoidable road accidents, (2) the path re-planning layer of a novel two-layer model predictive control (TL-MPC) that will re-plan a local trajectory and give a reference acceleration, and (3) the path tracking layer of the TL-MPC, that outputs steering wheel angle to follow the trajectory under the premise of ensuring safety constraints, is proposed to solve the CA problem in such scenario.

Secondly, in typical traffic scenarios characterized by the absence of distinct separations among traffic participants, such as mixed traffic or shared spaces, vehicles and pedestrians often coexist, leading to situations where the ego vehicle encounters multiple pedestrians within a relatively short interaction distance. Given the stochastic nature of pedestrian movements and the need to balance time efficiency with safety during the passing process, this thesis introduces two Collision Avoidance (CA) strategies for the ego vehicle. These strategies are based on Model Predictive Control (MPC) and the Social Force Model (SFM), aimed at addressing the CA challenge in such scenarios. The interaction dynamics between the ego vehicle and pedestrians are simplified into a Markov process, enabling the adoption of the SFM-based dynamic model. The validity of this simplification is supported by the analysis of real-world driving data. Furthermore, parameters associated with the SFM-based vehicle

## Abstract

model are recalibrated using Particle Swarm Optimization (PSO), and this calibration process is comprehensively examined from a physical standpoint.

Thirdly, to enhance the generalizability of the SFM-based Collision Avoidance (CA) strategy in handling increasingly intricate scenarios, an adaptive parameter approach is employed for the SFM-based vehicle model. Utilizing the real-time status of the interaction system comprising both the vehicle and pedestrian, the ego vehicle will derive optimal SFM-based parameters generated through offline Particle Swarm Optimization (PSO) to effectively avert collisions.

Fourthly, in view of problems existing in artificial neural network (ANN) and MPC when designing CA methods, such as ANN normally use human driver data set, which contains instability and huge amount of noise as training data, that will result in large trial and iteration epochs to obtain results, and MPC are not yet possible to control in real-time in the dynamic motion of the vehicle due to its huge computation when facing to complex scenario. This research also proposed an ANN based neural approximation-based feedback controller (NAFC) that its training data is collected from MPC in order to ensure stability of training data and can guaranteed real-time performance.

Finally, an SFM-based driver assistance system is conducted and examined in T3R Hardware-in-the-Loop (HIL) test bench. This driver assistance system generates a local reference path for the driver based on the real-time states of vehicle-pedestrian system. This path is then seamlessly projected onto the front windshield, providing the driver with a virtual representation of the environment. The empirical results stemming from the HIL tests affirm the feasibility of the proposed SFM-based driver assistance system in guiding drivers to safe path.

## List of nomenclatures

Serial number	Symbol	Notation	Unit
1	$U_k$	Control input sequence	-
2	$r(k)$	Reference input	-
3	$x(k)$	State	-
4	$y(k)$	Output	-
5	$U_k^*$	Optimal control input sequence	-
6		The distance between the ego vehicle and the front of the parked vehicle	m
7	$L_b$	Distance between the ego vehicle and the rear of the parked vehicle	m
8		Distance between the oncoming vehicle and the front of the parked vehicle	m
9	$v_{[*]}$	Velocity of $[*]$	m/s
10	$a_{[*]}$	Acceleration of $[*]$	m/s <sup>2</sup>
11	$D_{\text{safety}}$	Minimum safe distance	m
12	$PET_{\text{safe}}$	Safe time difference	s
13		Safe time difference with constant speed	s
14	$PET_{s1}$	Safe time difference with constant speed	s
15	$\eta_{up}$	Output vector in upper-layer MPC	m
16	$Q_{up}, R_{up}$	Weighting matrices for upper- layer MPC	-
17	$N_{[p,c]}$	Length of prediction/control horizon	-

## List of nomenclatures

18	$[x, y]$	[longitudinal, lateral] position in the ego vehicle body frame	m
19	$[X, Y]$	[longitudinal, lateral] position in world axis frame	m
20	$\varphi$	Vehicle yaw angle	rad
21	$a$	Vehicle acceleration	m/s <sup>2</sup>
22	$F$	Force	N
23	$\mu$	Road friction coefficient	-
24	$\zeta$	Small positive number	-
25	$u(t)$	Control input	-
26	$D_{[*]2[\blacksquare]}$	Distance between $[*]$ and $[\blacksquare]$	m
27	$R_{[\text{ub}, \text{lb}]}$	[upper, lower] bound constraint of the road	m
28	$a_{up}, b_{up}$	Coefficients of the fifth-order polynomial	-
29	$\alpha_{[f, r]}$	Slip angles of [front, rear] axle	-
30	$\delta_f$	Steering wheel angle	rad
31	$l_{[f, r]}$	Distances from the center of gravity to [front, rear] axles	m
32	$I_{zz}$	Yaw moment of inertia	kg · m <sup>2</sup>
33	$m_{[*]}$	Mass of $[*]$	kg
34	$s_{[f, r]}$	Slip rate of [front, rear] tire	-
35	$\bar{C}_{\alpha[f, r]}$	Longitudinal stiffness of [front, rear] tire	-
36	$\xi$	State sequence for MPC	-
37	$\gamma$	Output sequence for MPC	-
38	$T_s$	Sampling time for MPC	s
39	$W$	Weight for MPC	-
40	$\rho$	Relaxation factor coefficient for	-

MPC			
41	$TTCP$	Time to Conflict Point	s
42	$d_{[*]2[\blacksquare]}$	Distance between $[*]$ and $[\blacksquare]$	m
43	$v_{ev}^{col}$	Collision speed	m/s
44	$d_{ev}^{col}$	Collision distance	m
45	$\tilde{F}_{[*]2[\blacksquare]}^{i,t}$	Force from the i-th $[*]$ to $[\blacksquare]$ at time t	N
46	$P_{[*]}^t$	Position of $[*]$ at time t	m
47	$S_{[*]}^t$	State of $[*]$ at time t for SFM	-
48	$j_{ev}^t$	Jerk of acceleration	m/s <sup>3</sup>
49	$\Delta\delta_{ev}^t$	Jerk of steering wheel angle	rad/s
50	$\mathbb{F}_{\delta}$	Set of feasible $\delta_{ev}^t$	-
51	$\mathbb{F}_a$	Set of feasible $a_{ev}^{x,t}$	-
52	$A_{[*]2[\blacksquare]}$	Magnitude of force from $[*]$ to $[\blacksquare]$	N
53	$B_{[*]2[\blacksquare]}$	Decaying rate of force from $[*]$ to $[\blacksquare]$	-
54	$\lambda_{[*]2[\blacksquare]}$	Anisotropy rate of force from $[*]$ to $[\blacksquare]$	-
55	$\beta_{[*]2[\blacksquare]}$	Switch function of force from $[*]$ to $[\blacksquare]$	-
56	$\kappa_{des2[*]}$	Magnitude of force from destination to $[*]$	N
57	$\vec{F}_{[*]}^t$	Total force for $[*]$	N
58	$\vec{F}_{noise}^t$	Gaussian distribution-based noise	N
59	$\vec{F}_{brake}^t$	Force from controller for ego vehicle	N

## List of nomenclatures

60	$\phi_{[*]2[\blacksquare]}^t$	Interaction angle between $[*]$ and $[\blacksquare]$	rad
61	$d_{[*]}^{\text{swi}}$	Switch distance for $[*]$	m
62	$\Theta_i$	i-th particles swarm set	-
63	$v_{\text{ref4}}[*]$	Reference speed for $[*]$	m/s
64	$\omega_v$	Weight of tracking current reference speed	-
65	$\omega_p$	Weight of tracking reference path	-
66	$c_1$	Individual learning rate for PSO	-
67	$c_2$	Group learning rate for PSO	-
68	$r_1, r_2$	Random number for PSO	-

---



## Contents

Chapter1	Introduction .....	1
1.1	Preface.....	1
1.2	Motivation of research .....	1
1.2.1	Situation of traffic accidents .....	1
1.2.2	Shared space.....	3
1.2.3	Developing of autonomous vehicles .....	5
1.3	Previous research.....	9
1.3.1	Previous solution.....	9
1.3.2	Research gaps.....	12
1.4	The purpose this research.....	13
1.4.1	Research purpose .....	13
1.4.2	Research Challenges .....	14
1.5	Structure of this thesis .....	15
Chapter2	Active Collision Avoidance strategy .....	17
2.1	Preface.....	17
2.2	Introduction of Model Predictive Control .....	18
2.3	Solution for collision avoidance interacting with other vehicles .....	21
2.3.1	Scenario modeling .....	21
2.3.2	Behavior re-planning based on post-encroachment time (PET) .....	24
2.3.3	Multi-layer collision avoidance strategy .....	26
2.3.4	Upper-Layer MPC-based trajectory re-planning.....	27
2.3.5	Polynomial Fitting .....	32
2.3.6	Lower-Layer MPC-based trajectory tracking .....	32
2.3.7	Simulation results.....	37
2.4	Solution for collision avoidance interacting with pedestrians.....	45
2.4.1	Scenario modeling .....	45
2.4.2	Case of Multi-pedestrians .....	47

## Contents

2.4.3	Collision probability estimation.....	48
2.4.4	Two-layer MPC-based CA strategy .....	50
2.5	Existing Problems of MPC.....	52
2.6	Summary of this chapter .....	53
Chapter3	Passive Collision Avoidance Strategies.....	55
3.1	Preface.....	55
3.2	Social force model.....	56
3.2.1	Introduce of SFM.....	56
3.2.2	Rational explanation .....	58
3.2.3	SFM-based pedestrian model.....	66
3.2.4	SFM-based vehicle model.....	71
3.3	SFM-based solution for ego vehicle interacting with multi-pedestrians.....	73
3.3.1	Particle swarm optimization-based parameters calibration.....	76
3.3.2	Physical explanation of parameters optimization .....	79
3.3.3	Comparison of simulation results between MPC and SFM .....	86
3.4	Adaptive parameters method for SFM .....	90
3.4.1	Analysis of avoidance process .....	92
3.4.2	Two modes of Adaptive parameters method.....	96
3.4.3	Simulation results.....	102
3.5	SFM-based solution for ego vehicle interacting with bike.....	104
3.5.1	Scenario modeling .....	104
3.5.2	Modified SFM-based Vehicle Model.....	105
3.5.3	PSO-based parameters optimization .....	106
3.5.4	Simulation Results .....	108
3.6	Existing Problems of SFM .....	109
3.7	Neural Approximate Feedback Network.....	112
3.7.1	Application scenario .....	113
3.7.2	Training data collection.....	115
3.7.3	Structure of NAFC.....	117

3.7.4	Simulation results for NAFC .....	118
3.7.5	Existing Problems of NAFC .....	122
3.8	Summary of this chapter .....	123
Chapter4	SFM-based driver assistance system.....	125
4.1	Preface.....	125
4.2	Design of SFM-based driver assistance system .....	125
4.2.1	Test process for SFM-based driving assistant system.....	126
4.2.2	Local reference path generation .....	129
4.3	T3R simulator.....	131
4.4	Application of SFM-based driver assistance system in T3R.....	132
4.4.1	Pedestrian avoidance assistance .....	132
4.4.2	Lane keeping assistance .....	134
4.4.3	Experimental comparison .....	136
4.5	Summary of this chapter .....	138
Chapter5	Conclusion.....	139
5.1	Summary of this thesis .....	139
5.2	Future work .....	142
Reference	.....	143
Acknowledgment	.....	148
Achievement	.....	149



# Chapter1 Introduction

## 1.1 Preface

In this chapter, the motivation of the research is introduced in section 1.2. Previous researches are elaborated on in section 1.3. Then, based on the research gaps, the research purposes are illustrated in section 1.4. Section 1.5 gives the structure of this thesis.

## 1.2 Motivation of research

### 1.2.1 Situation of traffic accidents

With the development of science and technology, the safety performance of vehicles is increasingly enhanced due to the units such as antilock brake system (ABS) and electronic stability control (ESC), and the incidence of vehicle accidents is decreasing year by year. However, serious traffic accidents still happen nowadays.

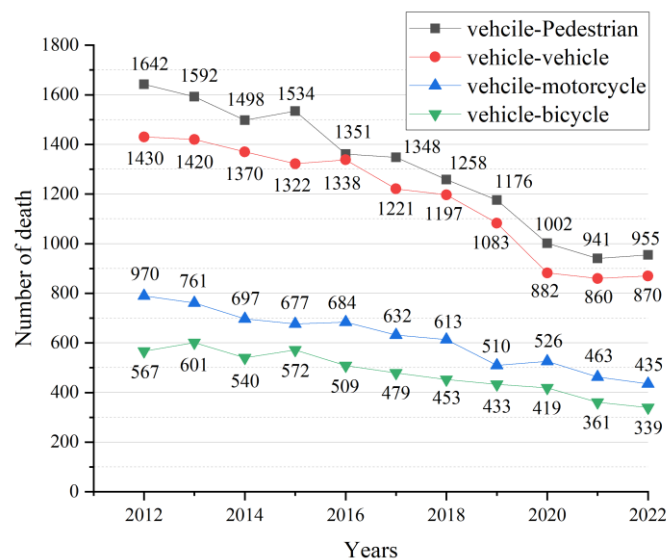


**Figure 1.1 Changes in the number of deaths by interaction[1]**

Figure 1.1 shows the number of death in different types of traffic accidents from 2012 to 2022

## Introduction

from national police agency of Japan[1]. From 2012 to 2022, the death toll of traffic accidents reduced. However, the number of accidents remains high, and companies in the automobile industry are continuing efforts to achieve zero traffic accidents. Besides, the death toll percent in in traffic accidents of interaction of vehicle-pedestrian (36.6% in the years of 2022) and vehicle-vehicle (33.3% in the years of 2022) is the highest.

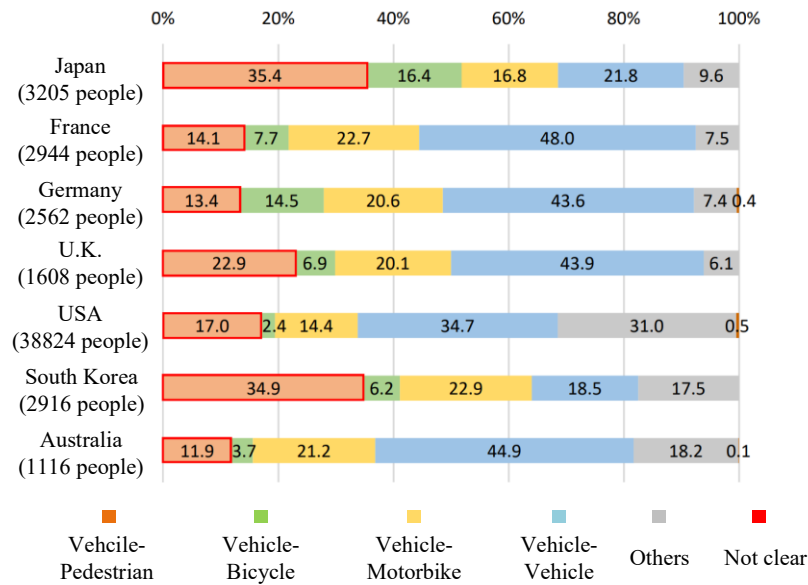


**Figure 1.2 Comparison of composition rates of the number of deaths within 30 days by country (2021)[1]**

Figure 1.2 shows comparison of composition rates of the number of deaths within 30 days by country in years of 2021. The comparison also gives a result, which is similar with results from Figure 1.1, that is death toll percent in traffic accidents of interaction of vehicle-pedestrian (orange part of Figure 1.2) and vehicle-vehicle (blue part of Figure 1.2) is the highest. Therefore, special attention should be paid when dealing with vehicle-pedestrian interaction and vehicle-vehicle interaction when dealing with collision avoidance.

Ensuring the safety of passengers, pedestrians, and the vehicle itself is a paramount concern. Therefore, the design of vehicle collision avoidance algorithms is essential due to the increasing need for safer and more efficient transportation in a world marked by urbanization and technological advancements. These algorithms have a significant impact on autonomous driving, robotics, and overall road safety, making them a critical area of research and development. For example, Figure 1.3 shows a typical vehicle-vehicle interaction in narrow road scenes in urban condition, which was a video frames

collected by Smart Mobility Research Center (SMRC)[2] of Tokyo University of Agriculture and Technology. When the ego vehicle wants to find a reasonable path to pass the parking vehicle without collide with the oncoming vehicle, the CA strategies need to be deeply discussed.

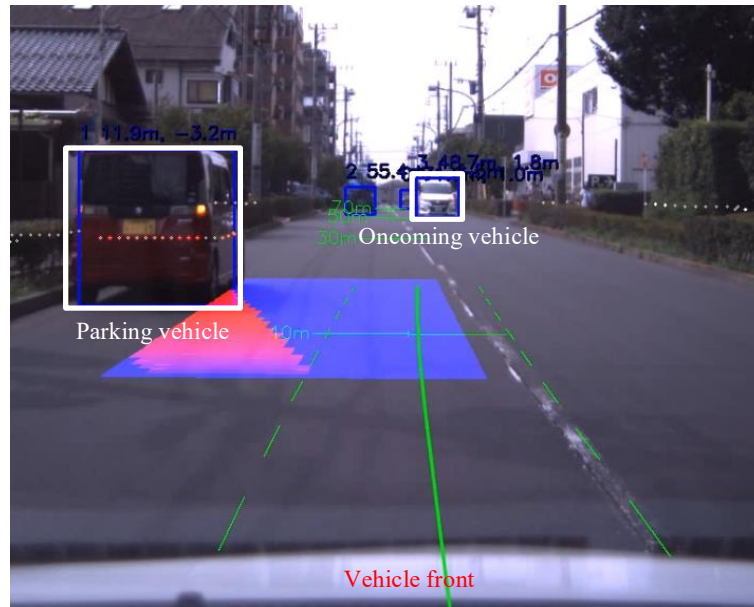


Figure 1.3 Vehicle-vehicle interaction in the urban condition

### 1.2.2 Shared space

Some countries in Southeast Asia, electric bikes are more and more involved in the interaction of traffic flow due to their convenience and quickness[3]. Users of this mode of transportation blur the distinction between vehicles and pedestrians, as all participants in traffic can freely share the same space. Simultaneously, the concept of shared space, employed to enhance the appeal of people traveling to public areas, is increasingly gaining prominence in Western countries as an alternative to conventional urban designs[4, 5]. Shared space, similar to mixed traffic, is a concept that fosters a heightened sense of alertness and accountability by minimizing delineations and physical separation between roadways and pedestrian zones[6].

Shared space represents a forward-thinking urban design and traffic management concept that challenges the conventional separation of road users and advocates for a more inclusive and collaborative approach to street design. It revolves around the notion of establishing public spaces

## Introduction

where pedestrians, cyclists, and vehicles coexist within the same roadway, often with minimal or no traffic control measures. The concept of space sharing, as illustrated in Table 1-1, was originally introduced through the woonerf (living playground) concept in the Netherlands during the late 1960s.

**Table 1-1 The characteristics of new design approaches[7]**

	Woonerf	Traffic calming	Shared space
Alternative names	Home zone residential yard	Traffic control	Naked intersection livable streets shared streets/zones
Land use	Residential	Any land use	Any land use
Is social interaction an aim?	Yes	No	Yes
Design approach	Flexible	Standardized	Flexible
Objective	Slow traffic to allow social interaction	Slow traffic	Multi-faceted
Who has the priority?	Pedestrians	Traffic	Identical
Initiated in	1960s	1980s	1991 (first applied in 2004)

And Figure 1.4 shows a vehicle-pedestrian interaction in narrow road scenes in residential areas, which was also a video frames collected by Smart Mobility Research Center (SMRC)[2] of Tokyo University of Agriculture and Technology, drivers need to carefully assess the collision risk although driving speed is relatively low. In such non-signalized areas, pedestrians typically have a relatively lower right-of-way priority, implying that vehicles are not required to come to a full stop to yield to pedestrians.

Hence, in cases where pedestrian movement is unpredictable, or when pedestrian crossings introduce stochastic elements from the driver's perspective, and considering the importance of time efficiency and swiftly navigating through uncertain risk areas, drivers or control agents must strike a

balance between maintaining higher relative velocities and ensuring an adequate safety distance during the avoidance process. Such situations are prevalent in shared spaces, and the development of a rational obstacle avoidance strategy in such scenarios is a pressing issue for researchers to address.

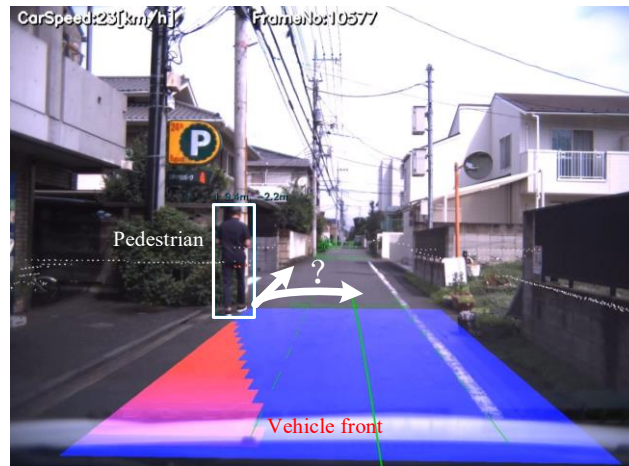


**Figure 1.4 Vehicle-pedestrian interaction in shared space**

### 1.2.3 Developing of autonomous vehicles

For intelligent control system or advanced driver assistance systems (ADAS) that are equipped in highly automated vehicles. Their main function is to maintain safer driving for both drivers and pedestrians[8-10], especially on non-signalized road in shared space.

Unmanned driving technology has made great achievements in the 20th century, from early radio remote control to radio guidance, to equipping vehicles with sensors, computing systems and control systems, giving vehicles "vision", intelligence and automation capabilities, making vehicles can achieve autonomous driving on structured roads, and the development direction of driverless technology has also shifted from the initial road intelligence to vehicle intelligence. But by the end of this century, research on autonomous driving technology was still concentrated in university laboratories or car company research institutes, and it failed to form a real industry. In the 21st century, an unmanned vehicle challenge organized by the U.S. Defense Advanced Research Projects Agency greatly promoted the development of autonomous driving, hereinafter referred to as "DARPA". It is precisely because of this competition that international currency technologies (ICT) companies around the world,

## Introduction

represented by Google, and Silicon Valley startups have joined in the research and development of smart cars, which has also triggered the "intelligent" transformation of the traditional automobile industry. The vehicle “Stanley”, shown in Figure 1.5, won the 2005 DARPA Challenge[11] and make the competition a milestone in the quest for self-driving cars.



**Figure 1.5 Stanley: The Robot that Won the 2005 DARPA Grand Challenge**

However, the playing environment is static and “Stanley” cannot navigate the traffic environment. Another autonomous vehicle named “boss”, shown as Figure 1.6, won the 2007 DARPA Urban Challenge[12] which designers should design a vehicle to obey all traffic rules while being able to detect and avoid other robots on the track. This is a particular challenge for vehicle software, as vehicles must make “intelligent” decisions in real time based on the actions of other vehicles.



**Figure 1.6 Boss, the autonomous Chevy Tahoe that won the 2007 DARPA Urban Challenge**

Till today, autonomous driving has made great progress[13]. OEMs around the world and companies with autonomous driving businesses have successively launched their own autonomous

driving solutions, such as the Autopilot developed by Tesla, Autonomous Driving Solution (ADS) developed by HUAWEI, *etc.*

In addition, SAE (Society of Automotive Engineers) introduced the concept of automated driving levels[14] (shown as Figure 1.7) to standardize and categorize the various degrees of automation in self-driving vehicles. This classification system was developed to promote clarity, safety, and consistency in the development and deployment of autonomous vehicles since its initial launch in 2014.

	SAE LEVEL 0™	SAE LEVEL 1™	SAE LEVEL 2™	SAE LEVEL 3™	SAE LEVEL 4™	SAE LEVEL 5™
What does the human in the driver's seat have to do?	You <b>are driving</b> whenever these driver support features are engaged – even if your feet are off the pedals and you are not steering			You <b>are not driving</b> when these automated driving features are engaged – even if you are seated in “the driver’s seat”		
	You must constantly supervise these support features; you must steer, brake or accelerate as needed to maintain safety			When the feature requests, you must drive	These automated driving features will not require you to take over driving	
What do these features do?	These are driver support features			These are automated driving features		
	These features are limited to providing warnings and momentary assistance	These features provide steering <b>OR</b> brake/acceleration support to the driver	These features provide steering <b>AND</b> brake/acceleration support to the driver	These features can drive the vehicle under limited conditions and will not operate unless all required conditions are met		This feature can drive the vehicle under all conditions
Example Features	<ul style="list-style-type: none"><li>• automatic emergency braking</li><li>• blind spot warning</li><li>• lane departure warning</li></ul>	<ul style="list-style-type: none"><li>• lane centering <b>OR</b></li><li>• adaptive cruise control</li></ul>	<ul style="list-style-type: none"><li>• lane centering <b>AND</b></li><li>• adaptive cruise control at the same time</li></ul>	<ul style="list-style-type: none"><li>• traffic jam chauffeur</li></ul>	<ul style="list-style-type: none"><li>• local driverless taxi</li><li>• pedals/steering wheel may or may not be installed</li></ul>	<ul style="list-style-type: none"><li>• same as level 4, but feature can drive everywhere in all conditions</li></ul>

**Figure 1.7 SAE J3016™ levels of driving automation**

Autonomous driving technology has revolutionized the automotive industry, offering numerous advantages in the domain of vehicle collision avoidance. Here are some key benefits[15-21]:

(1) Improved reaction time and precision: autonomous vehicles are equipped with advanced sensors and computer systems that can detect potential hazards and react within milliseconds. This rapid response time and precision surpasses human capabilities, leading to enhanced collision avoidance.

(2) Reduced human error: human errors, such as distracted driving, impaired judgment, and fatigue, are major contributors to accidents. Autonomous vehicles eliminate these factors, leading to a significant reduction in accidents caused by driver mistakes.

(3) Constant awareness: autonomous vehicles maintain 360-degree awareness of their

## Introduction

surroundings at all times, even in challenging conditions like heavy rain or fog. This constant vigilance minimizes the likelihood of collisions with unexpected obstacles.

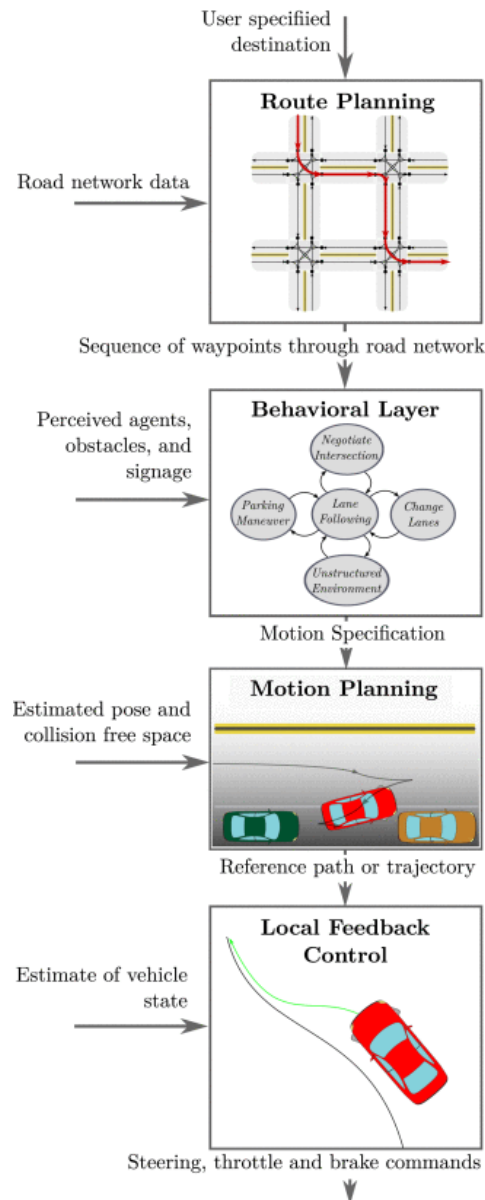


**Figure 1.8** The decision-making system of a typical self-driving car[13]

(4) Traffic management and communication: autonomous vehicles can communicate with each other and with traffic infrastructure, allowing them to coordinate movements and navigate congested areas efficiently. This can prevent collisions in high-traffic situations.

(5) Predictive analytics: advanced algorithms and machine learning enable autonomous vehicles to predict and anticipate potential collisions based on the behavior of other road users, further enhancing

their ability to avoid accidents.

(6) Adaptive maneuvering: Autonomous vehicles can execute complex and precise maneuvers, such as emergency braking, swerving, or changing lanes, to avoid collisions in real-time. These maneuvers are executed with a level of precision that exceeds human capabilities.

(7) Data sharing and learning: autonomous vehicle networks can share collision data and near-miss incidents, enabling collective learning and the continuous improvement of collision avoidance algorithms.

(8) Accessibility: autonomous driving technology can make transportation more accessible to individuals with disabilities, reducing barriers to mobility and enhancing safety for this segment of the population.

The decision-making system of a typical self-driving car is hierarchically decomposed into four components (cf. Figure 1.8): At the highest level a route is planned through the road network. This is followed by a behavioral layer, which decides on a local driving task that progresses the car towards the destination and abides by rules of the road. A motion planning module then selects a continuous path through the environment to accomplish a local navigational task. A control system then reactively corrects errors in the execution of the planned motion[13].

The designed CA strategies in this thesis are mainly based on behavioral layer, motion planning and local feedback control, that motion planning and local feedback control are also known as trajectory re-planning and local reference trajectory tracking, respectively.

## 1.3 Previous research

### 1.3.1 Previous solution

Vehicle active safety control technologies, such as advanced driver assistance systems (ADAS) that help the driving process automation are playing an important role in modern passenger cars and commercial vehicles. One of the main features of ADAS is the collision avoidance (CA) system. A sufficient CA architecture usually encompasses threat assessment, path planning and path tracking strategies [22]. As road collisions might happen in various scenarios, a successful CA system should have the ability to guide the avoidance navigation of the host vehicle in multi-scenario hazards. For

example, collisions at intersections, high-speed highway collisions, CA in crowded urban areas as well as collision mitigation of a priori unknown obstacles [23, 24]. There are at least two common types of CA design control architecture which have been proposed and implemented. For example, a multi-layer CA system[25], which contains modelling car-following strategies from a set of example driving sequences in offline and in online, the model is used to compute accelerations which replicate what a human driver would do in the same situation. Reference [26] considered collision risk potential prediction such as a pedestrian suddenly darting out from a poor-visibility blind corner and designed trajectory re-planning layer and tracking layer to theoretically calculate the desired yaw rate and the desired longitudinal deceleration by optimizing the potential field function in the framework of optimal control theory. This is the usual type of CA implementation and is also known as a guidance and navigation control system [27].

In addition, optimization algorithms based on different mathematical theories have been proposed and applied in the CA system. Threat assessment strategies provide an online evaluation of the potential threat to assist drivers in avoiding or evading collisions[28]. According to Gray et al. [29], threat assessment can be defined as a real-time judgment of a function which calculates the possibility of an unavoidable road accident. A path planning (PP) strategy as part of the full CA architecture can be widely used in the field of road vehicles and mobile robots. It is formulated to acquire a collision-free path while the vehicle independently navigates itself [24]. In the condition of the avoidance of single or multiple static obstacles, many studies have been carried out. Inspired by viscous fluid flowing between two parallel plates or around a cylinder, Cheng et al. proposed virtual fluid-flow-model based lane-keeping integrated with a collision avoidance control system to realize the function of both lane-keeping and collision avoidance [30]. The predictive nature and constraint handling capabilities of model predictive control (MPC) make it an attractive framework for leveraging these new technologies, and it is also adopted in CA., such as [31]presents a novel technique for creating haptic steering feedback based on a prediction of the system's need to intervene in the future. This feedback mirrors the tension between the two controller objectives of following the driver and maintaining a feasible path, [32] combined potential field with MPC in order to maintain the connectivity of a flock of agents in a leader-follower configuration with dynamic topology (they considered a group of agents navigating in an environment with obstacles towards their target. The followers avoid collisions with each other and

obstacles without using any communication links.) and [33] established solution formulated utilizing MPC includes decision making and trajectory planning to address the challenge of collision avoidance with dynamic surrounding vehicles in different driving situations. A machine learning approach, such as the artificial neural network [34, 35] and collision cone approach [36], depends on the driver behavior and the environment instead of the mapping information alone, making it reliable in the context of dynamic CA. The advantage of this method is, once a solution is found, it will be a shorter path. However, getting stuck in local minima is also an issue that should be addressed [37]. At the same time, its drawback is it requires a large trial to obtain the results, thus the computational time is also an issue.

Apart from roads that necessitate strict adherence to traffic regulations, such as intersections featuring signs or traffic lights, there exist traffic segments where there are no distinct demarcations between various road users. This type of environment is commonly referred to as shared space. When navigating such traffic sections, car drivers must diligently assess the risk of collisions, even though driving speeds tend to be relatively low. In these areas, pedestrians often have a lower right-of-way priority, which implies that vehicles usually don't need to come to a complete stop to yield the right-of-way to pedestrians. Consequently, considering the imperative for vehicle drivers to save time during their commutes or expedite their passage through similar areas, drivers or control agents must strike a delicate balance between maintaining relatively higher velocities and ensuring an appropriate safety distance during the avoidance process.

Focusing on such CA problems, a possible solution is to establish interaction relations between pedestrians and vehicles. A lot of research has been conducted to analyze pedestrian intention and vehicle-pedestrian interaction [38-40]. In [41] and [42], based on a statistical analysis of pedestrian behavior, a statistical framework to assess the risk of passing a non-signalized intersection for vehicles was established. Also, a predictive risk metric when a pedestrian appears was given quantitatively based on the pedestrian-aware risk model. The methods of precise prediction of the pedestrian's motion are also essential issues and taken into consideration by some researchers. In [43], a candidate trajectory planning method considering spatial and time sequences is proposed, and they conducted a pedestrian-vehicle interaction model to take the pedestrian's uncertain motion as a superposition of the Markov process without interference and the motion caused by the vehicle as well as predict the pedestrian's motion probabilistically. In [44], Long Short-Term Memory (LSTM) modules based recurrent neural

networks were adopted to make a pedestrian intent prediction. However, the prediction was based solely on the motion trajectory of the pedestrian. The above research mainly focused on the risk assessment of pedestrian crossing road intention. However, it is still difficult to indicate the pedestrian's trajectory in the actual vehicle-pedestrian interaction. Also, some research focused directly on the pedestrian behavior or motion. And the social force model (SFM) is the most used method for modeling users of such shared space in micro-simulation and has been continually improved and modified since its first introduction [45]. Kretz et al. analytically solved the SFM resultant equations for very simple cases and provided helpful comments on model calibration [46]. Besides, not all researches focus on the interactions among pedestrians. Dias et al. explored the applicability of an SFM based microscopic simulation model for personal mobility vehicles and multiple pedestrians in mixed traffic [47]. Based on fundamental patterns of multi-pedestrian interaction with a low speed vehicle (front, back, and lateral interaction in open space), Yang et al. proposed an SFM-based vehicle-pedestrians interaction model, and this model was calibrated by the genetic algorithm (GA) based on trajectory data of the same vehicle-pedestrian interaction patterns from controlled experiments [48].

### 1.3.2 Research gaps

However, the literatures mentioned above mostly focuses on the fixed obstacles, like [31], or moving obstacles in the same direction as the ego vehicle, like [49], and the speed of the ego vehicle and obstacles remains a constant. Most studies are based on the fact that the ego vehicle can safely avoid obstacles while maintaining the current speed. However, in the actual obstacle avoidance process, obstacles are usually dynamic with unpredictable motion. In this situation, the safest obstacle avoidance strategy is to require the ego vehicle to decelerate or even stop. Considering the travel time cost or convenience, we hope that the ego vehicle can avoid obstacles in accordance with the predetermined requirements under the premise of ensuring safety. In other words, if the vehicle can avoid obstacles at a constant speed or by acceleration, deceleration is unnecessary, which requires that the speed of the ego vehicle and trajectory re-planning is real-time controllable during obstacle avoidance. And the method of dealing with risks bring by unpredictable obstacles needs to be further discuss.

From the aspect of methodology, many advanced methods are adopted for vehicle dynamic control from 1980s. Typical methods includes neural networks, artificial potential field and model predictive

control. Recently, lots of researchers combine such methods for a better control effect. However, there still some problems. Neural network is considered a black box where there are no physical explainable models to define the interaction between vehicle and other traffic objects. Other method such as artificial potential field and virtual fluid which owns complex definition, will meet huge computational pressure especially when the scenario turns highly crowded. The cost for searching an optimal solution will turn unacceptable.

Besides, the most researches that developed CA strategies for autonomous vehicles may focus on the ego vehicle itself too much, less considering the dynamic of obstacles. For most research mentioned above, the motion of the obstacle was known in advance, such as being fixed in one position or moving along a predetermined trajectory by a given speed profile. Although other research, such as [3] and [50], adopted SFM for more realistic obstacle movement, there was also no randomness in the proposed SFM, which means the motion of obstacles can be predicted accurately in such researches. But, when considering the individual difference among pedestrians and the nuances of different shared space (like ages of pedestrians or visibility of area), the precise motion prediction of pedestrians is difficult to achieve, which also can be found in the result of research on modelling for similar mixed traffic scenario, such as [19].

## **1.4 The purpose this research**

### **1.4.1 Research purpose**

From discuss in the section1.3, this research aims to propose solutions to the following situations:

(1) Addressing the challenge of an automated vehicle needing to navigate multiple obstacles simultaneously, where the balance between travel time consumption and ensuring collision avoidance safety is of paramount importance. This is particularly crucial in cases involving the unpredictable motion of obstacles.

(2) Examining the methodology for defining an interaction system between the ego vehicle and pedestrians, with a specific focus on scenarios where pedestrian movements are unpredictable. Additionally, when the interaction system operates within a shared space where the distinctions in movement priorities between vehicles and pedestrians are minimal, this research aims to formulate a

mathematical model that possesses a tangible, physical interpretation.

(3) Evaluating control algorithms, such as Artificial Neural Networks (ANN), known for their drawback of requiring extensive trials and prolonged training processes to yield results. On the other hand, Model Predictive Control (MPC), which is suitable for slower dynamic processes and situations with lower real-time demands, still faces challenges in facilitating real-time control of high-speed vehicle dynamics due to its computational complexities. MPC also lacks the ability to draw from past experiences and tends to iteratively search for optimal solutions in similar scenarios, limiting its real-time applicability. Therefore, a core objective of this research is to introduce Collision Avoidance (CA) algorithms that hold the potential for real-time application.

In summary, the motivation of this research is to reduce the traffic accidents and increase the convenience of mobility used for autonomous vehicles: shuttles, delivery services in pedestrian areas.

### 1.4.2 Research Challenges

Focus on the (1)-(3) research targets in section 1.4.1, there are some research challenges:

(a) While the MPC-based controller exhibits a high level of competence in path rerouting and path tracking, it typically relies on accurate predictions of the states of traffic participants within the MPC prediction horizon. Consequently, when confronted with unpredictable obstacles leading to imprecise forecasting results, the adoption of an MPC-based controller poses challenges.

(b) Unpredictable pedestrian movements, influenced by individual and environmental variations, pose difficulties in formulating a mathematical interaction model between the ego vehicle and pedestrians.

(c) The examination of SFM-based pedestrian models is an area of focus in this research, which introduces the innovative incorporation of SFM into the vehicle dynamic model. Defining an SFM-based vehicle model is, therefore, a challenging endeavor. Additionally, the rationalization of utilizing the SFM-based interaction system for the ego vehicle in the design of collision avoidance strategies needs to be elaborated upon.

(d) Adapting calibrated SFM parameters for the SFM-based vehicle model to diverse collision avoidance scenarios is a formidable task, particularly when addressing pedestrians with unpredictable motion.

(e) Achieving real-time performance of the algorithm remains an ongoing pursuit for researchers in the field of traffic collision avoidance, presenting a challenge within the scope of this research.

## 1.5 Structure of this thesis

In Chapter1, the motivation of researches is introduced based on the current situation of traffic accidents especially in shared space. Then, the previous researches focusing on the CA strategies as well as the research gaps are discussed. Finally, the purpose of this thesis is elaborated.

In Chapter2, the MPC-based active collision avoidance strategies are established for the following cases:

(1) Focusing on interaction between multi-vehicles, consuming travel time and safety assurance of CA need to be carefully considered especially in the case related to unpredictable motion of obstacles. This chapter proposes a feasible solution to this situation by controlling speed and the steering wheel angle.

(2) Focusing on interaction between vehicle and pedestrians, MPC-based CA strategy that considers the unpredictable motion of the pedestrians, a novel speed re-planning layer combined with collision probability estimation, which is used to calculate an acceptable maximum safe speed for ego vehicle, is proposed.

In Chapter3, two categories of passive collision avoidance strategies have been developed: SFM-based and Neural Approximate Feedback Control (NAFC)-based. In the case of SFM-based CA strategies, the initial step involved simplifying the interaction system between the ego vehicle and pedestrians as a Markov process, enabling the utilization of the SFM-based dynamic model. Subsequently, a modified SFM-based vehicle-pedestrian interaction model was established, taking into account the random motion patterns of pedestrians. Then, the following cases are considered when adopting SFM to design CA strategies:

(1) Focusing on interaction between vehicle and pedestrians, particle swarm optimization (PSO) is adopted for searching the optimal parameters of SFM-based vehicle model and the calibration process has been analyzed physically in details;

(2) In order to improve the versatility of SFM-based CA strategy, the CA process is analyzed in details and a novel strategy using SFM-based adaptive parameters was proposed;

(3) Based on the current state of the interaction system that consists of vehicle and bicycle, an SFM-based strategy is proposed which helps the vehicle avoid bicycle appropriately.

Besides, a neural networks-based NAFC is proposed as a fast solver for MPC, and some simulation results are given to compare the effect of NAFC and MPC.

In Chapter4, on the basis of 3.2-3.5, that is, in addition to the application of SFM-based CA strategies in fully autonomous vehicles, we considered an SFM-based driver assistance system to help the driver deals with pedestrian with unpredictable motion in narrow road. The proposed driver assistance system is adopted and validated in T3R HIL test bench. A local reference path will be generated by the real-time states of the vehicle-pedestrian interaction system and virtually display on the front windshield for the driver. The results of HIL test shows the effectiveness of the SFM-based driver assistance system.

In Chapter5, the summary of this thesis and the future work which is based on the current research gaps of this thesis is given.

## Chapter2 Active Collision Avoidance strategy

### 2.1 Preface

The literatures mentioned in section 1.3.1 mostly focuses on the fixed obstacles and the speed of the ego vehicle and obstacles remains a constant. Many studies are grounded in the assumption that the ego vehicle can effectively evade obstacles while maintaining its current speed. However, in real-world obstacle avoidance scenarios, obstacles are often dynamic. In such situations, the safest obstacle avoidance strategy may necessitate the ego vehicle to decelerate or even come to a complete stop. Nevertheless, considering the trade-offs between travel time and convenience, the goal is for the ego vehicle to navigate around obstacles while adhering to predetermined safety requirements. In simpler terms, if the vehicle can circumvent obstacles without the need for deceleration and maintains a constant speed or accelerates, then real-time controllability of the ego vehicle's speed and trajectory re-planning during obstacle avoidance becomes essential. Focusing on such problems, this Chapter2 illustrates novel CA strategies that:

(1) A CA strategy is introduced, which comprises Behavior Re-Planning based on Post-Encroachment Time (BR-PET) and Trajectory Re-Planning and Tracking using a two-layer MPC system to address the CA challenge involving multi-vehicle interactions. The BR-PET module calculates alterations in the ego vehicle's speed by considering initial data related to the ego vehicle, static obstacles, dynamic obstacles, and the speed and acceleration constraints of the ego vehicle. Simultaneously, the real-time performance is ensured by selecting distinct dynamic vehicle models of varying complexity for the two separate MPCs employed in the path re-planning layer and the tracking layer.

(2) Taking into account the unpredictable movements of pedestrians, a comprehensive discussion on the collision probability estimation during the CA process is presented. Building upon this analysis, an active CA strategy based on MPC is introduced to address the CA challenge in scenarios involving interactions between multiple pedestrians and an ego vehicle.

## 2.2 Introduction of Model Predictive Control

Model predictive control, also known as moving horizon control, receding horizon control, dynamic matrix control and generalized predictive control, is a model-based feedback control strategy that has been widely discussed in recent years. The mechanism of MPC can be described as: at each sampling time, based on the current measurement information obtained, an open-loop optimization problem in a limited time horizon is solved online, and the first element of the obtained control sequence acts on the controlled agent. At the next sampling time, the above process is repeated, the optimization problem is refreshed with new measured values and solved again. The main difference between MPC and traditional control methods is that MPC is to solve the open-loop optimization problem online to obtain the open-loop optimization sequence, traditional control methods usually solve a feedback control law offline then the obtained feedback control law maintains the same in the control process.

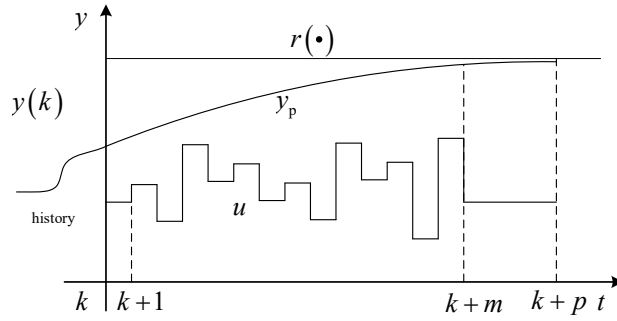


Figure 2.1 The basic principles of MPC

We take a simple given value control problem as an example to introduce the basic principles of MPC. Shown as Figure 2.1, in the current time  $k$ , we can the measured values  $y(k)$  from the controlled system. In the same time, there is a model for predicting future dynamics of the system (here we take state-space representation as example):

$$x(k+1) = f(x(k), u(k)), x(0) = 0 \quad (1)$$

$$y(k) = h(x(k), u(k)) \quad (2)$$

Where  $x(k) \in \mathbb{R}^n, u(k) \in \mathbb{R}^l, y(k) \in \mathbb{R}^q$  is the system state, control input and output, respectively.

Based on Equation (1), the future output of the system from  $y(k)$  could be obtained, defined as:

$$\{y_p(k+1|k), y_p(k+2|k), \dots, y_p(k+p|k)\} \quad (3)$$

where  $p$  is the prediction horizon,  $y_p(k+1|k)$  represents the predictive output at time  $k+1$  predicted at the current time  $k$ . Besides, notice that Equation (1) is difference equation, the current state  $x(k)$  is required as a start point of prediction. In the case of obtaining  $y(k)$ , state observers can be designed to estimate  $x(k)$ .

In order to predict the future output, the control input  $U_k$  needs to be calculated in prediction horizon, which is defined as

$$U_k \stackrel{\text{def}}{=} \{u(k|k), y_p(k+1|k), \dots, y_p(k+p-1|k)\} \quad (4)$$

The target of MPC is to make the system output  $y(\cdot)$  track the desired output, which is usually known as reference input (established as Equation (5)),

$$\{r(k+1), r(k+2), \dots, r(k+p)\} \quad (5)$$

in the constraints of output and control input (established as Equation)

$$\begin{cases} u_{\min} \leq u(k+i) \leq u_{\max}, i \geq 0 \\ y_{\min} \leq y(k+i) \leq y_{\max}, i \geq 0 \end{cases} \quad (6)$$

In other words, we aim to search an optimal control input to get a smallest deviation between predictive output and the reference. Therefore, a simple cost function is established to define the cumulative error between predictive output and the reference:

$$J(y(k), U_k) = \sum_{i=k+1}^{k+p} (r(i) - y_p(i|k))^2 \quad (7)$$

Then, the problem of search an optimal control input is transformed as the following optimization problem:

$$\begin{aligned} & \min_{U_k} J(y(k), U_k) \\ \text{s.t. } & u_{\min} \leq u(k+i) \leq u_{\max}, i = 0, 1, \dots, p-1 \\ & y_{\min} \leq y(k+i) \leq y_{\max}, i = 0, 1, \dots, p \end{aligned} \quad (8)$$

Equation (8) is also known as dynamic optimization problem because this optimization problem contains system dynamic function Equation (1) that the target function (8) is a cost defined along the dynamic trajectory of the system as well as the constrains (6) are the constrains for the dynamic trajectory of the system.

It is assumed there is a solution for optimization problem (1)-(2), and the optimal solution for the problem at time  $k$  is defined as:

$$U_k^* \stackrel{\text{def}}{=} \{u_k^*(k|k), u_k^*(k+1|k), \dots, u_k^*(k+p-1|k)\} \quad (9)$$

Obviously,  $U_k^*$  is a function of current output  $y(k)$ :

$$U_k^*(y(k)) = \arg \min_{U_k} J(y(k), U_k) \quad (10)$$

However, all elements of  $U_k^*$  cannot be applied to the system that the reasons contain:

(1) There are some deviations between the real output and predictive output of the system due to external disturbances and the model-plant mismatch.  $U_k^*$  is depend on the current output  $y(k)$  due to Equation (10). If the all elements of  $U_k^*$  are applied to the system, the output in time  $k + 1$  and later will be ignored, which means the external disturbances and model-plant mismatch information after time  $k$  cannot be used effectively. This may result in reduced system performance or even system instability.

(2) Commonly, it is hard to obtain an analytical expression for the problem described by Equation (1)-(2). The numerical solution is usually as an alternative, which means the length of prediction horizon  $p$  is finite. Even if all the elements in  $U_k^*$  are adopted, we only get the control input in finite time horizon  $p$  which cannot support the system working in a long period.

Therefore, only the first item  $u_k^*(k|k)$  of the optimal solution vector  $U_k^*$  in time step  $k$  will be adopted. And in the next time step  $k + 1$ , MPC re-predicts and solves based on the new measurement output  $y(k + 1)$ .

To sum up, the basic principles of MPC is that the new measurement in each sampling step is obtained to refresh optimization problem described by Equation (1)-(2), then solving the refreshed optimization problem and applying the first item of optimal solution vector to the system, repeating this process until terminal point(or  $k \rightarrow \infty$ ). In other words, MPC contains three steps:

- (1) Predict the future state of target system;
- (2) Obtain (numerical) solution of the optimization problem;
- (3) Apply the first item (or first part) of optimal solution to the system.

The above three step will be executed repeatedly in every sampling step.

MPC-based controller has developed considerably since it is initially adopted in slow industrial control processes[51, 52]. And now MPC can also be used in control with high real-time requirements[53, 54] such as vehicle dynamic control.

## 2.3 Solution for collision avoidance interacting with other vehicles

### 2.3.1 Scenario modeling

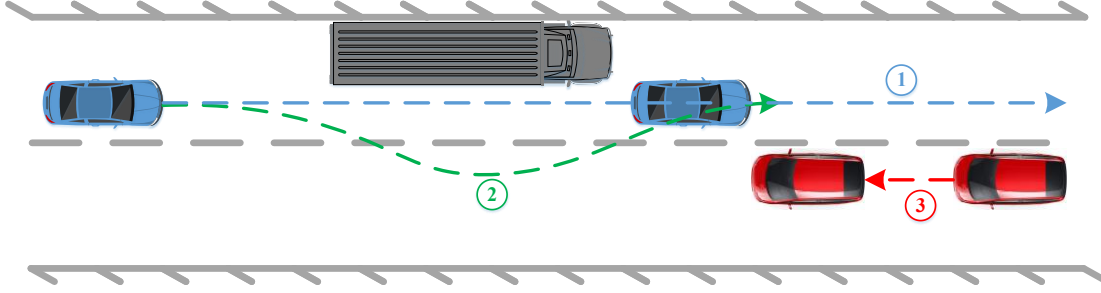


**Figure 2.2: Scenario of collision avoidance overtaking a parked vehicle and yielding an oncoming vehicle.**

The typical scenario Figure 1.3 could be modeled as Figure 2.2, the dotted line 3 is the trajectory of the oncoming vehicle and the dotted line 1 is the initial reference trajectory (also known as the global reference trajectory) of the ego vehicle. Due to the presence of a parked vehicle and an oncoming vehicle, the ego vehicle is compelled to adjust its local trajectory planning, as illustrated by the dashed line 2 in the scenario. Given variations in the initial position and speed changes in the oncoming vehicle's movement, it may not be safe for the ego vehicle to maintain its current speed or accelerate within the permissible speed limits or handling stability requirements. Consequently, the ego vehicle must inevitably decelerate to ensure safety in managing the driving situation. When dealing with dynamic obstacles like oncoming vehicles in the opposite lane, particularly when the future speed of the obstacle remains unpredictable, it becomes challenging for the controlled ego vehicle to exhibit the same level of judgment as a skilled and cautious human driver. Therefore, the question of the way to re-plan the motion behavior and local reference trajectory becomes a matter worthy of careful consideration.

Considering the different speed of oncoming vehicle, there are basically two situations when the ego vehicle and the oncoming vehicle meets, shown as Figure 2.3, A represents the ego vehicle, B signifies the parked vehicle, and C denotes the oncoming vehicle. A1 and C1 represent the positions where the ego vehicle and the oncoming vehicle intersect, with a similar correlation for A2 and C2.  $L_a$

and  $L_b$  are defined as the distances between the ego vehicle and the front or rear of the parked vehicle, respectively.  $L_c$  represents the distance between the oncoming vehicle and the front of the parked vehicle.  $D_{safety}$  is a reference safe distance utilized for controlling the speed of the ego vehicle. Unless otherwise specified, all distance measurements in this thesis are expressed in meters.

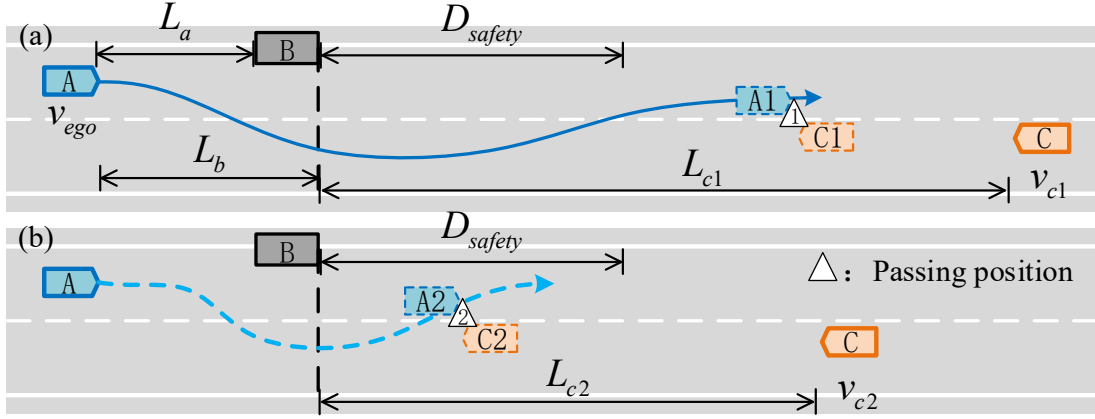


**Figure 2.3** Different passing position when ego vehicle keeps speed constant during overtaking (a) The passing position is at a safe position (b) The passing position is too close to the parked vehicle.

The objective of the research in this section is to introduce an upper-level control algorithm that enhances the safe avoidance of obstacles characterized by unpredictable speeds. Therefore, by default, the relative positional relationship between vehicles and the real-time speed of the oncoming vehicle can be accurately ascertained by the automotive radar installed in the ego vehicle. Moreover, given that the target scenario is anticipated to occur in narrow road conditions at low speeds, specific constraints have been established:

(1)  $L_a, L_b$  are global fixed parameters for the scenario, that means the initial relative position of the ego vehicle and the parked vehicle are not changed in any simulation;

(2)  $L_c$  is treated as a local invariant, that means the initial relative position of oncoming vehicle will only be changed as the initial condition of a simulation;

(3)  $0 \text{ m/s} \leq v_{ego} \leq 15 \text{ m/s}$ ,  $10 \text{ m/s} \leq v_c \leq 15 \text{ m/s}$ ;

(4)  $-3 \text{ m/s}^2 \leq a_{ego} \leq 1 \text{ m/s}^2$ ,  $-3 \text{ m/s}^2 \leq a_c \leq 1 \text{ m/s}^2$

Where  $v_{ego}$ ,  $a_{ego}$  represent the speed and acceleration/deceleration of the ego vehicle respectively.  $v_c$ ,  $a_c$  represent the speed and acceleration/deceleration of the oncoming vehicle

respectively.  $D_{\text{safety}}$  is a distance used to determine a safe passing position. It is obvious that such a scene often occurs in crowded urban traffic conditions.

The behavior of the ego vehicle will be re-planned by different situations when the ego vehicle and the oncoming vehicle meets, shown as follows:

(1) If the passing position is far enough away from the parked vehicle, as shown in Figure 2.3(a) at passing position 1, the ego vehicle will choose to keep speed unchanged or accelerate according to the oncoming vehicle speed  $v_{c1}$  and position  $L_{c1}$ ;

(2) Due to excessive speed  $v_{c1}$  or short initial distance  $L_{c2}$  of the oncoming vehicle, even if the ego vehicle accelerates to the maximum allowable speed, it cannot guarantee that their passing position is at a safe position, as shown in Figure 2.3(b) at passing position 2. The ego vehicle will decelerate until oncoming vehicle has already passed, shown as Figure 2.4, then it restarts and overtakes the parked vehicle.

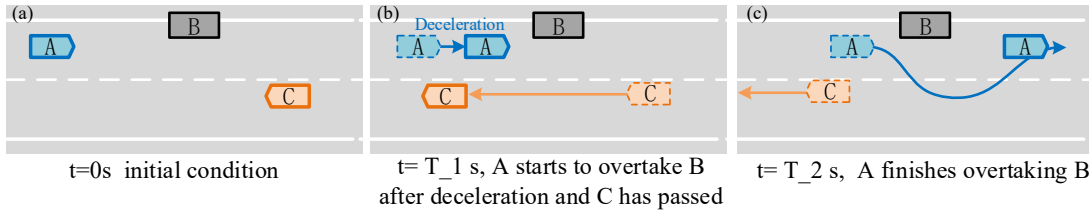


**Figure 2.4 The case of ego vehicle slowing down.(a) Relative positions between vehicles at  $t=0s$ ; (b) Relative positions between vehicles at  $t=T_1s$ ; (c) Relative positions between vehicles at  $t=T_2s$ .**

The issue at hand pertains to the real-time calculation of the passing position, speed control, and trajectory re-planning. The position can be straightforwardly determined based on the initial states of the three vehicles when their speeds remain constant throughout the entire process. However, if the future speed of the oncoming vehicle cannot be predicted, the passing position cannot be defined as a fixed point. Hence, it becomes imperative to employ a more intuitive safety indicator. The challenge of striking a balance between minimizing travel time consumption and ensuring safety will be addressed in the subsequent behavior re-planning section.

### 2.3.2 Behavior re-planning based on post-encroachment time (PET)

Using a safety indicator, this module is employed to perform behavior planning for the entire obstacle avoidance process of the ego vehicle. One widely utilized safety indicator for obstacle avoidance is Time to Collision (TTC) [55], which measures the time remaining before two vehicles collide if no evasive action is taken. However, this method is primarily based on the vehicle's speed and heading angle at the current moment and does not account for vehicle acceleration, leading to significant judgment errors. Another indicator known as Post-Encroachment Time (PET) is employed to estimate the criticality of a specific traffic situation. PET is defined as the elapsed time between the front of the leading vehicle passing a certain point on the roadway and the front of the following vehicle passing the same point [56]. In this research, PET is chosen as the safety indicator for behavior re-planning due to the unpredictable speed of the oncoming vehicle.

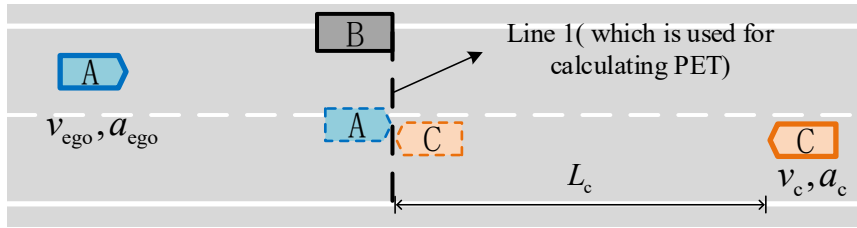


Figure 2.5 The site for calculating post-encroachment time

The location for PET calculation is established at the front side of the parked vehicle, as depicted by Line 1 in Figure 2.5. In this context, PET represents the time interval between A and C passing through Line 1. Given the congested nature of the urban road scenario and the unpredictability of the oncoming vehicle's future speed, prioritizing the safety of the ego vehicle during the obstacle avoidance process is paramount. Hence, it is assumed that the oncoming vehicle will accelerate to the maximum allowable speed without deceleration, even when it comes into close proximity with the ego vehicle. To maintain safety, a safe distance, denoted as  $D_{\text{safety}}$ , is established at 20 meters.

Then the equivalent PET is defined as:

$$PET_{\text{safe}}^{\text{max}} = D_{\text{safety}}/v_{a\_ini} + D_{\text{safety}}/v_{c\_max} \approx 3.33s \rightarrow 3.5s \quad (11)$$

$$PET_{\text{safe}}^{\text{max}} = D_{\text{safety}}/v_{a\_max} + D_{\text{safety}}/v_{c\_max} \approx 2.66s \rightarrow 3s \quad (12)$$

where  $PET_{safe}^{max}$  defines the maximum time difference between two vehicles passing through the set site while  $PET_{safe}^{min}$  defines the minimum time difference. These two items are close to each other so that the safe PET is set as 3.5 s for convenience. In order to visualize the result, the case where the initial speed of the ego vehicle is 11 m/s is selected. The result can be easily extended to the entire allowed speed span of the ego vehicle.

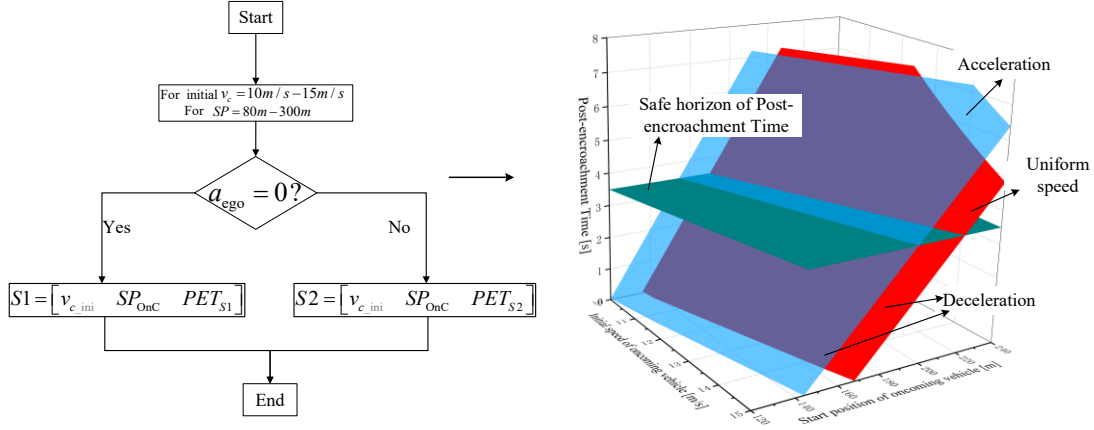


Figure 2.6 Calculation flow of post-encroachment time (PET)

As Figure 2.6 shows, the behavior re-planning module is obtained by the following steps. Firstly, after traversing all allowable speeds and allowable positions of the oncoming vehicle, the PET under the condition of the ego vehicle keeping the initial velocity unchanged ( $PET_{s1}$ ) and accelerating ( $PET_{s2}$ ) will be calculated separately. Then, the initial data of oncoming vehicle and calculated PET will be stored as two different arrays according to whether the ego vehicle needs to accelerate. In Figure 2.6, the blue surface consists of point set  $S1$  while the red surface consists of point set  $S2$ . Finally, the logic of behavior re-planning is as follows:

Case 1: If  $PET_{s2} > PET_{safe}$ , then ego vehicle will keep speed as initial speed unchanged in the whole avoidance process.

Case 2: If  $PET_{s2} < PET_{safe}$  and  $PET_{s1} > PET_{safe}$  which means the ego vehicle cannot avoid obstacles by an unchanged speed unless acceleration, then ego vehicle will be required to accelerate.

Case 3: If  $PET_{s2} < PET_{safe}$  and  $PET_{s1} < PET_{safe}$  which means even if the ego vehicle accelerates to maximum allowable speed, it cannot avoid obstacles safely, then the ego vehicle will be required to decelerate.

### 2.3.3 Multi-layer collision avoidance strategy

The control flow of the proposed Collision Avoidance (CA) system is depicted in Figure 2.7. Here's a step-by-step overview of the process:

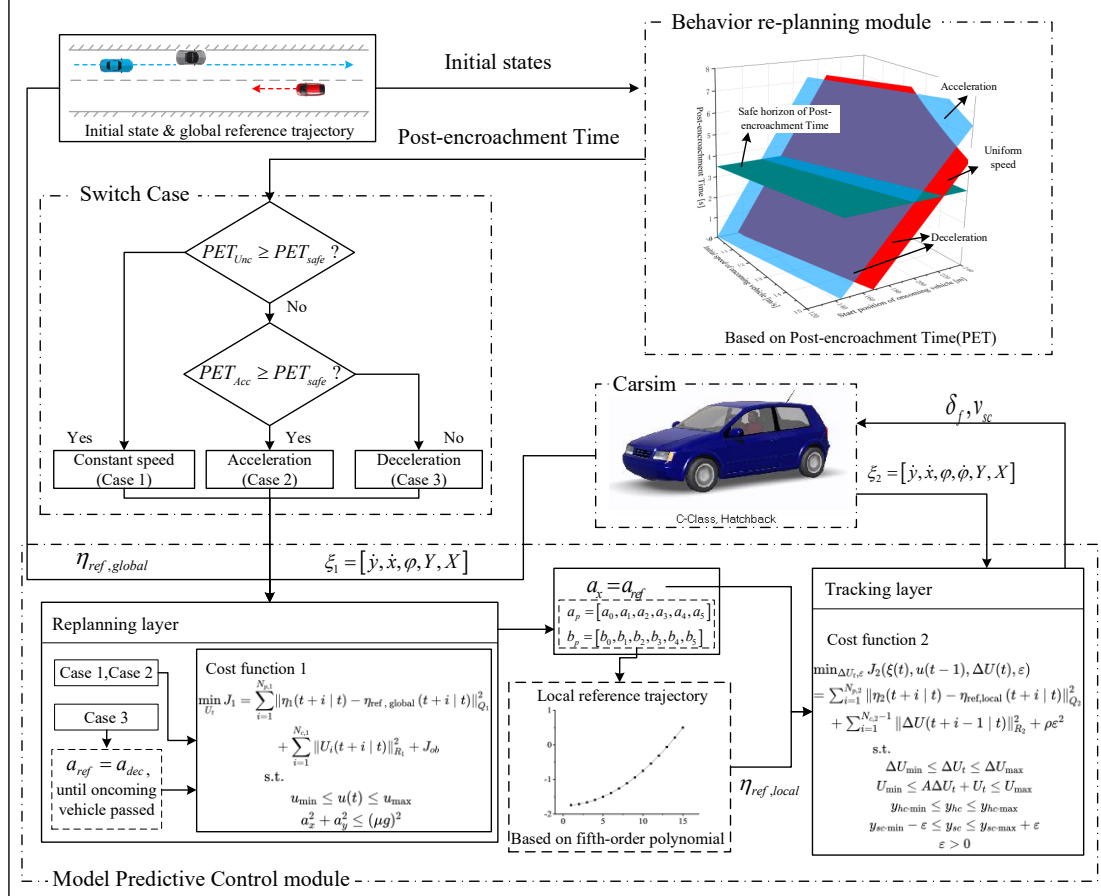


Figure 2.7 Control flow of multi-layer MPC-based collision avoidance (CA) system

(1) Predictive State Calculation: The real-time position and velocity of the oncoming vehicle are used to calculate its predictive state.

(2) Recognition Layer: The recognition layer determines the ego vehicle's movement (acceleration, constant speed, or deceleration) throughout the entire obstacle avoidance process. This decision is based on the Post-Encroachment Time (PET) calculated from the initial states of the ego vehicle and obstacles.

(3) Vehicle Control Unit (VCU): Using the calculated PET, the Vehicle Control Unit (VCU) decides on the next action, which can involve maintaining speed, accelerating, or decelerating.

(4) Re-Planning Layer (Upper-MPC Controller): In the re-planning layer, the local reference path

is transmitted to the tracking layer in the form of fitted curve parameters. Simultaneously, the reference longitudinal acceleration is derived and sent to the tracking layer.

(5) Tracking Layer (Operation Layer): In the tracking layer, also known as the operation layer, the optimal front wheel steering angle and reference speed are determined using the vehicle dynamics model MPC controller. Control signals are then forwarded to the Carsim module.

(6) Data Update: The state of the ego vehicle output by Carsim updates the data in the recognition layer, creating a feedback loop.

The two-layer MPC control system will be described in detail in the subsequent sections.

### 2.3.4 Upper-Layer MPC-based trajectory re-planning

Following behavior re-planning, the global reference path is recalculated based on the real-time relative position of the ego vehicle and obstacles at the upper layer. Subsequently, this reconfigured path is tracked at the lower layer.

In constructing a mathematical model for the vehicle, it is imperative to take into account factors like performance and computational speed. Given the substantial computational load introduced by the re-planning layer's algorithm, the primary aim of introducing MPC is to ensure that the re-planning results adhere to the constraints of vehicle dynamics and kinematics. Therefore, opting for a more complex model does not offer any advantages but contributes to increased computational demands. A comparison conducted has demonstrated that using a relatively lower precision model at the re-planning layer and a relatively higher precision model at the tracking layer strikes a balance between control performance and computational speed. Accordingly, a bicycle model is adopted at the re-planning layer, and a point mass model is chosen for the tracking layer.

The fundamental task of this layer is to devise a rational evaluation function that achieves obstacle avoidance, minimizes deviation between the re-planned path and the global reference path, all while conforming to the specified constraints. Subsequently, the local reference path fitting function and the reference longitudinal acceleration are transmitted to the tracking layer. In this layer, the cost function is defined as follows:

$$J_{up} = \sum_{i=1}^{N_{p,up}} \|\eta_{up}(t + i|t) - \eta_{ref,global}(t + i|t)\|_{Q_{up}}^2 + \sum_{i=1}^{N_{c,1}} \|U_i(t + i|t)\|_{R_{up}}^2 + J_{ob} \quad (13)$$

where  $\eta_{up}(t + i|t) = Y(t + i|t)$  is the output vector.  $\eta_{ref,global}(t + i|t)$ , with  $i = 1, \dots, N_{p,up}$ , is the initial trajectory reference, for the output tracking variable.  $U_i = [a_x \ a_y]^T$  is control vector.  $N_{p,up}$ ,  $N_{c,up}$  are the prediction horizon in replanning layer and the control horizon in re-planning layer, respectively.  $Q_{up} \in \mathbb{R}^{p_{y,up} \times p_{y,up}}$ ,  $R_{up} \in \mathbb{R}^{m_{up} \times m_{up}}$  are weighting matrices.  $J_{ob} = J_{Parking} + J_{road} + J_{onc}$  is the total cost of obstacles avoidance. The above-mentioned variables and constraints will be elucidated in comprehensive detail in the subsequent subsections. Within this function, the initial term serves to minimize lateral deviation and heading deviation of the ego vehicle concerning the reference trajectory. The second element stipulates that the ego vehicle should maintain its speed as consistently as possible, thereby ensuring a comfortable ride.

In this layer, the vehicle is treated as a point with a given mass  $m$ , i.e., no orientation is defined and the yaw dynamics is neglected[57], shown as Figure 2.8.

The state of motion and the state of force can be expressed as:

$$\dot{X} = \dot{x}\cos\varphi - \dot{y}\sin\varphi \quad (14)$$

$$\dot{Y} = \dot{x}\sin\varphi + \dot{y}\cos\varphi \quad (15)$$

$$ma_y = F_y \quad (16)$$

$$ma_x = F_x - F_d \quad (17)$$

where subscript  $[x, y]$  is the [longitudinal, lateral] axle in the ego vehicle body frame.  $[X, Y]$  are the Cartesian coordinates that belong to the world axis frame.  $F_x, F_y$  are the resultant force in longitudinal and lateral axes in the ego vehicle body frame, respectively.  $F_d = ma_d$  represents the resultant force of resistance in the longitudinal axle.

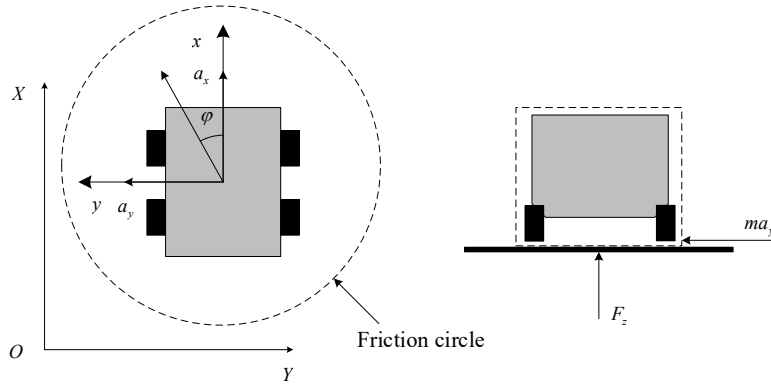


Figure 2.8 Point mass vehicle model for trajectory re-planning layer

The maximum tire forces should be constrained by the maximum adhesion provided by ground. In particular, for a given friction coefficient  $\mu$  and the tire normal force  $F_z$ , the lateral and longitudinal forces are constrained as follows:

$$F_x^2 + F_y^2 \leq (\mu F_z)^2 \quad (18)$$

Therefore the vehicle dynamics described by the Equations (14)-(17) can be rewritten in the following compact form:

$$\begin{aligned} \dot{\kappa}(t) &= f^{pm}(\kappa(t), u(t)) \\ s. t. \quad &u_{min} \leq u(t) \leq u_{max} \\ &a_x^2 + a_y^2 \leq (\mu g)^2 \end{aligned} \quad (19)$$

where the state vector is  $\kappa = [\dot{y} \ \dot{x} \ \varphi \ Y \ X]^T$  and the input vector is  $u = [a_x \ a_y]^T$ .

Given that the point-mass vehicle model overlooks body size information, it becomes necessary to extend the representation of obstacles. Simultaneously, the obstacles should be divided into segments at a specific resolution to avoid situations where vehicles could pass through the obstacle when it is too large, shown as Figure 2.9.

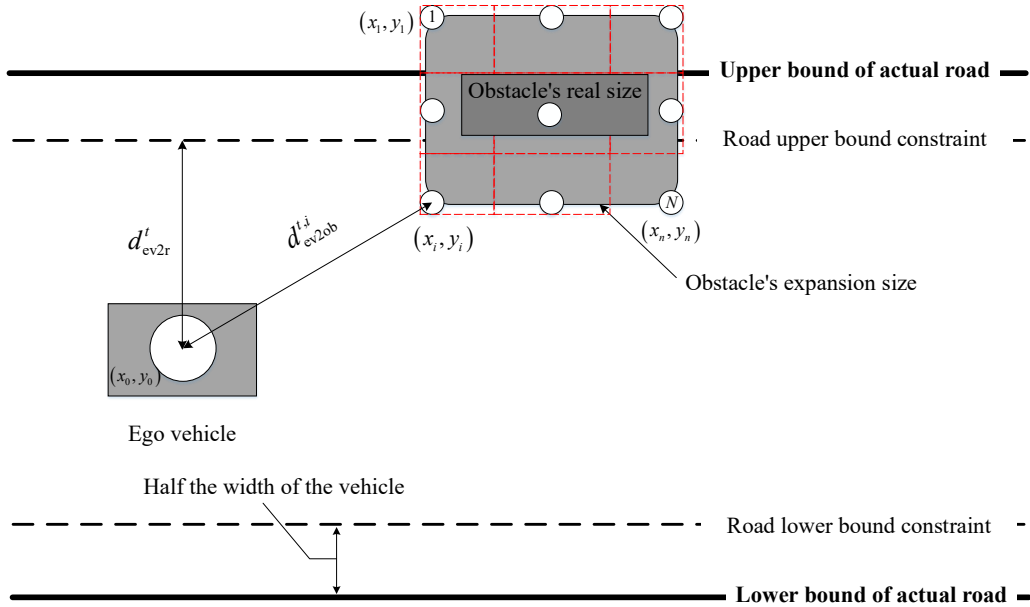


Figure 2.9 Obstacle expansion

The processing principles for road boundaries and parked vehicles are as follows:

- (1) The actual road boundary is preprocessed based on the width of the ego vehicle.

(2) The parked vehicle is broken down into multiple discrete smaller obstacles.

(3) The cost function is modified in consideration of the vehicle's speed and the distance deviation between the obstacle points and the vehicle.

The cost function of the distance between the ego vehicle and parked vehicle is established as:

$$J_{\text{Parking}} = \sum_{i=1}^{N_{p,\text{up}}} \sum_{n=1}^{n_{\text{parking}}} \frac{W_1}{(X_i - X_{0,i})^2 + (Y_i - Y_{0,i})^2 + \zeta_1} \quad (20)$$

where  $W_1$  is the weight coefficient.  $\zeta_1$  is a small positive number that prevents the denominator from being zero.  $n_{\text{parking}}$  is total number of copies after the parked vehicle is segmented.  $X_{0,i}$  is the predictive position of the ego vehicle at step  $i$ .

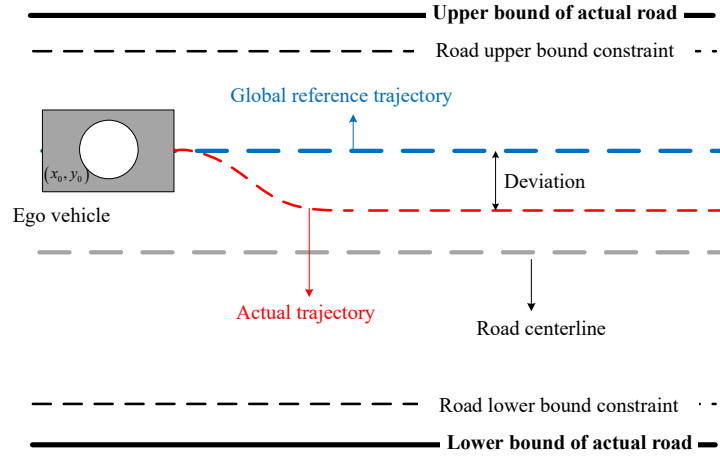


Figure 2.10 Cost caused by road bounds

Furthermore, we take into account that the road is partitioned into two opposing lanes, and the global reference path lies within one of them, as illustrated in Figure 2.10. Consequently, to minimize the deviation between the actual trajectory and the reference trajectory, the cost function for the road segment is modified based on the relative position between the ego vehicle and the road boundaries.

$$J_{\text{road}} = \begin{cases} 0, & D_{\text{ev2Road},i} \geq D_{\min}; \\ \sum_{i=1}^{N_{p,\text{up}}} \frac{W_2}{D_{\text{ev2Road},i} + \zeta_2}, & D_{\text{ev2Road},i} < D_{\min} \end{cases} \quad (21)$$

where  $W_2$  is the weight coefficient.  $\zeta_2$  is a small positive number that prevents the denominator from being zero.  $D_{\min}$  is the allowable minimum distance between the ego vehicle and the road bounds.  $D_{\text{ev2Road},i}$  is defined as:

$$D_{\text{ev2Road},i} = \begin{cases} |Y_{\text{ev},i} - R_{\text{ub}}|, Y_{\text{ev}} - R_{\text{ub}} \leq Y_{\text{ev}} - R_{\text{lb}}; \\ |Y_{\text{ev},i} - R_{\text{lb}}|, Y_{\text{ev}} - R_{\text{ub}} \geq Y_{\text{ev}} - R_{\text{lb}} \end{cases} \quad (22)$$

where  $Y_{\text{ev}}$  is the longitudinal coordinate of the ego vehicle in world axis frame.  $R_{[\text{ub},\text{lb}]}$  is the [upper, lower] bound constraint of the road.

Analogous to the case of a parked vehicle and considering the position prediction of the oncoming vehicle, the cost function for the oncoming vehicle segment is defined as follows:

$$J_{\text{OnC}} = \sum_{i=1}^{N_{p,\text{up}}} \sum_{n=1}^{n_{\text{OnC}}} \frac{W_3}{D_{\text{ev2OnC}}|_{n,T=i+\zeta_3}} \quad (23)$$

where  $W_3$  is the weight coefficient.  $\zeta_3$  is a small positive number that prevents the denominator from being zero.  $n_{\text{onc}}$  is total number of copies after the oncoming vehicle is segmented.  $D_{\text{ev2onc}}|_{n,T=i}$  is defined as:

$$D_{\text{ev2OnC}}|_{n,T=i} = (X_{n,i} - X_{0,i})^2 + (Y_{n,i} - Y_{0,i})^2 \quad (24)$$

where  $X_{n,i}$  is the predictive position of oncoming vehicle's  $n$ -th block after being segmented at step  $i$ .

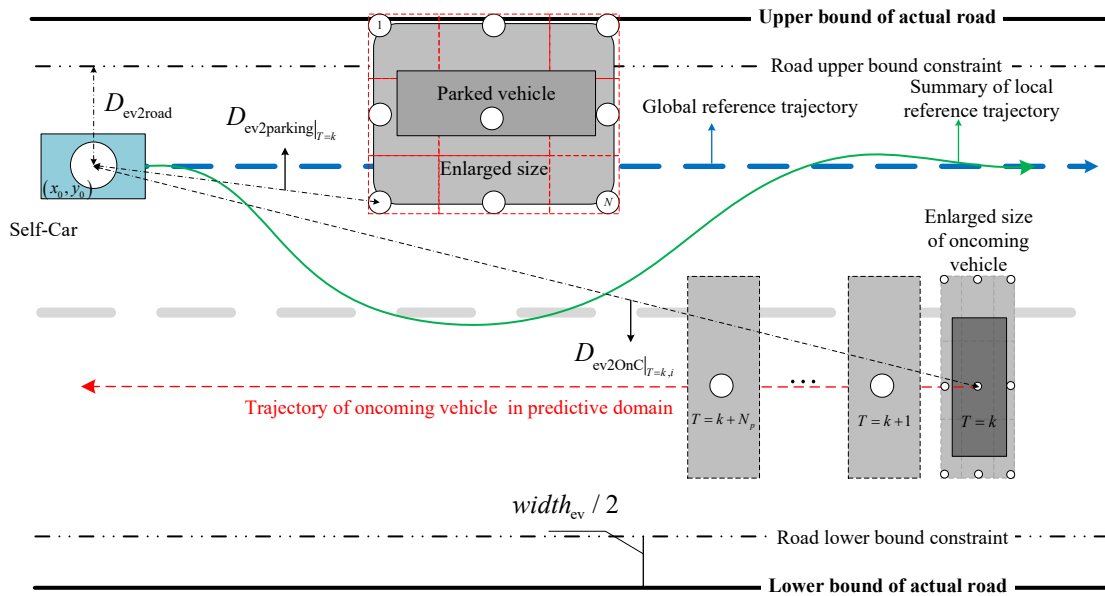


**Figure 2.11 The whole process of generating local reference trajectory**

When merging the road, parked vehicle and the oncoming vehicle, as depicted in Figure 2.11, this section address the following optimization problem at each time step:

$$\begin{aligned}
& \min_{U_t} J_{up}(\kappa(t), u(t)) \\
& s. t. \quad u_{min} \leq u(t) \leq u_{max} \\
& \quad \quad a_x^2 + a_y^2 \leq (\mu g)^2
\end{aligned} \tag{25}$$

With the non-linear problem solver, the solution  $U_t^* = [u_{t,t}^*, \dots, u_{t+N_{c,2},t}^*]^T$  is obtained. Then, with the  $u_{t,t}^* = [a_{x,t}^* \ a_{y,t}^*]^T$ , the predictive state of the ego vehicle from the time  $t$ , that is  $[X_{0,t+i|t} \ Y_{0,t+i|t} \ \varphi_{0,t+i|t}]$  with  $i = 1, \dots, N_{p,up}$ , is obtained by Equations (14)-(17).

### 2.3.5 Polynomial Fitting

The re-planned path is represented by discrete points within the prediction time domain. Directly inputting these points into the tracking layer would significantly occupy input interfaces. Additionally, as the prediction horizon changes, the number of points also varies, which complicates the standardized design of the controller. Furthermore, the control period of the re-planning layer differs from that of the tracking layer, making it challenging for the tracking layer's controller to follow discrete reference trajectory points [58].

To mitigate computational demands, ensure continuity in position change, yaw angle change, and acceleration change, and minimize disturbances, a fifth-order polynomial is employed as the fitting curve.

$$\begin{aligned}
Y_{ref} &= a_0 t^5 + a_1 t^4 + a_2 t^3 + a_3 t^2 + a_4 t + a_5 \\
\varphi_{ref} &= b_0 t^5 + b_1 t^4 + b_2 t^3 + b_3 t^2 + b_4 t + b_5
\end{aligned} \tag{26}$$

The output of the re-planning layer are coefficients of the fifth-order polynomial,  $a_{up} = [a_0 \ a_1 \ a_2 \ a_3 \ a_4 \ a_5]$  and  $b_{up} = [b_0 \ b_1 \ b_2 \ b_3 \ b_4 \ b_5]$ , and the reference longitudinal acceleration  $a_{x,ref}$ .

### 2.3.6 Lower-Layer MPC-based trajectory tracking

The objective of the MPC controller in this layer is to track the local reference trajectory re-planned by the MPC controller in the trajectory re-planning layer. Much like the re-planning layer, the cost function is defined as follows:

$$\begin{aligned}
& \min_{\Delta U_t, \varepsilon} J_{low}(\xi(t), u(t-1), \Delta U(t), \varepsilon) = \\
& \sum_{i=1}^{N_{p,low}} \|\eta_{low}(t+i|t) - \eta_{ref,local}(t+i|t)\|_{Q_{low}}^2 \\
& \quad + \sum_{i=1}^{N_{c,low}-1} \|\Delta U(t+i-1|t)\|_{R_{low}}^2 + \rho \varepsilon^2
\end{aligned} \tag{27}$$

where  $\eta_{ref,local}(t + i|t)$ , with  $i = 1, \dots, N_{p,low}$ , is the reference, which is generated by re-planning layer, for the output tracking variable.  $U = \delta_f$  is control vector.  $Q_{low} \in \mathbb{R}^{p_{y,low} \times p_{y,low}}$ ,  $R_{low} \in \mathbb{R}^{m_{low} \times m_{low}}$  are weighting matrices.  $\varepsilon$  is a slack variable. A comprehensive explanation of the aforementioned variables and constraints will be provided in the following sections. In this cost function, the initial term serves to minimize the lateral deviation and heading deviation of the ego vehicle concerning the reference trajectory. The subsequent element ensures a smooth change in the control inputs.

Given the focus of this study on low-to-medium-speed urban conditions without emergencies, and considering the two-layer MPC structure, this layer employs a bicycle model (as shown in Figure 2.12), which offers computational advantages.

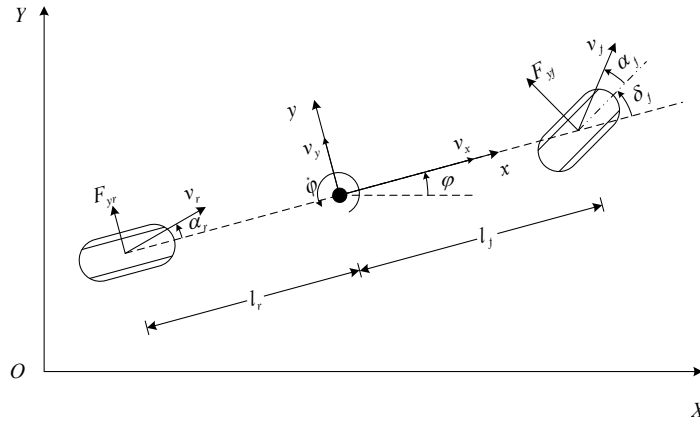


Figure 2.12 Bicycle model for trajectory tracking layer

In this particular scenario, the vehicle tires function within the linear region when subjected to small lateral acceleration. As a result, the calculation of vehicle lateral forces is based on the straightforward linear tire model, which employs the equivalent tire cornering stiffness  $\bar{C}_{\alpha f}$  and  $\bar{C}_{\alpha r}$ :

$$F_{yf} = \bar{C}_{\alpha f} \alpha_f \quad (28)$$

$$F_{yr} = \bar{C}_{\alpha r} \alpha_r \quad (29)$$

where  $\alpha_f, \alpha_r$  denote slip angles of the front and rear axle, respectively. Moreover, due to the small tire deflection, the tire slip angles,  $\alpha_f, \alpha_r$ , can be expressed as:

$$\alpha_f = \arctan\left(\frac{v_y + l_f \dot{\phi}}{v_x}\right) - \delta_f \approx \frac{v_y + l_f \dot{\phi}}{v_x} - \delta_f \quad (30)$$

$$\alpha_r = \arctan\left(\frac{v_y - l_r r}{v_x}\right) \approx \frac{v_y - l_r \dot{\varphi}}{v_x} \quad (31)$$

where  $v$  is the velocity.  $r$  is the yaw rate.  $l_f$  and  $l_r$  are the distances from the center of gravity to the front and rear axles, respectively.  $\varphi$  and  $\delta_f$  are the yaw angle and the front wheel steering angle, respectively.

Hence, leveraging the small deflection angle of the front wheels and the linear tire model, the vehicle dynamics can be described through the following mathematical equations:

$$m\dot{v}_y = -mv_x\dot{\varphi} + 2\left[\bar{C}_{\alpha f}\left(\delta_f - \frac{v_y + l_f\dot{\varphi}}{v_x}\right) + \bar{C}_{\alpha r}\frac{l_r\dot{\varphi} - v_y}{v_x}\right] \quad (32)$$

$$m\dot{v}_x = mv_y\dot{\varphi} + 2\left[C_{lf}s_f + \bar{C}_{\alpha f}\left(\delta_f - \frac{v_y + l_f\dot{\varphi}}{v_x}\right)\delta_f + C_{lr}s_r\right] \quad (33)$$

$$I_{zz}\ddot{\varphi} = 2\left[l_f\bar{C}_{\alpha f}\left(\delta_f - \frac{v_y + l_f\dot{\varphi}}{v_x}\right) - l_r\bar{C}_{\alpha r}\frac{l_r\dot{\varphi} - v_y}{v_x}\right] \quad (34)$$

$$\dot{\varphi} = r \quad (35)$$

$$\dot{Y} = v_x \sin\varphi + v_y \cos\varphi \quad (36)$$

$$\dot{X} = v_x \cos\varphi - v_y \sin\varphi \quad (37)$$

where  $m$  is the vehicle mass. The yaw moment of inertia and vehicle mass are represented by  $m$  and  $I_{zz}$ .  $s_{[f,r]}$  is the slip rate of [front, rear] tire.  $\bar{C}_{\alpha[f,r]}$  is the longitudinal stiffness of [front, rear] tire. The state vector is  $\xi = [\dot{y} \ \dot{x} \ \varphi \ \dot{\varphi} \ Y \ X]^T$  and the input vector is  $u = \delta_f$ . And we define that  $-10^\circ \leq \delta_f \leq 10^\circ$ ,  $-0.85 \leq \Delta\delta_f \leq 0.85$ .

The vehicle nonlinear dynamic model is:

$$\dot{\xi} = f(\xi, u) \quad (38)$$

To establish an MPC problem, the bicycle model is first linearized using Taylor series expansion at the reference point and subsequently discretized using the Forward-Euler method as follows:

$$\xi(k+1) = A_k \xi(k) + B_k u(k) + d(k) \quad (39)$$

$$\eta_{\text{low}}(k) = C_k \xi(k) \quad (40)$$

where  $A_k = I + A_t$ ,  $B_k = T_s B_t$  and  $d(k) = \xi_{ref}(k+1) - A_k \xi_{ref}(k) - B_k u(k)$ .  $A_t = \left.\frac{\partial f}{\partial \xi}\right|_{\xi_t, u_t}$ ,  $B_t = \left.\frac{\partial f}{\partial u}\right|_{\xi_t, u_t}$ .  $T_{s,2} = 0.01$  s is the simulation step.  $\eta_{\text{low}}(k) = [\varphi \ Y]^T$  is the output vector and  $C_k$  is an output selection matrix.

To facilitate the introduction of the control input increment  $\Delta U$  and simplify calculations, the state space is reconstructed as follows:

$$\tilde{\xi}(k) = \begin{bmatrix} \xi(k) \\ u(k-1) \end{bmatrix} \quad (41)$$

$$\tilde{\eta}_2(k) = \tilde{C}_k \tilde{\xi}(k) \quad (42)$$

The predictive state is defined as:

$$\tilde{\xi}(k+1) = \tilde{A}_k \tilde{\xi}(k) + \tilde{B}_k \Delta u(k) + \tilde{d}(k) \quad (43)$$

where  $\tilde{A}_k = \begin{bmatrix} A_k & B_k \\ 0_{m \times n} & I_m \end{bmatrix}$ ;  $\tilde{B}_k = \begin{bmatrix} B_k \\ I_m \end{bmatrix}$ ;  $\tilde{C}_k = [C_k \ 0]$ ;  $\tilde{d}(k) = \begin{bmatrix} d(k) \\ 0_m \end{bmatrix}$ ;  $\Delta u(k) = u(k) - u(k-1)$   $m$

is the dimension of control amount while  $n$  is the dimension of state amounts.

Therefore, the final output expression can be expressed as:

$$\gamma(k+1) = \psi \xi(k) + \theta \Delta u(k) + \Gamma \Phi(k) \quad (44)$$

where

$$\gamma(k+1) = \begin{bmatrix} \eta_{\text{low}}(k+1) \\ \vdots \\ \eta_{\text{low}}(k+N_{c,\text{low}}) \\ \vdots \\ \eta_{\text{low}}(k+N_{p,\text{low}}) \end{bmatrix}, \psi = \begin{bmatrix} \tilde{C}_k \tilde{A}_k \\ \vdots \\ \tilde{C}_k \tilde{A}_k^{N_{c,\text{low}}} \\ \vdots \\ \tilde{C}_k \tilde{A}_k^{N_{p,\text{low}}} \end{bmatrix}, \quad (45)$$

$$\Delta U(k) = \begin{bmatrix} \Delta u(k) \\ \Delta u(k+1) \\ \vdots \\ \Delta u(k+N_{c,\text{low}}-1) \end{bmatrix} \quad (46)$$

$$\theta = \begin{bmatrix} \tilde{C}_k \tilde{B}_k & 0 & 0 & 0 \\ \vdots & \vdots & \vdots & \vdots \\ \tilde{C}_k \tilde{A}_k^{N_{c,\text{low}}-1} \tilde{B}_k & \tilde{C}_k \tilde{A}_k^{N_{c,\text{low}}-2} \tilde{B}_k & \cdots & \tilde{C}_k \tilde{B}_k \\ \vdots & \vdots & \ddots & \vdots \\ \tilde{C}_k \tilde{A}_k^{N_{p,\text{low}}-1} \tilde{B}_k & \tilde{C}_k \tilde{A}_k^{N_{p,\text{low}}-2} \tilde{B}_k & \cdots & \tilde{C}_k \tilde{A}_k^{N_{p,\text{low}}-N_{c,\text{low}}} \tilde{B}_k \end{bmatrix} \quad (47)$$

$$\Gamma = \begin{bmatrix} \tilde{C}_k & \cdots & 0 \\ \vdots & \ddots & \vdots \\ \tilde{C}_k \tilde{A}_k^{N_{p,\text{low}}-1} & \cdots & C \end{bmatrix}, \quad (48)$$

$$\Phi(k) = \begin{bmatrix} \tilde{d}(k) \\ \vdots \\ \tilde{d}(k+N_{p,\text{low}}-1) \end{bmatrix} \quad (49)$$

and  $N_{p,\text{low}}$ ,  $N_{c,\text{low}}$  are the prediction horizon in tracking layer and the control horizon in tracking layer, respectively. At each time step we solve the following optimization problem:

$$\begin{aligned} & \min_{\Delta U_t, \varepsilon} J_{\text{low}}(\xi(t), u(t), \Delta U(t), \varepsilon) \\ & s. t. \quad \Delta U_{\min} \leq \Delta U_t \leq \Delta U_{\max} \\ & \quad U_{\min} \leq A \Delta U_t + U_t \leq U_{\max} \\ & \quad y_{hc,\min} \leq y_{hc} \leq y_{hc,\max} \\ & \quad y_{sc,\min} - \varepsilon \leq y_{sc} \leq y_{sc,\max} + \varepsilon \\ & \quad \varepsilon > 0 \end{aligned} \quad (50)$$

where  $y_{hc,[min,max]}$  is the [upper, lower] bound on output variables to be hard constrained;  $y_{sc,[min,max]}$  is the [upper, lower] bound on output variables to be soft constrained. As it is a convex optimization problem, the function can be reconstructed as a standard quadratic form:

$$J_{low}(\xi(t), u(t-1), \Delta U(t), \varepsilon) = [\Delta U(t)^T, \varepsilon]^T H_t [\Delta U(t)^T, \varepsilon] + G_t [\Delta U(t)^T, \varepsilon] + P_t \quad (51)$$

where  $H = \begin{pmatrix} \theta^T Q_e \theta + R_e & 0 \\ 0 & \rho \end{pmatrix}$ ,  $G_t = [2E^T Q_e \theta \quad 0]$ ,  $P_t = E^T Q_e E$  and  $E$  is defined as a tracking error between the free response of the linearized system and the reference trajectory, i.e.,  $E = \gamma_{ref} - \psi \xi(t) - \Gamma \Phi(t)$  with  $\gamma_{ref} = [\eta_{ref,local}(t+1|t), \dots, \eta_{ref,local}(t+N_p|t)]^T$ . The matrices  $Q_e$  and  $R_e$  are block diagonal matrices of appropriate dimensions with  $Q$  and  $R$  on the main diagonal, respectively.

With QP problem solver, the solution  $U_t^* = [\Delta u_{t,t}^*, \dots, \Delta u_{t+N_{c,1}-1,t}^*]^T$  at time  $t$  for the current state  $\xi(t)$  and the previous input  $u(t-1)$  are obtained. The resulting feedback control law is given by:

$$u(t, \xi(t)) = u(t-1) + \Delta u_{t,t}^*(\xi(t)) \quad (52)$$

At time  $t+1$  the optimization problem is formulated and solved over a shifted horizon. Controller parameters and weights are shown as Table 2-1.

In Table 2-1,  $I_*$  is an identity matrix of dimension \*.  $k_1 = k_3 = 3$  and  $k_2 = 1$  are the weights of speed.  $W_1$ ,  $W_2$  and  $W_3$  are the weight coefficients of avoiding the parked vehicle, road bounds and the oncoming vehicle, respectively. They depend on the vehicle's velocity to ensure driving safety and lateral stability. Consequently, the cost of collision avoidance will rise with the vehicle's speed, particularly in relatively high-speed conditions.

Table 2-1 Parameters of MPC

MPC parameters in motion re-planning layer		
Symbol	Value	Unit
$N_{p,up}$	60	(none)
$N_{c,up}$	2	(none)
$Q_{up}$	$100 \times I_{N_{p,up}}$	(none)

$R_{up}$	$10 \times I_{N_{c,up}}$	(none)
$T_{s,up}$	0.02	s
$W_1$	$900 + k_1 \times v_a$	(none)
$W_2$	$2000 + k_2 \times v_a$	(none)
$W_3$	$900 + k_3 \times (v_a + v_{onc})$	(none)
<b>MPC parameters in the motion tracking layer</b>		
Symbol	Value	Unit
$N_{p,low}$	30	(none)
$N_{c,low}$	3	(none)
$Q_{low}$	$\begin{bmatrix} 2000 & 0 \\ 0 & 10,000 \end{bmatrix}$	(none)
$R_{low}$	$5 \times 10^5 \times I_{N_{c,low}}$	(none)
$\rho$	1000	(none)
$T_{s,low}$	0.01	s

### 2.3.7 Simulation results

To assess the effectiveness of the obstacle avoidance strategy based on PET and a two-layer MPC approach, a co-simulation is conducted using CarSim and MATLAB. The simulation employs a front-wheel-drive C-class hatchback model from CarSim software, with a sample time of 0.01 seconds. Three distinct scenarios are considered, each based on different PET values as established in Section 2, and are discussed in this section.

To generate varying PET values, it is assumed that the distance between the ego vehicle and the parked vehicle remains constant, while the initial position of the oncoming vehicle is adjusted. Concurrently, the initial speed of the ego vehicle is set at 11 m/s for all three simulations.

In the case of uniform speed, the computed  $PET_{s2}$  is greater than the predefined  $PET_{safe}$  threshold. Consequently, the ego vehicle maintains its initial speed throughout the entire avoidance process. Figure 2.13 depict the acceleration, steering wheel angle, and vehicle longitudinal speed for case 1.

## Active Collision Avoidance strategy

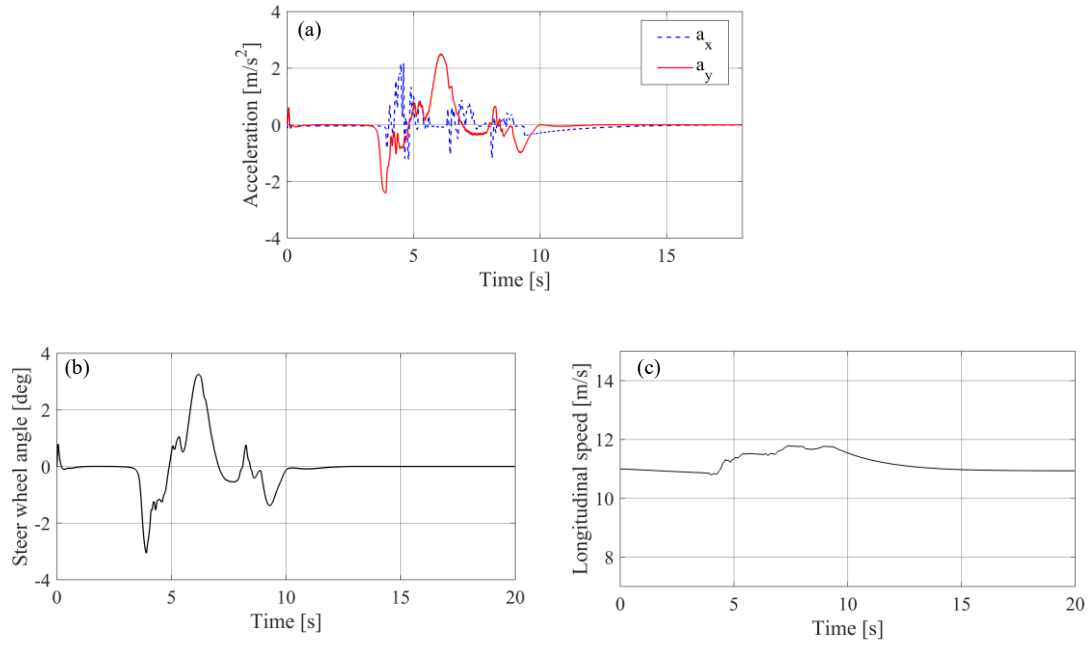


**Figure 2.13(a) Longitudinal and lateral acceleration, (b) Steer wheel angle and (c) longitudinal speed of ego vehicle in uniform speed case (ego car just keeps speed unchanged when overtaking obstacles)**

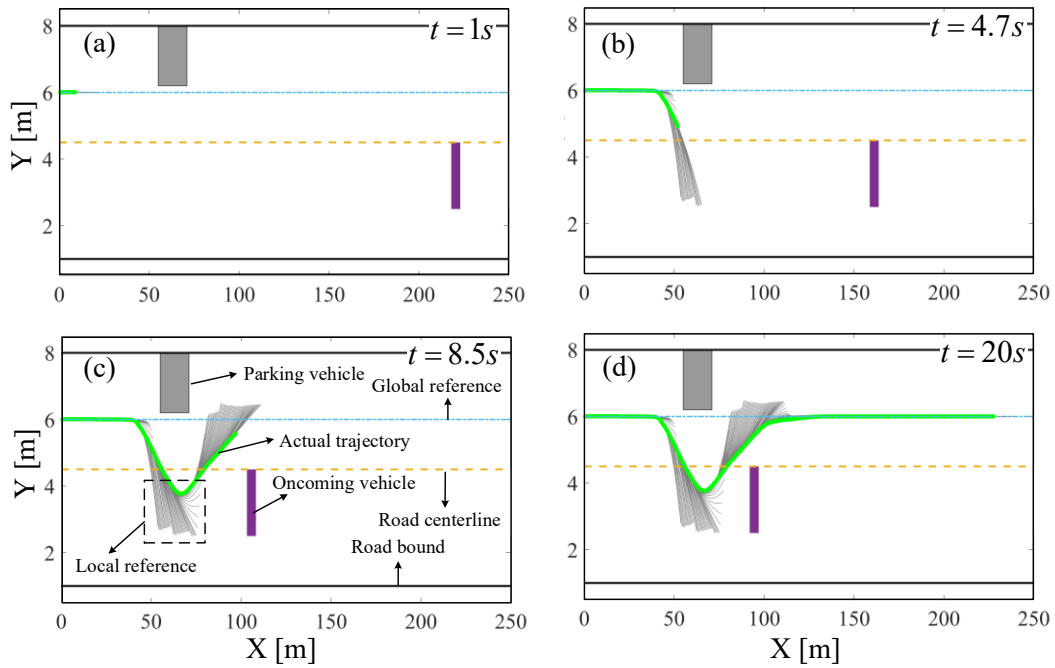


**Figure 2.14 Collision avoidance process of ego vehicle under case 1. (a) Relative positions between vehicles at  $t=1s$ ; (b) Relative positions between vehicles at  $t=4.7s$ ; (c) Relative positions between vehicles at  $t=8.5s$ ; (d) Relative positions between vehicles at  $t=20s$**

Figure 2.14 illustrates the Collision Avoidance (CA) process of the ego vehicle in the case of uniform speed. The CA process is simulated using Simulink/MATLAB, and various elements within the CA process, such as the parked vehicle, the oncoming vehicle, and the re-planned local reference, are annotated in Figure 2.14 (c). The local reference path, displayed as a short gray curve alongside the actual trajectory (green curve), is generated by the upper-layer MPC controller in the trajectory re-planning layer (as referenced in Figure 2.7) for this time step, signifying the reference trajectory for the subsequent time step.

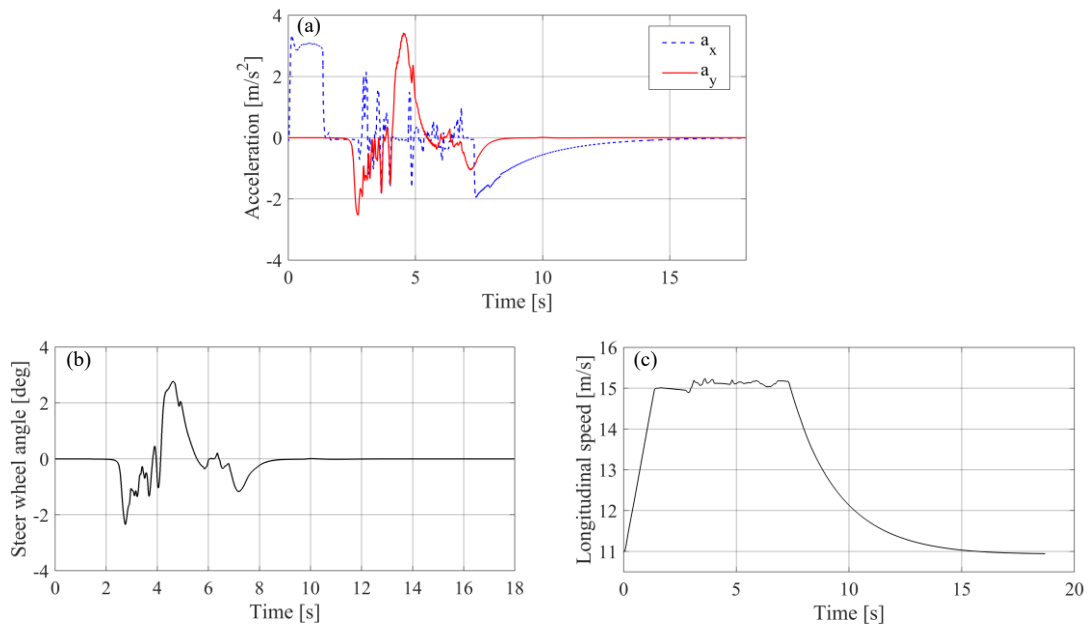
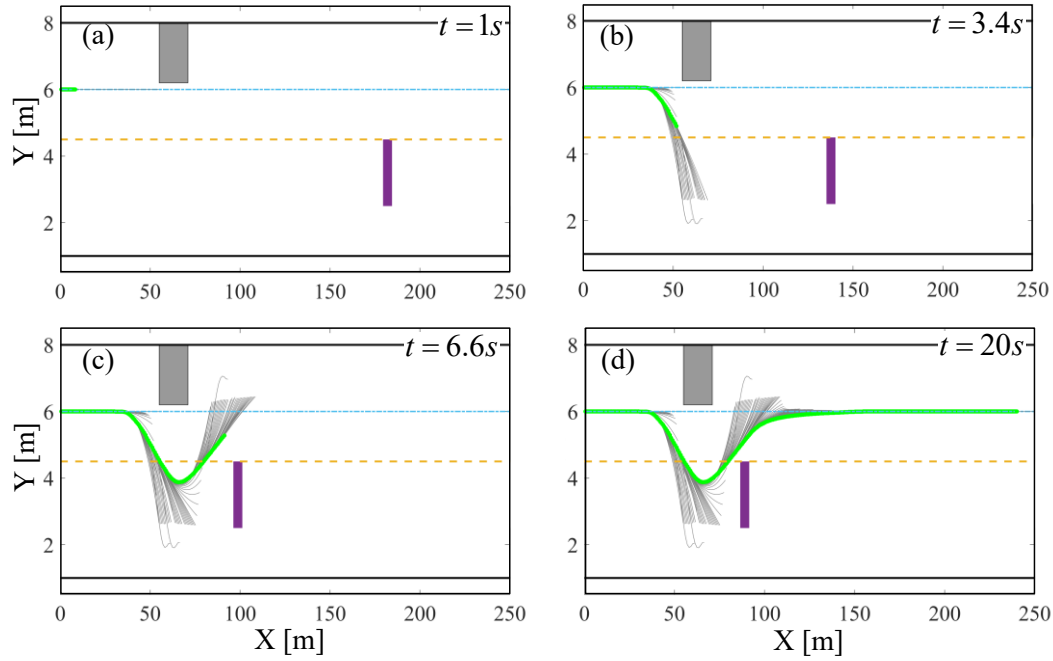


**Figure 2.15 (a) Longitudinal and lateral acceleration, (b) Steer wheel angle and (c) longitudinal speed of ego vehicle in acceleration case (ego car needs to accelerate for a safe overtaking)**

In the case of acceleration, the computed  $PET_{s2}$  is smaller than  $PET_{safe}$ , while  $PET_{s1}$  is greater than  $PET_{safe}$ . Consequently, the ego vehicle is required to accelerate. Figure 2.15 depict the acceleration, steering wheel angle, and vehicle longitudinal speed for the acceleration case.

Figure 2.16 presents the Collision Avoidance (CA) process of the ego vehicle in the case of acceleration. When there is a potential collision risk during the CA process if the ego vehicle maintains its speed, but this risk can be mitigated by accelerating the ego vehicle to the permissible maximum speed, the ego vehicle is mandated to accelerate. While deceleration and waiting for the oncoming

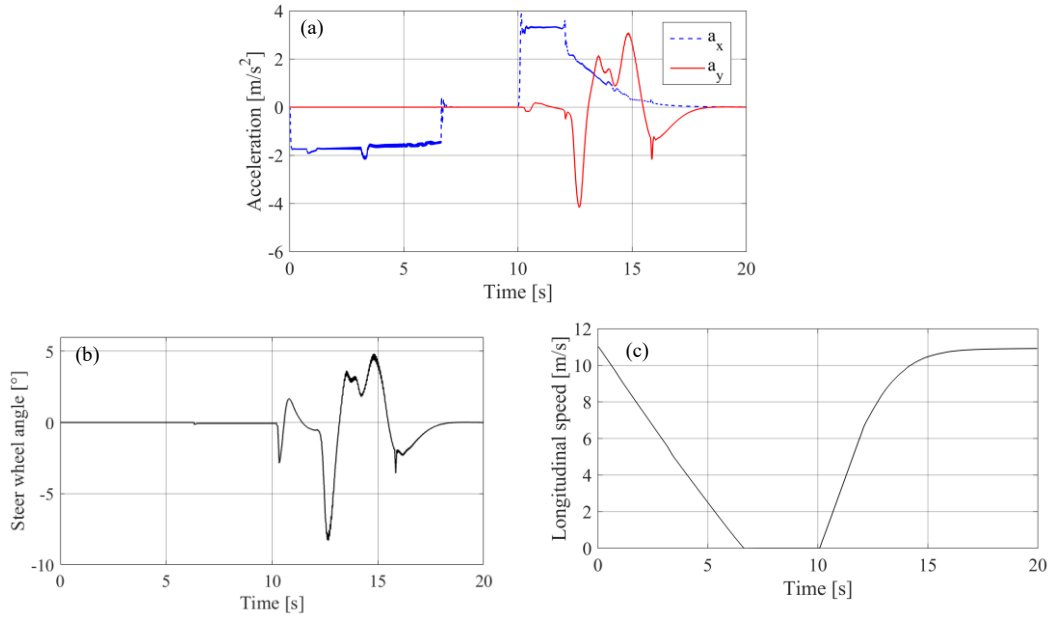
vehicle to pass the parked vehicle is an alternative option for the ego vehicle, the choice of acceleration is deemed optimal, considering factors such as time efficiency and convenience, all while ensuring safety.



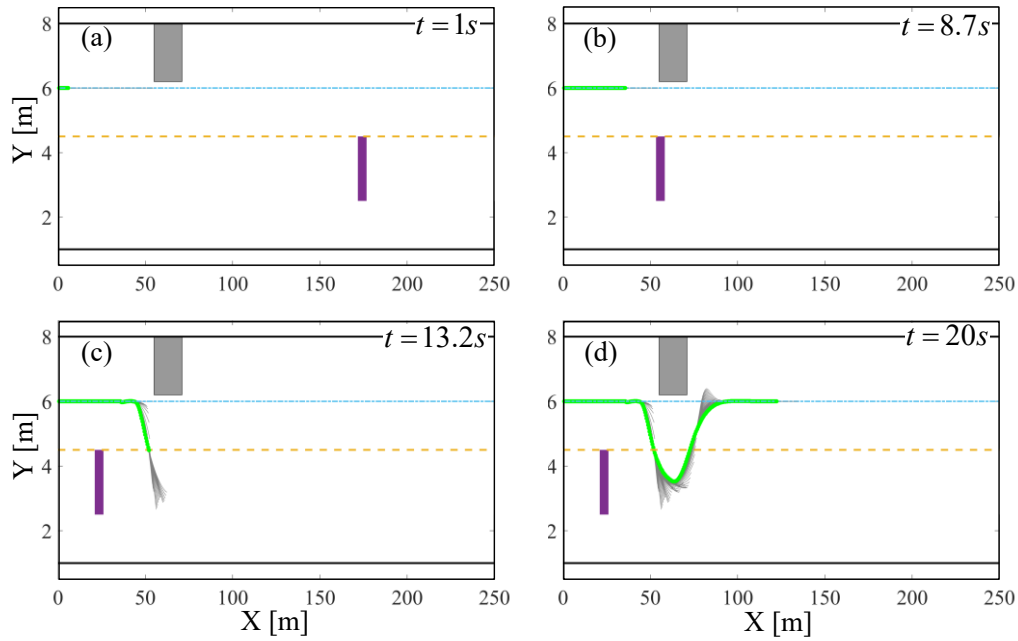
**Figure 2.16 Collision avoidance process of ego vehicle under case 2. (a) Relative positions between vehicles at  $t=1s$ ; (b) Relative positions between vehicles at  $t=3.4s$ ; (c) Relative positions between vehicles at  $t=6.6s$ ; (d) Relative positions between vehicles at  $t=20s$ .**

In the case of deceleration, the computed PET is smaller than  $PET_{safe}$ , necessitating the ego vehicle to decelerate. Figure 2.17 depict the acceleration, steering wheel angle, and vehicle longitudinal speed for the deceleration case.

Figure 2.18 illustrates the Collision Avoidance (CA) process of the ego vehicle in the deceleration case. When the calculation reveals that it is unsafe to maintain uniform speed or accelerate to avoid both the parked vehicle and the oncoming vehicle simultaneously, the ego vehicle is instructed to decelerate. This allows the ego vehicle to wait for the oncoming vehicle to pass the parked vehicle first, as indicated Figure 2.18(c). After the oncoming vehicle has passed, the ego vehicle then restarts and continues the CA process.



**Figure 2.17 (a) Longitudinal and lateral acceleration, (b) Steer wheel angle and (c) longitudinal speed of ego vehicle in deceleration (ego car needs to decelerate for a safe overtaking)**



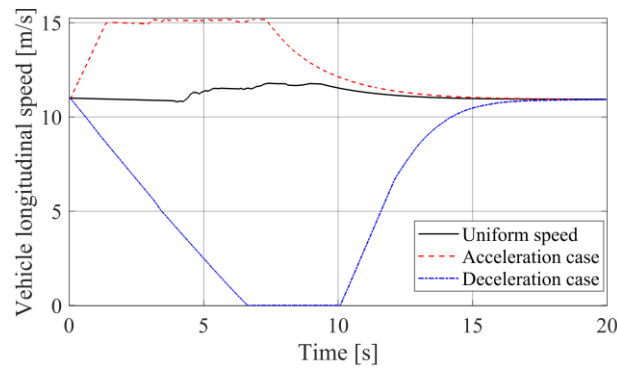
**Figure 2.18 Collision avoidance process of ego vehicle under case 3. (a) Relative positions between vehicles at  $t=1s$ ; (b) Relative positions between vehicles at  $t=8.7s$ ; (c) Relative positions between vehicles at  $t=13.2s$ ; (d) Relative positions between vehicles at  $t=20s$ .**

Figure 2.13(a), Figure 2.15(a), Figure 2.17(a) depict the acceleration the vehicle throughout the

entire obstacle avoidance process. Figure 2.13(c), Figure 2.15(c), Figure 2.17(c) illustrate the velocity of the vehicle during the entire obstacle avoidance process, respectively. The choice of the vehicle's behavior is determined by the specific *PET* value, as reflected in the acceleration and velocity plots.

As observed in Figure 2.13(b), Figure 2.15(b) and Figure 2.17(b), given the low-speed urban conditions, the vehicle's front wheel steering angle remains relatively small in all three different cases. When the ego vehicle initiates a turn, the steering wheel angle also exhibits minor fluctuations, with the maximum steering wheel angle reaching approximately  $8^\circ$ .

The comparison of the longitudinal speed under three cases is shown in Figure 2.19.



**Figure 2.19 Speed comparison under different cases**

Examining Figure 2.19, a comparison of vehicle speeds in the three different cases is presented. In the uniform speed case, the vehicle's velocity remains at approximately 11 m/s, with minor fluctuations, aligning with the requirement to maintain the speed as a reference whenever circumstances permit.

In the acceleration case, the vehicle opts to accelerate for obstacle avoidance, effectively reducing the time spent while ensuring safety. Both the vehicle's speed and acceleration fall within the predefined boundaries. Once the obstacles are successfully cleared, the vehicle decelerates back to the reference speed.

Conversely, in the deceleration case, the vehicle cannot safely avoid obstacles even with maximum allowable acceleration. Therefore, the ego vehicle initiates deceleration until the oncoming vehicle has passed. Subsequently, the ego vehicle resumes its movement and successfully navigates around the parked vehicle. In all three cases, the ego vehicle's final speeds are adjusted to return to the reference speed after completing the obstacle avoidance maneuvers.

Simultaneously, a time history of TTC between the ego vehicle and the oncoming vehicle is established, as illustrated in Figure 2.20. As both vehicles are moving toward each other, the TTC eventually reaches zero. A smaller initial TTC implies a higher safety risk during the CA process. If the ego vehicle can safely avert a collision through acceleration, deceleration becomes unnecessary. This approach ensures the prompt passage of the ego vehicle, preventing congestion and saving passengers' time.

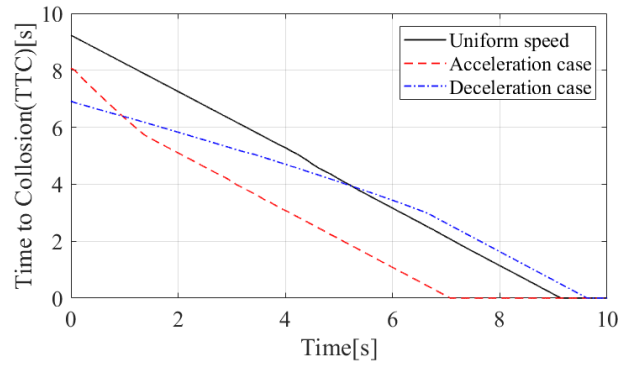


**Figure 2.20 The time history of the time-to-collision between ego vehicle and the oncoming vehicle under different cases.**

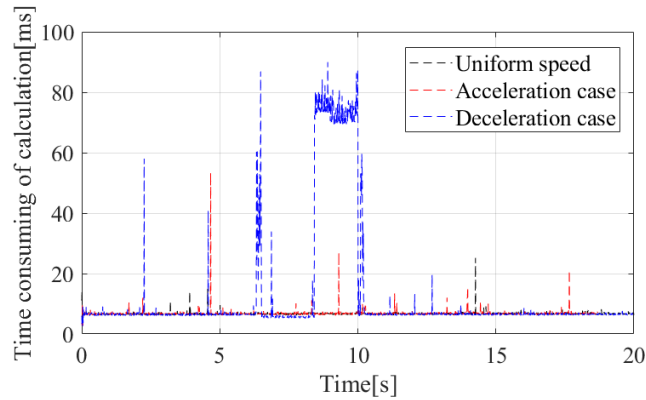


**Figure 2.21 Time consuming of simulation calculation under different cases**

The time consumption of the simulation calculations serves as an effective indicator to assess the real-time performance of the proposed algorithm. As depicted in Figure 2.21, in the uniform speed case and the acceleration case where the ego vehicle is not required to decelerate, the calculation time typically hovers around 8 milliseconds with minor fluctuations. Although some simulation calculations

in the acceleration case exhibit relatively longer durations, they do not exceed 100 milliseconds. Furthermore, these lengthier computations predominantly occur between the 7th and 10th seconds of the simulation in the acceleration case. During this period, the ego vehicle is stationary, waiting for the oncoming vehicle to pass first (as referenced in Figure 2.19). Hence, these extended computation times do not compromise the safety of obstacle avoidance or the real-time decision-making process when the ego vehicle is in motion.

Table 2-2 illustrates alterations in relevant parameters while the ego vehicle is in motion. The data presented in the table substantiates the ego vehicle's smooth and secure obstacle avoidance capabilities within the predefined speed and acceleration limits. This reaffirms the reliability of the proposed algorithm.

**Table 2-2 Related parameters while the ego vehicle is running**

Uniform speed case		
Symbol	Range	Unit
Longitudinal speed	10.8~11.8	m/s
Steering wheel angle	-3.1~3.2	°(degree)
Longitudinal acceleration	-1.2~2.2	m/s <sup>2</sup>
Lateral acceleration	-2.4~2.5	m/s <sup>2</sup>
Acceleration case		
Symbol	Range	Unit
Longitudinal speed	11~15.2	m/s
Steering wheel angle	-2.3~2.8	°(degree)
Longitudinal acceleration	-1.9~3.1	m/s <sup>2</sup>
Lateral acceleration	-2.5~3.3	m/s <sup>2</sup>
Deceleration case		
Symbol	Range	Unit
Longitudinal speed	0~11	m/s
Steering wheel angle	-8.3~4.8	°(degree)
Longitudinal acceleration	-2.1~3.3	m/s <sup>2</sup>
Lateral acceleration	-4.1~3.1	m/s <sup>2</sup>

Figure 2.22 displays the actual trajectories of the ego vehicle in three different cases. Additionally, the minimum distances between the ego vehicle and the obstacles are as follows: 0.52 meters (in the uniform speed case), 0.24 meters (in the acceleration case), and 0.5 meters (in the deceleration case). These outcomes serve as evidence confirming the effectiveness of the proposed algorithm in performing

obstacle avoidance and maintaining lane discipline within the context of urban traffic conditions.

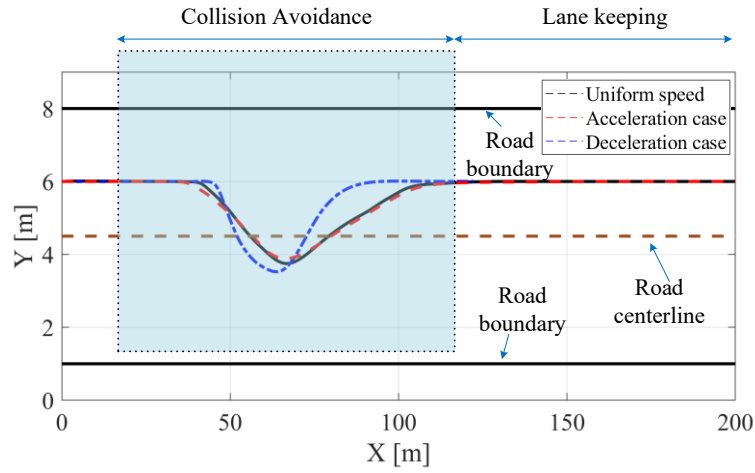


**Figure 2.22 Real trajectories comparison under different cases**

## 2.4 Solution for collision avoidance interacting with pedestrians

Moreover, the interaction between the ego vehicle and multiple pedestrians is taken into account to broaden the scope of the proposed MPC-based CA algorithm.

### 2.4.1 Scenario modeling

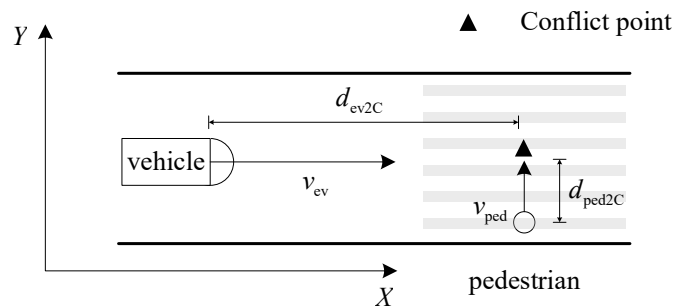


**Figure 2.23 Case of single pedestrian**

In the initial phase, the interaction between the ego vehicle and a single pedestrian, as illustrated in Figure 2.23, is examined to elucidate an adapted social force-based pedestrian motion model and a

methodology for determining the maximum speed for the ego vehicle during the CA process.

The conflict point denotes the intersection of the initial reference paths for the ego vehicle and the pedestrian. Here,  $d_{ev2P}$  represents the distance between the ego vehicle and the conflict point, while  $d_{ped2C}$  signifies the distance between the pedestrian and the conflict point.  $v_{ev}$  and  $v_{ped}$  denote the respective speeds of the vehicle and pedestrian. Additionally,  $X, Y$  represent Cartesian coordinates situated within the world axis frame.

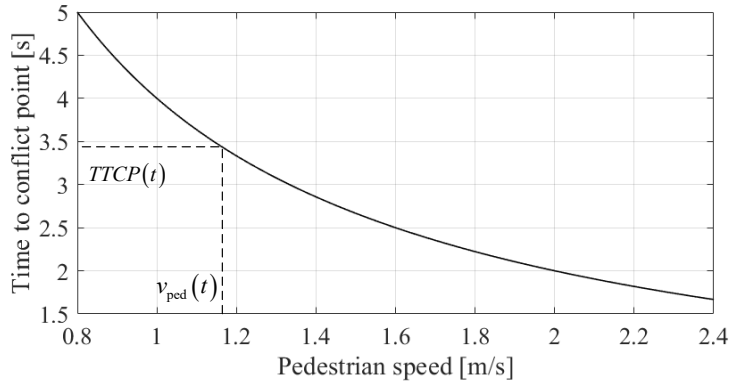


**Figure 2.24 Time to collision calculated by constant pedestrian speed**

Typically, vehicles opt to halt and wait when confronted with pedestrians crossing the road. Nonetheless, in congested sections lacking traffic lights or other signals, drivers usually aim to maintain a relatively low speed for passage. The Time to Conflict Point (TTCP) on the pedestrian side[55], as defined in this scenario, serves as a commonly employed safety indicator to guide the selection of a safe passing speed for the ego vehicle, and it is defined as follows:

$$TTCP = d_{ped2P}/v_{ped} \quad (53)$$

Based on the initial setting of the scenario given in section 2.4.2, TTCP under different pedestrian initial speed is obtained shown as Figure 2.24. If the current pedestrian speed  $v_{ped}(t)$  is obtained, the collision speed  $v_{ev}^{col}(t)$  based on vehicle current position or the collision distance  $d_{ev}^{col}(t)$  based on current vehicle speed could be obtained based on current  $TTCP(t)$ .

$$v_{ev}^{col}(t) = \frac{d_{ev2C}(t)}{TTCP(t)} \quad (54)$$

$$d_{ev}^{col}(t) = v_{ev}(t) \cdot TTCP(t) \quad (55)$$

So if the current vehicle speed  $v_{ev}(t) < v_{ev}^{col}(t)$  or current vehicle position  $d_{ev2C}(t) > d_{ev}^{col}(t)$ ,

it is considered that vehicle can safely avoid the pedestrian.

## 2.4.2 Case of Multi-pedestrians

Usually, the ego vehicle will interact with multiple pedestrians in urban scenario, that means the discusses in the section 2.4 is based on a scenario which is similar to Figure 2.25.

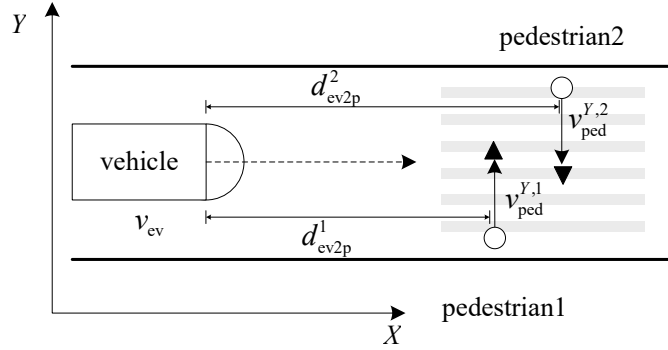


**Figure 2.25 Case of multiple pedestrians**

While this case considers only two pedestrians, extending it to scenarios with three or more pedestrians is relatively straightforward since it solely focuses on the motion of pedestrians in the  $Y$ -axis direction. The initial settings are as follows:

- (1) Vehicle initial speed  $v_{ev}^{ini}$  is  $6\text{ m/s}$  and the range of acceleration for vehicle is  $[-5\text{ m/s}^2 \quad 2.5\text{ m/s}^2]$ ;
- (2) The distance between vehicle and pedestrian 1  $d_{ev2ped}^1$  is  $20\text{ m}$  while the distance between vehicle and pedestrian 2  $d_{ev2p}^2$  is  $22\text{ m}$ ;
- (3) Vehicle mass  $m_{ev}$  is  $1700\text{ kg}$  while both pedestrians mass  $m_{ped}^1$  and  $m_{ped}^2$  are  $75\text{ kg}$ ;
- (4) Pedestrian 1 initial speed  $v_{ped}^{Y,1,ini}$  is  $1.2\text{ m/s}$  and Pedestrian 2 initial speed  $v_{ped}^{Y,2,ini}$  is  $1\text{ m/s}$ .  
The range of acceleration for pedestrians is  $[-2.5\text{ m/s}^2 \quad 2.5\text{ m/s}^2]$ ;
- (5) Driveway is dry road with a good vision whose road friction coefficient  $\mu$  is  $0.8$ ;
- (6) The distance to collision point of pedestrian 1  $d_{ped2p}^1$  and pedestrian 2  $d_{ped2p}^2$  are both equal to  $4\text{ m}$ .

### 2.4.3 Collision probability estimation

In section 2.4, we addressed pedestrians with unpredictable motion, emphasizing the importance of establishing a suitable dynamic model for moving pedestrians. A detailed social force model-based pedestrian dynamic model is provided in section 3.2.3 in details. And in this section, we focus on discussing the method of dealing with pedestrian own unpredictable speed when adopting MPC-based CA strategy.

Given the unpredictability of pedestrian speed, obtaining a definitive solution for MPC that ensures safety is challenging. Therefore, we consider estimating the collision probability during the interaction between the ego vehicle and the pedestrian. Specifically, if the maneuver calculated by MPC for the ego vehicle at its current state guarantees a collision probability with the pedestrian below a specific threshold, this maneuver is deemed acceptable.

For the target scenario depicted in Figure 2.25, based on the current state and the predicted future motion of both the vehicle and the pedestrian, MPC can yield a maximum safe speed ( $v_{ev}^{\max, safe}$ ) and a reference acceleration ( $a_{ev}^{ref}$ ) for the ego vehicle, as illustrated in Figure 2.26.

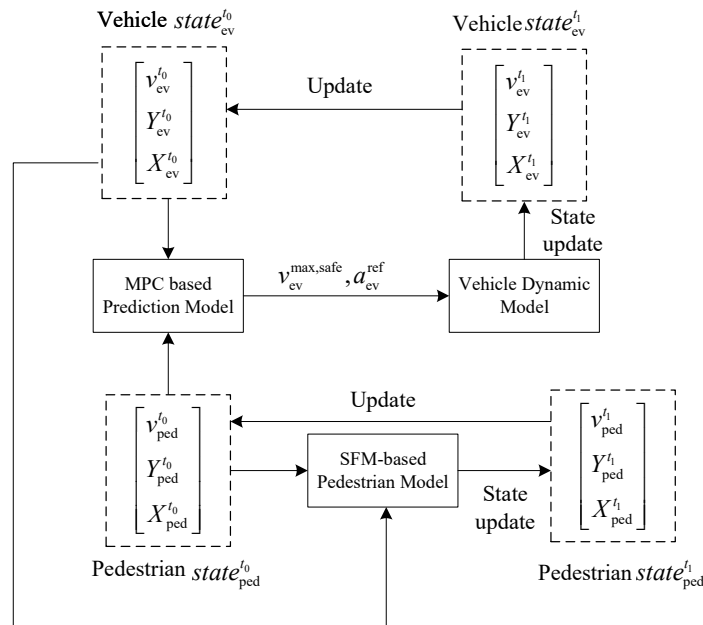
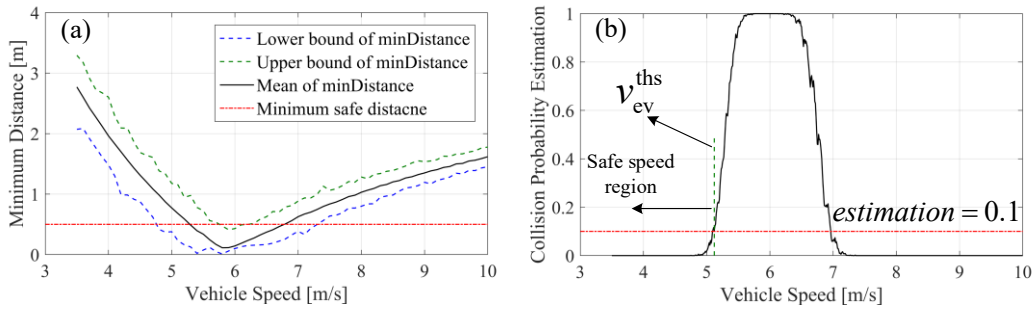


Figure 2.26 MPC-based CA strategy for ego vehicle interacting with multi-pedestrians

Referring to Figure 2.25, by setting  $d_{ev2P}$  is set as 20 m,  $d_{ped2P}$  is 4 m and knowing the

current pedestrian speed is  $1.2 \text{ m/s}$ , the minimum distance between the ego vehicle and the pedestrian can be calculated for various current vehicle speeds (assuming constant speed for the ego vehicle). To estimate the collision probability under different vehicle speeds, a simulation of 1000 iterations is conducted for each different vehicle speed, ranging from  $3.5 \text{ m/s}$  to  $10 \text{ m/s}$  with a  $0.1 \text{ m/s}$  interval. The results are presented in Figure 2.27(a), highlighting the variability in the minimum distances between the ego vehicle and the pedestrian among different iterations, while the initial speed of the ego vehicle remains constant due to the randomness of pedestrian motion.



**Figure 2.27 (a) Range of minimum interaction distance under different initial speed of ego vehicle; (b) Collision probability estimation under different initial speed of ego vehicle**

With a minimum safe distance assumed to be  $0.5 \text{ m}$ , the collision probability estimation is obtained from the collected data, as shown in Figure 2.27 (b). During the speed re-planning process, the collision estimate is considered acceptable when the speed is below a certain value. For instance, if a collision estimation of  $\leq 0.1$  is acceptable, then the safe speed range for the vehicle is less than  $5.1 \text{ m/s}$  (denoted as  $v_{ev}^{ths}$ ) under the current initial settings. As illustrated in Figure 2.28, 100 iterations with a same initial speed ( $5.1 \text{ m/s}$ ) of vehicle is established. Due to the randomness of pedestrian motion, as depicted in Figure 2.28 (a), the distance curves between the vehicle and the pedestrian vary among different iterations, despite the initial settings being identical, as displayed in Figure 2.28 (b). Although some minimum distances are smaller than the set safe distance, the number of times the danger distance is breached is very low in the total iterations. It is worth noting that pedestrians typically tend to avoid vehicles in real-world scenarios. Therefore, if the collision probability estimation for a chosen vehicle speed is lower than a threshold, that speed is considered acceptable.

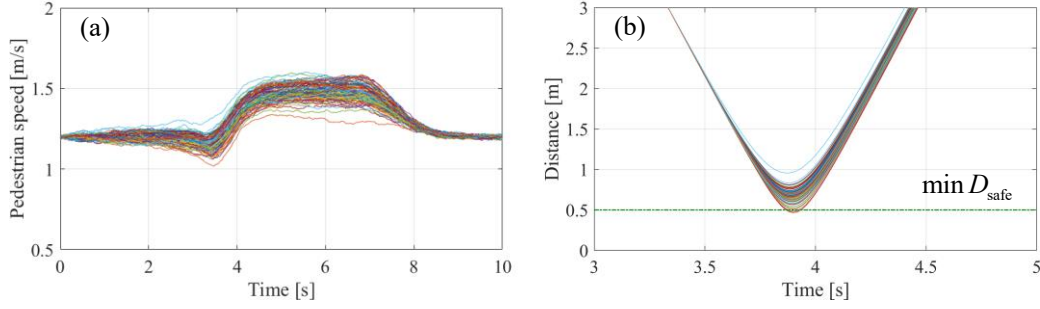


**Figure 2.28(a) Longitudinal speed of pedestrian when considering randomness; (b) Distance between vehicle and pedestrian when considering randomness**

#### 2.4.4 Two-layer MPC-based CA strategy

The MPC-based controller can be divided into two layers: the upper layer is the speed re-planning layer, and the lower layer is the optimal acceleration generation layer. In the re-planning layer, the process of obtaining an acceptable speed for the ego vehicle when interacting with the first pedestrian can be summarized as shown in Figure 2.29:

- (1) Obtain current states of vehicle and pedestrians ( $state_{ev}^t = [v_{ev}^t \ Y_{ev}^t \ X_{ev}^t]$ ,  $state_{ped}^t = [v_{ped}^t \ Y_{ped}^t \ X_{ped}^t]$ );
- (2) For  $v_{ev}^i = v_{ev}^{\max} (= v_{ev}^t) \rightarrow 0$ , start traversing down;
- (3) For each optional vehicle speed iteration from 1 to  $\max Times$ , calculate  $\min D_{ev2ped}^1$ ;
- (4) Is  $\min D_{ev2ped}^1 > \min D_{safe}$ ? If yes, go to step (5), else go back to (2);
- (5) Is  $iteration_{now} = \max Times$ ? If yes, go to step (6), else go back to (3);
- (6) Output the reference re-planning speed  $v_{ev}^{ref4p,1} = v_{ev}^i$ .

For safety, the vehicle is not allowed to accelerate before the CA process is over. So, in step (2), the maximum traversal speed  $v_{ev}^{\max}$  is the current speed  $v_{ev}^t$ . Besides, if the  $\max Times$  for iteration is defined as

$$\max Times = \frac{1}{collision\ estimation} \quad (56)$$

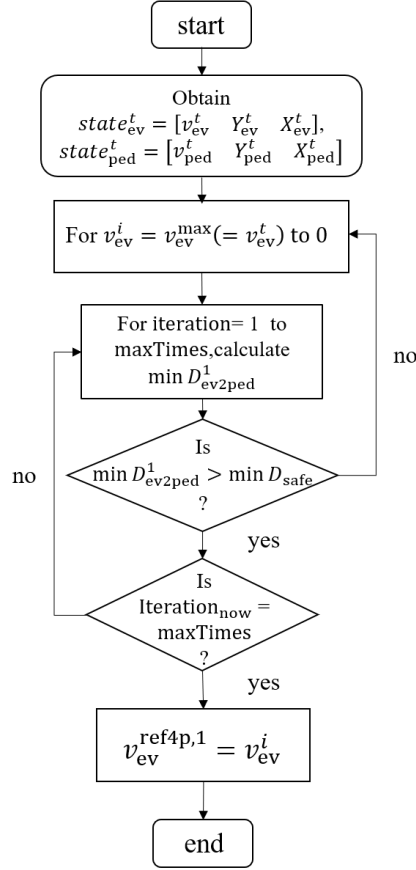


**Figure 2.29** The process of obtaining acceptable speed for ego vehicle when interacting with a pedestrian

Under this framework, it is not necessary to traverse all optional speeds and iterations, which enhances the real-time performance of the algorithm. When calculating acceptable speeds for other pedestrians, the only change is adopting the reference speed for the previous pedestrian, denoted as  $v_{ev}^{\text{ref4p},i}$  as the maximum traversal speed  $v_{ev}^{\text{max}}$  in step (2). This means that the reference speed calculated from the final pedestrian is always the minimum one.

In the optimal acceleration generation layer, considering that a vehicle with a straight reference path normally will not be required to change lanes when facing pedestrians coming from both sides, the lateral dynamics of the vehicle are not considered in this section. A first-order inertial system is used for vehicle longitudinal speed control, defined as follows

$$\dot{a} = \frac{K}{\tau_d} (a_{\text{ref}} - a) \quad (57)$$

where  $K$  is a system gain,  $\tau_d$  is the time constant,  $a$  is the vehicle acceleration while  $a_{\text{ref}}$  is the reference acceleration (or the optimal acceleration). And to form an MPC problem, this system model

discretized by the Forward-Euler method as follows:

$$x(k+1) = A_k x(k) + B_k u(k) \quad (58)$$

$$y(k) = C_k x(k) \quad (59)$$

where  $x = [v \ a]^T$  is the state vector,  $u = a_{des}$  is the control input.  $A_k = \begin{bmatrix} 1 & T_s \\ 0 & 1 - \frac{T_s}{\tau_d} \end{bmatrix}$  and  $B_k = \begin{bmatrix} 0 \\ \frac{KT_s}{\tau_d} \end{bmatrix}$ ,  $T_s = 0.01s$  is the simulation step.  $C_k = [1 \ 0]$  is an output selection matrix.

The cost function is defined as

$$\begin{aligned} \min_{\Delta u(k)} J(x(k), u(k-1), \Delta u(k)) = & \sum_{i=1}^{N_p} \|y(k+i|k) - y_{ref}(k+i|k)\|_{Q^{MPC}}^2 + \sum_{i=1}^{N_c} \|\Delta u(k+i)\|_{R^{MPC}}^2 \\ \text{s.t. } & u_{\min} \leq u(k+i) \leq u_{\max}, i = 0, 1, \dots, N_c - 1 \\ & \Delta u_{\min} \leq \Delta u(k+i) \leq \Delta u_{\max}, i = 0, 1, \dots, N_c - 1 \end{aligned} \quad (60)$$

where  $y_{ref}(k+i|k)$ , with  $i = 1, \dots, N_p$ , is the reference, which is generated by re-planning layer, for the output tracking variable.  $N_p = 30$  and  $N_c = 10$  are the prediction horizon and the control horizon, respectively.

And considering the total duration time of prediction horizon is  $0.3s$  and the vehicle speed is relatively slow in this scenario, we assume that  $y_{ref}(k+i|k, i = 1, \dots, N_p) = y_{ref}(k+i|k, i = 1)$  for simplifying the calculation.  $Q^{MPC} \in \mathbb{R}^{p_y \times p_y}$ ,  $R^{MPC} \in \mathbb{R}^{m \times m}$  are weighting matrices.  $\varepsilon$  is a slack variable.  $u_{\min}$  and  $u_{\max}$  are the threshold for acceleration while  $\Delta u_{\min}$  and  $\Delta u_{\max}$  are the threshold for acceleration increments. In this function, the first term penalizes the deviation of the ego vehicle's longitudinal speed from the initial reference speed, while the second term ensures a smooth change in the control variable.

For a better view of comparison with social force model-based strategy, the simulation results of MPC-based CA strategy in this section are all shown in section 3.3.3.

## 2.5 Existing Problems of MPC

MPC is a popular control strategy used in various industrial processes and systems to optimize the performance of a system by predicting its future behavior and adjusting control inputs accordingly. Including this thesis, it has also been used in the field of vehicle collision avoidance algorithm design.

However, there are several existing issues and challenges associated with MPC[53, 54]:

(1) Computational complexity: MPC involves solving optimization problems at each time step to find the optimal control inputs. As the prediction horizon and control horizon increase, the computational burden grows significantly, making real-time implementation challenging for complex systems;

(2) Tuning: tuning MPC controllers can be a complex and time-consuming task. Selecting appropriate control horizons, prediction horizons, and penalty weights in the cost function requires domain expertise and may not always lead to optimal results;

(3) Model mismatch: MPC relies on an accurate model of the system being controlled. If there is a mismatch between the actual system and the model used in the controller, the control performance can degrade. This is especially problematic in dynamic or nonlinear systems;

(4) Constraints handling: Handling constraints on control inputs and state variables is an essential aspect of MPC. Ensuring feasibility and stability while adhering to constraints can be challenging, especially in situations where constraints are stringent or time-varying;

(5) Real-Time implementation: implementing MPC in real-time systems can be challenging due to its computational demands. Hardware limitations or delays in computation can lead to performance degradation or instability.

The above problems limit the application of MPC. Though, layering control strategies and applying vehicle models of different complexity and collision probability estimation that proposed in this section can partially solve these problems, there are still problems exist:

(1) Reasonable mathematical models are needed to describe interactive systems such as vehicle-vehicle interaction and vehicle-pedestrian interaction;

(2) The MPC-based controller proposed in this section mainly focus on low-speed urban traffic conditions, therefore, CA problem under extreme adhesion or at relative high-speed conditions needs to be further discussed.

(3) Real-Time implementation is still a problem when the CA scenario is complex.

## 2.6 Summary of this chapter

When dealing with collision avoidance problems in shared spaces, the goal is to enable the ego

vehicle to navigate around obstacles while considering travel time and convenience. The aim is for the vehicle to avoid obstacles while maintaining a constant speed or accelerating, eliminating the need for deceleration. This necessitates real-time control over the vehicle's speed and trajectory adjustments during obstacle avoidance. In addressing these challenges, this chapter introduces innovative CA that aim to achieve these objectives:

(1) In the context of vehicle interactions, a collision avoidance (CA) strategy is presented, which involves behavior re-planning based on post-encroachment time (BR-PET) and trajectory re-planning and tracking utilizing a two-layer MPC system. The BR-PET module calculates necessary speed adjustments for the ego vehicle by considering initial information about the ego vehicle, static and dynamic obstacles, and speed and acceleration limits. Additionally, the real-time performance is ensured by employing different dynamic vehicle models with varying complexities for the two MPCs used in the path re-planning and tracking layers.

(2) Focusing on scenarios involving vehicle-pedestrian interactions, an MPC-based active CA strategy is proposed to address unpredictable pedestrian movements. This strategy is based on a detailed discussion of collision probability estimation during the CA process, considering the randomness in pedestrian motion. This approach enhances the safety and effectiveness of CA in situations involving pedestrians with unpredictable behaviors.

Finally, the existing problems of MPC-based CA strategies are analyzed.

## Chapter3    Passive Collision Avoidance Strategies

### 3.1 Preface

Previous research on developing collision avoidance (CA) strategies for autonomous vehicles has often focused primarily on the ego vehicle itself, giving less consideration to the dynamics of obstacles. Many of the existing studies assume that obstacle motions are known in advance, either fixed in one position or following predetermined trajectories with given speed profiles. Even research using Social Force Models (SFM), such as [3] and [50], lacks randomness in obstacle motions, implying that obstacles' movements can be accurately predicted.

However, when accounting for individual differences among pedestrians and variations in shared spaces (like variations in pedestrian ages or visibility), precise motion predictions of pedestrians become challenging. This challenge is evident in research focused on modeling for mixed traffic scenarios, such as [48]. Therefore, in line with the goals of Model Predictive Control (MPC)-based CA strategies, which aim to design strategies ensuring quick and safe passage of the ego vehicle on roads with collision risks, we acknowledge the uncertainty in pedestrians' motions. Consequently, we propose novel SFM-based methods that allow the ego vehicle to make avoidance decisions without predicting pedestrian motions but rather rely on force balancing principles.

Additionally, when considering control algorithms such as artificial neural networks (ANN), it's worth noting their drawback of requiring extensive trials and prolonged training processes to yield results. On the other hand, control algorithms like Model Predictive Control (MPC), although suitable for slow dynamic processes and conditions with low real-time requirements, still face challenges in real-time high-speed vehicle dynamic control due to their computationally intensive nature. Furthermore, MPC lacks the ability to reference past experiences and relies on iterative search for optimal solutions in similar scenarios, which limits its real-time applicability. In response to these challenges, we propose a novel method based on an ANN architecture, known as NAFC (Neural Approximate Feedback Control). The training data for NAFC is derived from a well-calibrated MPC controller. During training, a series of states of the MPC-based ego vehicle are used as input data, and the optimal output from MPC corresponding to the current state serves as the output data. NAFC can

be regarded as a rapid implicit solution solver for MPC, offering a more efficient and real-time approach to vehicle control.

## 3.2 Social force model

### 3.2.1 Introduce of SFM

The social force model (SFM) is a model based on Newtonian mechanics and it was originally proposed to explain the motion of pedestrians. It is suggested that the motion of pedestrians can be described as if they would be subject to "social forces." These "forces" are not directly exerted by the pedestrians' personal environment, but they are a measure for the internal motivations of the individuals to perform certain actions (movements)[45]. SFM assumes that pedestrians are accelerated by social forces and move. In this model, the pedestrian is affected by three forces at the same time, namely the driving force (or force from destination), the force between people, and the force between people and obstacles. Since we focus on the interaction between ego vehicle and the pedestrian, a schematic diagram of force exerted on pedestrian is established as Figure 3.1.

In Figure 3.1,  $\vec{F}_{obj2p}^{i,t}$  represents the force from the  $i$ -th objectors (other than vehicles) to the pedestrian in the time  $t$ . Simply,  $\vec{F}_{obj2p}^{i,t}$  is the sum of forces which can be defined as the forces from road boundaries, buildings or other inaccessible areas. Therefore,  $\vec{F}_{obj2p}^{i,t}$  is usually defined as the repulsive force that keeps pedestrians away from corresponding object.  $\vec{F}_{ev2p}^{i,t}$  is part of  $\vec{F}_{obj2p}^{i,t}$ , actually. It represents the force from the  $i$ -th vehicle to the pedestrian in the time  $t$ . The function of  $\vec{F}_{ev2p}^{i,t}$  is similar to that of  $\vec{F}_{obj2p}^{i,t}$ . When the vehicle is in front of the motion direction of pedestrian,  $\vec{F}_{ev2p}^{i,t}$  usually manifests as resistance to movement of the pedestrian. On the contrary,  $\vec{F}_{ev2p}^{i,t}$  will appear as a driving force to movement of the pedestrian when the vehicle is behind the motion direction of pedestrian.  $\vec{F}_{des2p}^t$  is the force from "the destination" that the pedestrian wants to arrive. "The destination" is a broad concept, it not only can be a place, such as a point, an area or just the other side of the road(for the pedestrian who want to cross the road), but also can be a reference trajectory that contains the reference speed  $\vec{v}_p^t$  for the pedestrian in current time  $t$  or a reference path (such as the

pedestrian is just walk along the road).

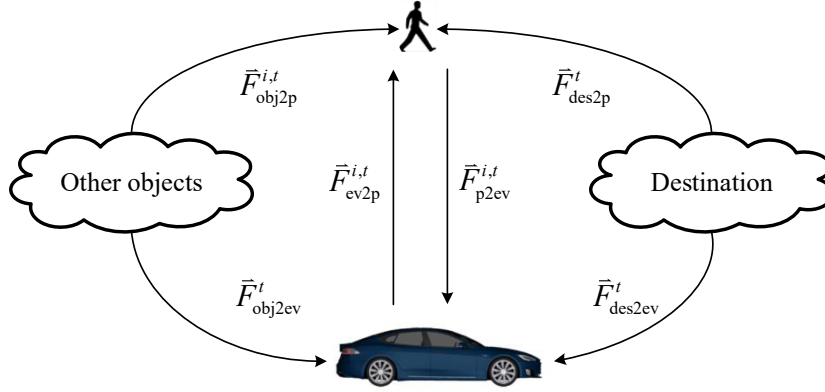


**Figure 3.1 Schematic diagram of social force exerted on pedestrian and vehicle**

The resultant force generated by these three forces acts on the pedestrian generating an acceleration to drive pedestrian movement. To sum up, among them, the force from destination  $\vec{F}_{des2p}^t$  is the social force exerted by the individual on himself, which reflects his/her need to move to the destination under the influence of subjective consciousness; the interaction force between people and objects is the social force exerted on the individual by other surrounding. It reflects their need to keep a certain distance from others as much as possible; the force between a person and a vehicle is the social force exerted by the vehicle in the traffic on the individual, which reflects his/her need to keep a certain distance from the vehicle. Although all these forces are virtual, they are easily explainable and reasonable.

Similarly, when we consider the motion of the ego vehicle, SFM-based model could also be adopted. The forms of forces exerted on the pedestrian and the ego vehicle are similar, however the magnitude of the parameters in each force for the pedestrian and the ego vehicle is different. Detailed mathematical modeling of forces will be established in section 3.2.3 and section 3.2.4.

The interaction forces are only based on the current states of the traffic participants which means the historical data is ignored. And the determination of these forces does not require prediction of future changes in traffic flow either. To some extent, the SFM-based CA process is Markov-like process. Therefore, when parameters of the SFM-based vehicle are well-calibrated offline, the online solution for CA problem based on SFM is real-time (it can be viewed as simply a numerical calculation).

The following section 3.2.2 will explain the real traffic follows a Markov-like process that SFM-

based vehicle model can be adopted in designing CA methods.

### 3.2.2 Rational explanation

The point of modifying SFM-based pedestrian model to vehicle dynamic model and adopting SFM-based vehicle model for CA strategy design is to explain the CA process of the interactive system consisting of the ego vehicle and the pedestrian follows the Markov process.

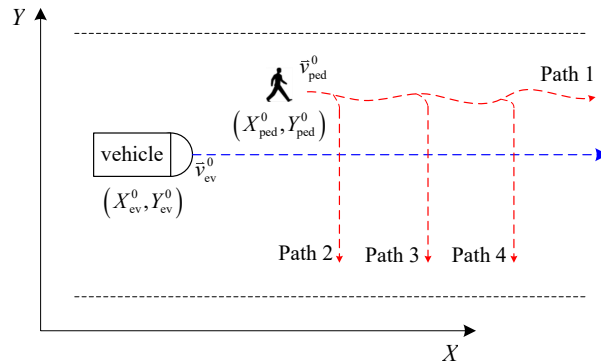


**Figure 3.2 Typical interaction scenario between vehicle and pedestrian**

Here, we consider the following typical interaction scenario between ego vehicle and pedestrian under urban traffic case, shown as Figure 3.2.

In Figure 3.2, the Cartesian coordinates are defined by  $X$  and  $Y$ , respectively. Superscript 0 represents the initial states or parameters and subscript ped is the abbreviate of pedestrian where ev represents the ego vehicle. The future motion of the pedestrian is qualitatively defined as the following four possible realizations:

- (1) Path 1: The pedestrian walks straightly without changing direction. In this case, the ego vehicle does not need to take on avoidance operation.
- (2) Path 2 or 4: The crossing road behavior of the pedestrian is too early (or too late), and the ego vehicle has not approached yet (already passed). And in this case, the ego vehicle does not need to take avoidance operation as well.
- (3) Path 3: If the ego vehicle does not avoid the pedestrian in time, the minimum distance between them will be smaller than a threshold safety distance ( $\min D_{\text{safe}}$ ) that indicates whether the collision avoidance process is safe or not. In this case, the ego vehicle must yield to avoid danger.

With the above analysis, In the case of the pedestrian in paths 1, 2, and 4, the ego vehicle just needs to follow the initial trajectory and speed, which is considered the optimal operation when facing a pedestrian with potential crossing road intention. However, appropriate collision avoidance maneuverings in the case of path 3 need to be further discussed.

As shown in Figure 3.2, the available information at time  $t$  is listed as:

- (1) The current velocity and position of the ego vehicle:  $v_{ev}^t$  and  $P_{ev}^t = [X_{ev}^t, Y_{ev}^t]$ ;
- (2) The current velocity, position and moving direction of the pedestrian:  $v_{ped}^t, P_{ped}^t = [X_{ped}^t, Y_{ped}^t]$  and  $\delta_{ped}^t$ ;

$\delta_{obs}^t$  is the observation of  $\delta_{ped}^t$  by vehicle sensors, which is used for judgment of ego vehicle that which path the pedestrian will choose:

$$\delta_{obs}^t \begin{cases} \in [-\delta_{ped}^{thr}, \delta_{ped}^{thr}], \text{ path 1} \\ < -\delta_{ped}^{thr}, \text{ path 2 - 4} \end{cases} \quad (61)$$

Besides, the interaction between the ego vehicle and the pedestrian is essential. As the ego vehicle and the pedestrian are both the participants of traffic flow, the behavior of the participants is not only determined by their own will, but is usually influenced by the surrounding environment. Taking the pedestrian that decides to cross the road currently as an example, shown in Figure 3.3.

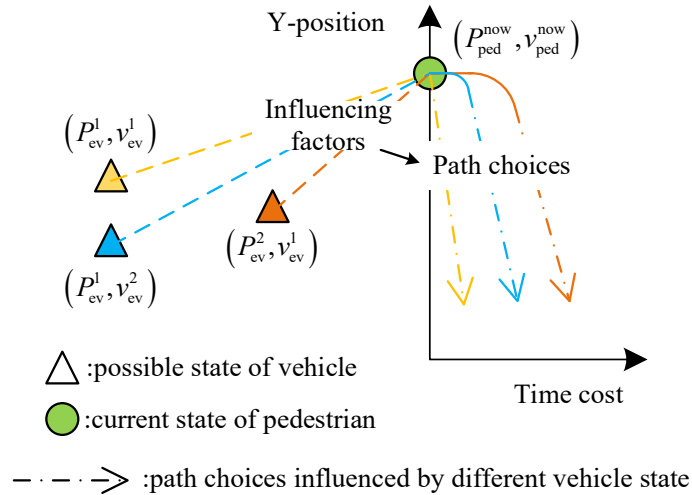


**Figure 3.3 Possible path choices of pedestrian influenced by vehicle with different state**

In Figure 3.3, the pedestrian, shown as green circle, is fixed currently as the shown state

$(P_{\text{ped}}^{\text{now}}, v_{\text{ped}}^{\text{now}})$ . The ego vehicle, shown as triangle, owns different possible states that follow:

$$\begin{cases} \|P_{\text{ped}}^{\text{now}} - P_{\text{ev}}^1\|_2 < \|P_{\text{ped}}^{\text{now}} - P_{\text{ev}}^2\|_2 \\ v_{\text{ev}}^1 < v_{\text{ev}}^2 \end{cases} \quad (62)$$

Figure 3.3 gives the possible path choices for pedestrian-crossing when the pedestrian faces the vehicle owning different states.

A pedestrian path that is with more time consuming, such as the path with red color, means the pedestrian slows his speed down for a safe crossing. When a pedestrian faces a closer or faster oncoming vehicle, the pedestrian will change its future his future behavior. Previous works proposed some methods to describe this kind of interaction and most of them were based on [45-48].

Therefore, the states of these two participants are integrated as one system state which is written as:

$$S^t = (S_{\text{ev}}^t, S_{\text{ped}}^t) \quad (63)$$

where  $S_{\text{ev}}^t = [v_{\text{ev}}^t, P_{\text{ev}}^t]$  and  $S_{\text{ped}}^t = [v_{\text{ped}}^t, P_{\text{ped}}^t]$  are the state of the ego vehicle and the pedestrian at current time  $t$ , respectively.

Generally, the whole CA process should be considered. However, when the future trajectory of the pedestrian follows an unknowable profile and is stochastic, the future state of the interaction system can be described by a transition probability matrix based on the current state, which is simplified as a Markov process. And Markov process has been adopted by many similar traffic processes [59-62].

Although some previous research used the Markov process to illustrate similar traffic processes, they rarely justified the use of the Markov process.

To catch the key to improving safety driving by analyzing the interaction of ego vehicle and other traffic participants, some traffic data collected by our SMRC is adopted [2]. Interaction events between pedestrians and the ego vehicle on a non-signalized road are used for illustrating the rationality of adopting Markov process. The record signals include the following items:

- (1) Video data containing cumulative frames and running time during interactions on the non-signalized road;
- (2) Time series of vehicle lateral acceleration  $a_{\text{ev}}^y(\cdot)$ ;
- (3) Time series of lateral distance between ego vehicle and the  $i$ -th pedestrian  $d_{\text{ev2p}}^{y,i}(\cdot)$ .

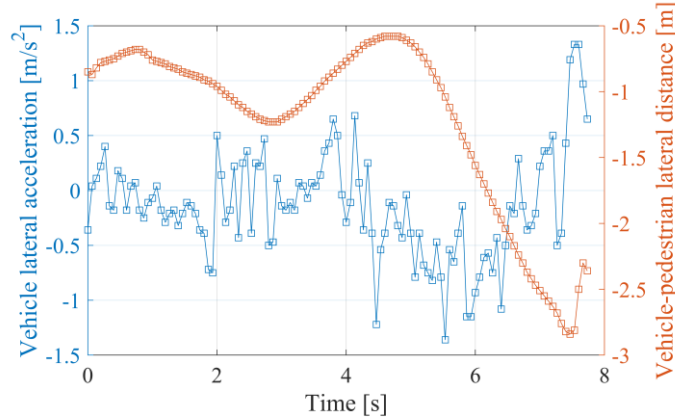
5 typical time series data sets consist of  $a_{ev}^y(\cdot)$  and  $d_{ev2p}^{y,i}(\cdot)$  are selected and used for correlation analysis. The collected data is shown in Figure 3.4. (In order to show concisely, here we only give the image of one data set in the total 5 sets, because their distributions are similar.)

Figure 3.4 shows some correlation in the time domain between  $a_{ev}^y$  and  $d_{ev2p}^{y,i}$ . The cross-correlation sequence of two joint stationary stochastic processes  $x_n, y_n$  was given by [63] as follows:

$$\hat{R}_{xy}(m) = \begin{cases} \sum_{n=0}^{N-m-1} x_{n+m} y_n^*, & m \geq 0 \\ \hat{R}_{xy}^*(-m), & m < 0 \end{cases} \quad (64)$$

where  $N$  is the length of time series data and  $*$  denotes complex conjugation. The Equation (64) can only estimate the sequence because, in practice, only a finite segment of one realization of the infinite-length random process is available. In general, the correlation function requires normalization to produce an accurate estimate by the following equation:

$$\hat{R}_{xy,coeff}(m) = \frac{1}{\sqrt{\hat{R}_{xx}(0)\hat{R}_{yy}(0)}} \hat{R}_{xy}(m) \quad (65)$$



**Figure 3.4 The time series of vehicle lateral acceleration and corresponding vehicle-pedestrian distance**

And the results are shown in Figure 3.5. It shows that:

(1) As the correlation between the  $a_{ev}^y$  and  $d_{ev2p}^{y,i}$  increases as the time delay decreases, it shows that the input of lateral acceleration directly affects the vehicle-pedestrian distance. The lateral acceleration is caused by the vehicle steering wheel angle which is considered system input, and the vehicle-pedestrian distance is the system state. So, the vehicle-pedestrian interaction system state of next time is transformed by the current system state and the system input.

(2) The correlation between the two sets of data drops sharply as the time delay increases, which means earlier historical input of lateral acceleration has little influence in the current state. This feature can be approximated as a non-aftereffect.

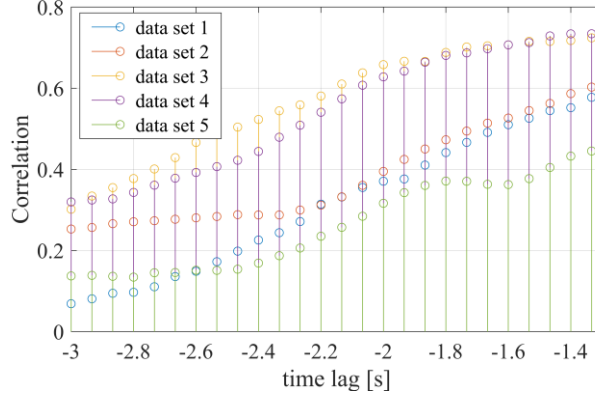


**Figure 3.5 Normalization correlation analysis of vehicle-pedestrian interaction events**

And the above analysis shows the rationality of approximating the vehicle-pedestrian system as a Markov process. Actually, from physical-view consideration, the future behavior of pedestrians and drivers, such as crossing road or accelerating/decelerating vehicles, is also mainly based on the current positions and respective velocity.

Therefore, the transition function of the interactive system could be established as:

$$\begin{cases} p_{ev}(\mathbb{S}_{ev}^{t+1} | \mathbb{S}^t, \dots, \mathbb{S}^0) = p_{ev}(\mathbb{S}_{ev}^{t+1} | \mathbb{S}^t) \\ p_{ped}(\mathbb{S}_{ped}^{t+1} | \mathbb{S}^t, \dots, \mathbb{S}^0) = p_{ped}(\mathbb{S}_{ped}^{t+1} | \mathbb{S}^t) \end{cases} \quad (66)$$

where  $p_{ev}$  and  $p_{ped}$  are the transition function of ego vehicle and the pedestrian, respectively.

Furthermore, the accessible maneuver for the ego vehicle during CA process is defined as a set of steering and acceleration in  $x$ -direction:

$$m_{ev}^t = (\delta_{ev}^t, a_{ev}^{x,t}) \quad (67)$$

where  $\delta_{ev}^t$  is the steering wheel angle at time  $t$  and  $a_{ev}^{x,t}$  represents the acceleration in  $x$ -direction at time  $t$ . And the velocity  $v_{ev}^t$ , acceleration  $a_{ev}^{x,t}$ , and steering wheel angle  $\delta_{ev}^t$  are within the proper bounds:

$$v_{ev}^t \in [0, v_{ev}^{max}], \forall t \in (t_0, t_{end}) \quad (68)$$

$$a_{ev}^t \in [-a_{ev}^{max}, a_{ev}^{max}], \forall t \in (t_0, t_{end}) \quad (69)$$

$$j_{ev}^t \in [-j_{ev}^{max}, j_{ev}^{max}], \forall t \in (t_0, t_{end}) \quad (70)$$

$$\delta_{ev}^t \in [-\delta_{ev}^{max}, \delta_{ev}^{max}], \forall t \in (t_0, t_{end}) \quad (71)$$

$$\Delta\delta_{ev}^t \in [-\Delta\delta_{ev}^{max}, \Delta\delta_{ev}^{max}], \forall t \in (t_0, t_{end}) \quad (72)$$

where  $j_{ev}^t$  and  $\Delta\delta_{ev}^t$  are the jerk of acceleration and steering wheel angle at the current time, respectively.  $t_0$  and  $t_{end}$  are the time when CA process starts and ends, respectively. Noticing that the lower bound of velocity is posed equally to zero in order to avoid unwanted backward movements. The bounds of  $a_{ev}^t$  and  $\delta_{ev}^t$  are set to ensure that the trajectory of the vehicle is within a reasonable range in the real world. At the same time, the limits of change rates for the  $a_{ev}^t$  and  $\delta_{ev}^t$  are used to reduce impact.

Besides, some limits are added to the pedestrian for the rationality of the movement as well:

$$v_{ped}^t \in [0, v_{ped}^{max}], \forall t \in (t_0, t_{end}) \quad (73)$$

$$a_{ped}^t \in [-a_{ped}^{max}, a_{ped}^{max}], \forall t \in (t_0, t_{end}) \quad (74)$$

Considering the state  $\mathbb{S}^{t+1}$  is decided by  $\mathbb{S}^t$  and the maneuver  $m_{ev}^t$  the transition function is updated as:

$$p(\mathbb{S}^{t+1}|\mathbb{S}^t) \rightarrow p(\mathbb{S}^{t+1}|\mathbb{S}^t, m_{ev}^t) \quad (75)$$

The choices of different maneuver for the ego vehicle bring different transition possibilities based on the same current state of the interaction system. As shown in Figure 3.6. (a) of Figure 3.6 represents the current system state, that is defined as  $\mathbb{S}^0$ . The pedestrian is shown as a circle while the ego vehicle is simplified as a triangle. Considering two different maneuvers for the ego vehicle which are  $m_{ev}^1$  and  $m_{ev}^2$ . And in  $m_{ev}^2$ , the acceleration  $a_{ev}^{x,2}$  is larger than that of  $a_{ev}^{x,1}$ . Then, the possibility of reaching the next states  $\mathbb{S}^1$  and  $\mathbb{S}^2$  will be different:

$$\begin{cases} p(\mathbb{S}^1|\mathbb{S}^0, m_{ev}^1) \gg p(\mathbb{S}^2|\mathbb{S}^0, m_{ev}^1) \\ p(\mathbb{S}^1|\mathbb{S}^0, m_{ev}^2) \ll p(\mathbb{S}^2|\mathbb{S}^0, m_{ev}^2) \end{cases} \quad (76)$$

The larger acceleration may bring farther moving distance for vehicle and greater avoidance for pedestrian, which means the possibility of reaching state  $\mathbb{S}^2$  in (c) of Figure 3.6 is larger than that of  $\mathbb{S}^1$  when taking maneuver  $m_{ev}^2$  under the same initial state  $\mathbb{S}^0$ . However, there is still some possibility of reaching  $\mathbb{S}^1$  when taking maneuver  $m_{ev}^2$  such as  $a_{ev}^{x,1}$  is the upper limit of current state  $\mathbb{S}^0$ .

Figure 3.6 and Equation (76) are just established to explain that different maneuver taken by the ego vehicle may lead to different interaction system states of the next time step, and this is the reason for modifying the transition possibility function as Equation (75).

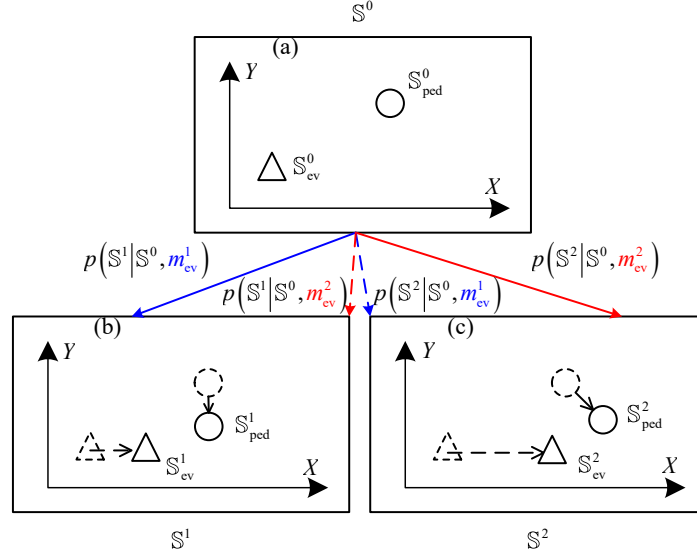


Figure 3.6 Different probabilistic trajectories of the interactive system based on different  $m_{ev}^t$

Furthermore, for the system state  $\mathbb{S}^0$ , we aim to find the optimal maneuver  $m_{ev}^{*,t}$  that is accessible currently to reach the optimal state  $\mathbb{S}^{*,t+1}$ . So, a reward function is established to evaluate the currently chosen maneuver  $m_{ev}^t$ :

$$r(\mathbb{S}^t, m_{ev}^t, \mathbb{S}^{t+1}) = - \left( w_{\text{ref}} \|P_{ev}^{t+1} - P_{ev}^{\text{ref},t+1}\|_2 + w_v |v_{ev}^{X,t+1} - v_{ev}^{X,*,t+1}| - w_{\text{ped}} \|P_{ev}^{t+1} - P_{ped}^{t+1}\|_2 \right) \quad (77)$$

where  $P_{ev}^{\text{ref},t}$  is the reference path for the ego vehicle, and  $v_{ev}^{X,*,t+1}$  represents the optimal speed of the ego vehicle in the  $X$ -direction at time  $t$ .  $w_{\text{ref}}$ ,  $w_v$  and  $w_{\text{ped}}$  are the weights of evaluation indexes, respectively. This reward function requires the ego vehicle to balance tracking the reference path, tracking optimal velocity and keeping away from the pedestrian. And the purpose is to maximize this reward at every time step.

When the initial state  $\mathbb{S}^0$  is determined, the purpose is to find the optimal policy  $\pi^*$  that could maximize the expect future reward  $V^*(\mathbb{S}^0)$  from the following system state  $\mathbb{S}^1, \dots, \mathbb{S}^{t_{\text{end}}}$  by selecting the optimal maneuver  $m_{ev}^* \in M_{ev}$  at each time step for ego vehicle, which could be considered as a Markov decision process(MDP):

$$V^*(\mathbb{S}^0) = \max_{\pi \in \Pi} \mathbb{E} \left[ \sum_{t=t_0}^{t_{\text{end}}} \gamma^t r(\mathbb{S}^t, m_{ev}^t, \mathbb{S}^{t+1}) | \pi \right] \quad (78)$$

Where  $\gamma \in (0,1)$  is a discount factor. Generally, the Bellman Optimal Equation is adopted to solve the MDP:

$$V^*(\mathbb{S}^t) = \max_{m_{ev}} \left( r(\mathbb{S}^t, m_{ev}^t, \mathbb{S}^{t+1}) + \gamma \sum_{\mathbb{S}^{t+1} \in \mathbb{S}_{all}} p(\mathbb{S}^{t+1} | \mathbb{S}^t, m_{ev}^t) V^*(\mathbb{S}^{t+1}) \right) \quad (79)$$

However, a fundamental problem with MDP is that the size of the state space  $\mathbb{S}$  and the size of the action space  $M$  both can grow quickly due to the high dimensionality of the space, or due to increasingly fine-grained discretization to approach a continuous representation. Which is referred to as the curse of dimensionality by Bellman [64]. For the MDP problem addressed in this section, noticing the reference path in the target scenario (shown as Figure 3.2) maintains a straight line, and the optimal speed profile  $v_{ev}^{x,*}$  in Equation (77) is inaccessible during the solution, the reward function  $r(\mathbb{S}^t, m_{ev}^t, \mathbb{S}^{t+1})$  at each time step is replaced by a  $R$  that defines the total reward of the whole CA process for simplification:

$$R = W_{ref} \cdot d_{ev2ref}^{min} + W_v \bar{v}_{ev}^X - W_{ped} d_{ev2ped}^{min} \quad (80)$$

where

$$d_{ev2ref}^{min} = \min \left\{ \|Y_{ev}^t - Y_{ev}^{ref}\| \mid t \in (t_0, t_{end}) \right\} \quad (81)$$

$$\bar{v}_{ev}^X = \frac{\sum_{i=1}^{end} v_{ev}^{X,i} \cdot T_s}{t_{end} - t_0} \quad (82)$$

$$d_{ev2ped}^{min} = \min \left\{ \|P_{ev}^t - P_{ped}^t\|_2 \mid t \in (t_0, t_{end}) \right\} \quad (83)$$

where  $T_s$  is the sampling time. And when the initial state  $\mathbb{S}^0$  is determined, the  $V^*(\mathbb{S}^0)$  is approximated to the maximum value of  $R$ :

$$V^*(\mathbb{S}^0) = \max R \quad (84)$$

Then, instead of searching the optimal policy  $\pi^*$ , it is possible to directly obtain the optimal maneuver profile  $m_{ev}^*$  by the total reward  $R$ . Combining Equation (80)-(84), the first item of function  $R$ , which is from Equation (81), , requires the ego vehicle to follow the reference path that is corresponding to the requirement of slight steering. The second item, which is from Equation (82), gives the average  $X$ -direction vehicle speed during the CA process that is corresponding to the requirement of quick passing. And the final item, which is from Equation (83), is corresponding to the requirement of safe passing.

Due to the above assignments, it is possible to define a feasible profile  $a_{ev}^{x,t}$  and  $\delta_{ev}^t$  as follows:

**Definition:** Curves  $a_{ev}^{x,t}$  and  $\delta_{ev}^t$  are feasible if they are  $l^{-1}$  continuity and satisfy conditions

Equation (68) (74). The set of feasible  $a_{ev}^{x,t}$  and  $\delta_{ev}^t$  are written as  $\mathbb{F}_a$  and  $\mathbb{F}_\delta$ , respectively.

In summary, the SFM-based CA strategy needs to address the following maneuver planning problem:

**Problem 1:** Given the determinate initial state  $\mathbb{S}^0$  and reward function  $R$  to calculate the optimal maneuver profile  $m_{ev}^{*,t}, \forall t \in [t_0, t_{end}]$  which satisfies:

$$m_{ev}^* = \underset{m_{ev}^t \in (\mathbb{F}_\delta \cap \mathbb{F}_a)}{\operatorname{argmax}} R \quad (85)$$

Considering the vehicle-pedestrian interaction has been thoroughly researched, here we make the following assumption:

**Assumption 1:** Considering  $\mathbb{S}^0$  follows conditions a series of specific initial conditions and  $m_{ev}^t \in (\mathbb{F}_\delta \cap \mathbb{F}_a)$  is a finite set, the transition function  $p(\mathbb{S}^{t+1}|\mathbb{S}^t, m_{ev}^t)$  is approximated by an explicit equation that describes a system state  $\mathbb{S}^{t+1}$  that reaches from  $\mathbb{S}^t$  by ego vehicle taking a specific maneuver  $m_{ev}^t$ :

$$\mathbb{S}^{t+1} = f_{env}(\mathbb{S}^t, m_{ev}^t) \quad (86)$$

Besides, as the target scenario Figure 3.2 is not complex, an explicit dynamic equation  $f_{env}$  is used to approximate transition possibility function  $p$ , which is defined as **Assumption 1**. It is convenient to calculate the total reward  $R$  of Equation (80), which is essential for solving **Problem 1**, after establishing  $f_{env}$ . Therefore, the interaction between ego vehicle and the pedestrian is essential, which is defined as problem 2:

**Problem 2:** Given the current state of ego vehicle  $\mathbb{S}_{ev}^t$ , pedestrian  $\mathbb{S}_{ped}^t$  and the limit conditions (68) (74), to calculate  $\mathbb{S}_{ev}^{t+1}$  and  $\mathbb{S}_{ped}^{t+1}$  based on the interaction between these two participants:

$$\begin{cases} \mathbb{S}_{ev}^{t+1} = f_{env, ev}(\mathbb{S}_{ped}^t, \mathbb{S}_{ev}^t) \\ \mathbb{S}_{ped}^{t+1} = f_{env, ped}(\mathbb{S}_{ped}^t, \mathbb{S}_{ev}^t) \end{cases} \quad (87)$$

s. t. Equation (68) – (74)

To solve **Problem 2**, force-based interaction models for the pedestrian and the ego vehicle were established in the following section 3.2.3 and section 3.2.4.

### 3.2.3 SFM-based pedestrian model

In complex urban scenarios, behavior of a pedestrian is affected by various types of traffic participants, which in most cases are surrounding pedestrians and vehicles.

Figure 3.7 shows a simple illustration of SFM-based model for pedestrian 1. The pedestrian 1 is affected by surrounding elements which lead to his changing of the path to the destination. These effects can be viewed as some force exerting on the pedestrian 1, such as the force from vehicle  $F_{ev2p}$ , the force from other pedestrians  $F_{p2p}$  and the force from destination  $F_{des2p}$ . However, the interaction force is only based on the current states of the traffic participants which means the historical data is ignored. To some extent, the SFM-based CA process is Markov-like process. So, SFM-based dynamic model is suitable in the proposed scenario.

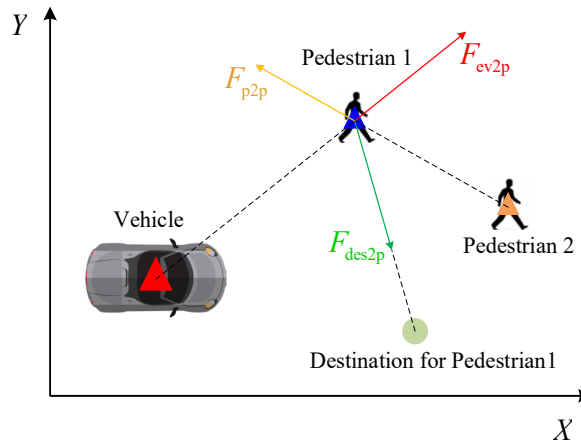


Figure 3.7 SFM-based pedestrian model

Pedestrians are regarded as a point mass in the social force model, whose dynamic is defined as:

$$\dot{X}_{ped} = v_{ped}^X \quad (88)$$

$$\dot{Y}_{ped} = v_{ped}^Y \quad (89)$$

$$\dot{v}_{ped}^X = a_{ped}^X = \frac{F_{ped}^{X,t}}{m_{ped}} \quad (90)$$

$$\dot{v}_{ped}^Y = a_{ped}^Y = \frac{F_{ped}^{Y,t}}{m_{ped}} \quad (91)$$

where superscript  $[X, Y]$  are the Cartesian coordinates that belong to the world axis frame.  $F_{ped}^{X,t}$ ,  $F_{ped}^{Y,t}$  are the total force imposing on pedestrian at current time  $t$  in lateral and longitudinal axes, respectively.  $m_{ped}$  represents the mass of pedestrian. The total force  $\vec{F}_{ped}^t$  at time  $t$ , that is formed by  $F_{ped}^{Y,t}$  and  $F_{ped}^{X,t}$  is the summation of multisource effect:

$$\vec{F}_{\text{ped}}^t = \vec{F}_{\text{ev2p}}^t + \vec{F}_{\text{p2p}}^t + \vec{F}_{\text{des2p}}^t + \vec{F}_{\text{noise}}^t \quad (92)$$

where  $\vec{F}_{\text{ev2p}}^t$  represents the force from interaction with vehicle.  $\vec{F}_{\text{des2p}}^t$  is the force from destination which is simplified in this study to the pedestrian's willingness to keep the initial speed constant.  $\vec{F}_{\text{p2p}}^t$  is pedestrian-pedestrian interaction force. As this study mainly focus on CA avoidance strategies for vehicle, and the scenario given by Figure 3.2 only contains one pedestrian and this section mainly focus on designing an SFM-based vehicle CA strategy. So, the interaction among pedestrians  $\vec{F}_{\text{p2p}}^t$  is ignored here. Besides, the force model cannot fully generalize all factors that can affect pedestrians, so a Gaussian distribution-based noise  $\vec{F}_{\text{noise}}^t$  is added to SFM-based pedestrian model to simulate some uncertainty.

And components of  $\vec{F}_{\text{ped}}^t$  are defined as:

$$\vec{F}_{\text{ev2p}}^t = f_{\text{exp}}(d_{\text{ev2p}}^t, A_{\text{ev2p}}, B_{\text{ev2p}}) A_{\text{sin}}(\phi_{\text{ev2p}}^t, \lambda_{\text{ev2p}}) \quad (93)$$

$$\vec{F}_{\text{des2p}}^t = \beta_{\text{ev2p}} \cdot \kappa_{\text{des2p}} \cdot (\vec{v}_{\text{ped}}^t - \vec{v}_{\text{ped}}^0) \quad (94)$$

$$\vec{F}_{\text{noise}}^t = \kappa_{\text{noi}} \cdot \chi, \chi \sim N(\mu, \sigma) \quad (95)$$

where  $\kappa_{\text{des2p}}$  is a feedback gain for the destination force,  $v_{\text{ped}}^0 = v_{\text{ped}}^{\text{ini}}$  represents a pedestrian desired speed which is assumed as the initial speed and  $\kappa_{\text{noi}}$  is a gain for Gaussian based white noise (where  $\mu = 0$  and  $\sigma = 1$ ).

The other parameters of each force are described as following:

$$f_{\text{exp}} = A_{\text{ev2p}} \cdot e^{(-B_{\text{ev2p}} \cdot d_{\text{ev2p}}^t)} \quad (96)$$

This function represents a decaying function that the magnitude of force  $F_{\text{ev2p}}^t$  decreases monotonically as the distance between the ego pedestrian to the target agent increases. Besides, there are some other forms of decaying function such as linear decaying in addition to exponential decaying. The exponential decaying is more accurate in simulating the interaction of vehicles and pedestrians while linear decaying is more commonly used in pedestrian-pedestrian interaction.  $d_{\text{ev2p}}^t$  is a variable representing the distance between the ego pedestrian and the target agent, and  $A_{\text{ev2p}}, B_{\text{ev2p}}$  are parameters adjusting the characteristics of the decaying function. It can be shown visually in Figure 3.8 that with the  $d_{\text{ev2p}}^t$  increases, the force from vehicle decreases. Besides, considering pedestrian owns

different shapes, we set a unified safety radius as  $0.5\text{ m}$  (the offset shown in Figure 3.8) for convenience.

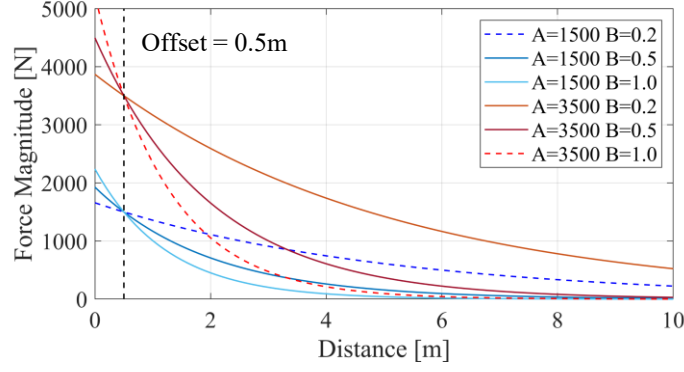


**Figure 3.8 Decaying function**

The anisotropy function is defined as:

$$\mathbf{A}_{\text{sin}} = \lambda_{\text{ev2p}} + (1 - \lambda_{\text{ev2p}}) \frac{1 + \cos|\phi_{\text{ev2p}}^t|}{2} \quad (97)$$

This function represents anisotropy function that its output is a scalar ranging from 0 to 1, representing how the influence attenuates as the angle between pedestrian's walking direction and his direction to the target agent increases. Besides,  $\phi_{\text{ev2p}}^t \in [-\pi \quad \pi]$  is a variable representing the interaction angle, shown as Figure 3.9, and  $\lambda_{\text{ev2p}}$  is the parameter adjusting the anisotropy characteristics[48].

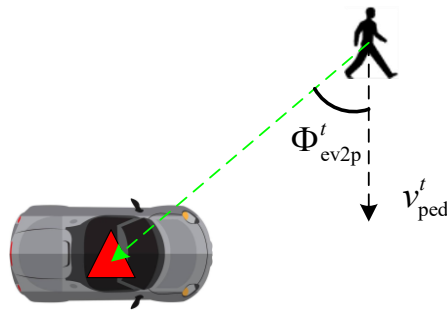


**Figure 3.9 Interaction angle  $\phi_{\text{ev2p}}^t$**

Figure 3.10 shows a virtually trend of anisotropy value based on different interaction angle  $\phi_{\text{ev2p}}^t$  and different  $\lambda_{\text{ev2p}}$ . Simply, considering the same  $\lambda_{\text{ev2p}}$ , when the vehicle is directly in front of the pedestrian, the force from vehicle to pedestrian  $F_{\text{ev2p}}^t$  is the largest, and when a vehicle is directly behind

a pedestrian, the magnitude of force  $F_{ev2p}^t$  will be smallest.

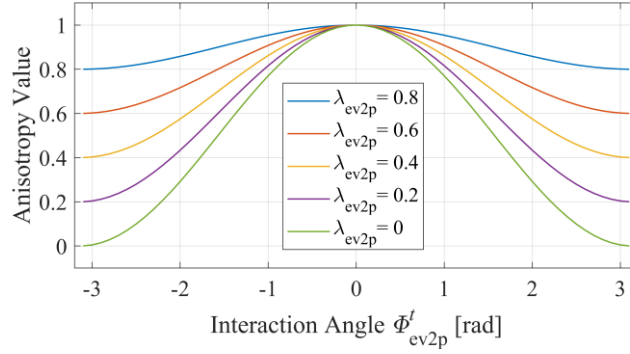


**Figure 3.10 anisotropy function**

$$\beta_{ev2p} = \max \left\{ \min \left\{ \frac{d_{ev2p}^t - d_{ped}^{swi}}{d_{ped}^{swi}} \right\}, 0 \right\} \quad (98)$$

This represents a switch function which allows the pedestrian to switch from mainly focusing on reaching the destination to avoiding the collision with vehicle. This function will be explained in detail in section of SFM based vehicle model (section 3.2.4). And the calibrated parameters of SFM-based pedestrian model are provided by [48].

In previous researches, when considering vehicle-pedestrian interaction during CA process, the movement of pedestrians was usually considered to be uniform or moving according to given profiles of speed and trajectory. However, in actual scenarios, pedestrian movement will be affected by different external factors. To show the difference bringing by noise  $\vec{F}_{noise}^t$ , a comparison based on scenario in Figure 2.23 is given. The initial position and speed of pedestrian are fixed, that  $v_{ped}$ ,  $d_{ped2C}$  are equal to  $1.2 \text{ m/s}$  and  $4\text{m}$ , respectively. The initial position of vehicle is fixed that  $d_{veh2C}$  is  $20\text{m}$ . Only the initial speed of vehicle is changed in different iterations. With different initial speed of vehicle (varies from  $3.5 \text{ m/s}$  to  $10 \text{ m/s}$  with an interval of  $0.1 \text{ m/s}$ ), the minimum distance comparison, that is the minimum distance between a constant speed vehicle and pedestrian during the whole CA process, of the total force with and without noise item is shown as Figure 3.11

It is assumed that if the minimum distance between vehicle and pedestrian (defined as  $\min D_{ev2p}$ ) is less than  $0.5 \text{ m}$  (defined as  $\min D_{safe}$ , as the green line shows), the collision occurs. When there is no noise item, the pedestrian motion can be considered as a certainty motion which is only decided by the initial situation of vehicle and pedestrian (such as initial speed and position of vehicle, initial speed

and position of pedestrian). This is impractical. When the noise item is added, the pedestrian motion is more reasonable. At the same time, the noise item can be interpreted as the influence of unquantifiable external or internal factors such as weather conditions or psychological factors on pedestrian motion.

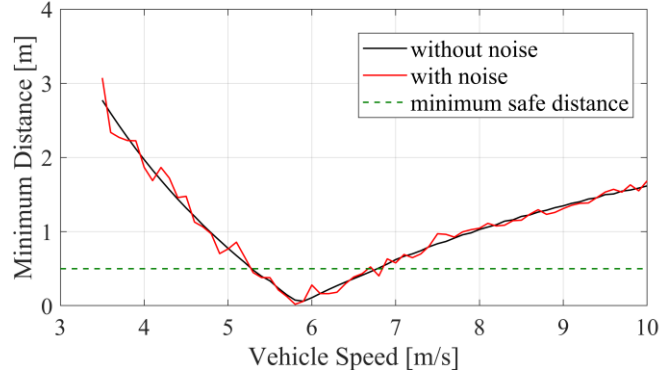


**Figure 3.11 Minimum interaction distance comparison**

### 3.2.4 SFM-based vehicle model

In most previous researches, social force model is mainly used in pedestrian dynamic modeling. The vehicle motion generally considered to be along a given trajectory and provide the vehicle-based force for optimizing the SFM based pedestrian model [65]. Although a small group of researchers also considered SFM-based vehicle models, like [3] that changing lane is determined by strategy (not by force balance), which means the SF only provides a signal to identify whether the current situation poses a risk of collision without directly affecting lane changing. Meanwhile, only the vehicle-vehicle interaction is under consideration rather considering the interaction between vehicle and pedestrians.

Based on the proposed scenario, a vehicle longitudinal dynamic model that is fully controlled by SFM is proposed, which is a modified version of SF based pedestrian model. It is defined as:

$$\dot{X}_{ev} = v_{ev}^X \quad (99)$$

$$\dot{Y}_{ev} = v_{ev}^Y \quad (100)$$

$$\dot{v}_{ev}^X = a_{ev}^X = \frac{F_{ev}^{X,t}}{m_{ev}} \quad (101)$$

$$\dot{v}_{ev}^Y = a_{ev}^Y = \frac{F_{ev}^{Y,t}}{m_{ev}} \quad (102)$$

where  $F_{ev}^{X,t}$  and  $F_{ev}^{Y,t}$  are the components of the total force  $\vec{F}_{ev}^t$  exerted on ego vehicle in  $[X, Y]$  direction.

$$\vec{F}_{ev}^t = \vec{F}_{p2ev}^{i,t} + \vec{F}_{des2ev}^t \quad (103)$$

In SFM-based vehicle model, the definition of  $F_{p2ev}^{i,t}$  is similar with that of pedestrian, and the force from destination  $\vec{F}_{des2ev}^t$  could be considered as the force that requires vehicle to track the reference trajectory, which are established as following:

$$\vec{F}_{p2ev}^t = f_{exp}(d_{p2ev}^t, A_{p2ev}, B_{p2ev}) \mathbf{A}_{sin}(\phi_{p2ev}^t, \lambda_{p2ev}) \quad (104)$$

$$\vec{F}_{des2ev}^t = \beta_{p2ev} \cdot \kappa_{des2ev} \cdot \omega_v(\vec{v}_{ev}^t - \vec{v}_{ref4ev}^t) \cdot \omega_p(\vec{p}_{ev}^t - \vec{p}_{ev}^0) \quad (105)$$

where  $\vec{v}_{ref4ev}^t$  is the reference speed for current time  $t$ .  $\omega_v$  and  $\omega_p$  are the weight of tracking current reference speed and the weight of tracking reference path, respectively. This research only considers the upper-layer obstacle avoidance strategy, it is assumed that the ego vehicle will perfectly execute the acceleration and deceleration caused by SFM. Therefore, the force of noise  $\vec{F}_{noise}^t$  is removed.

Consider longitudinal and lateral motions of the vehicle for coupling and to reduce the influence of its profile on the interaction force as well as simplifying the calculation, the mass point model is adopted for ego vehicle, which is defined as:

$$\dot{X}_{ev}^t = v_{ev}^{x,t} \cos \varphi - v_{ev}^{y,t} \sin \varphi \quad (106)$$

$$\dot{Y}_{ev}^t = v_{ev}^{x,t} \sin \varphi + v_{ev}^{y,t} \cos \varphi \quad (107)$$

$$m_{ev} a_{ev}^{Y,t} = F_{ev}^{Y,t} \quad (108)$$

$$m_{ev} a_{ev}^{X,t} = F_{ev}^{X,t} \quad (109)$$

where  $\varphi$  is the yaw angle, and the resultant force on the vehicle tires should satisfy the friction circle constraint:

$$(a_{ev}^{X,t})^2 + (a_{ev}^{Y,t})^2 \leq (k\mu g)^2 \quad (110)$$

where  $\mu$  is the road friction coefficient and  $k \leq 1$  is a gain to limit saturation of tire friction.

After both SFM-based vehicle and pedestrian model are established above, the **Problem 2**, which is defined as:

*Given the current state of ego vehicle  $S_{ev}^t$ , pedestrian  $S_{ped}^t$  and the limit conditions (68) (74), to calculate  $S_{ev}^{t+1}$  and  $S_{ped}^{t+1}$  based on the interaction between these two participants*

is successfully solved. Then we aim to solve the **Problem 1**, which is defined as:

*Given the determinate initial state  $\mathbb{S}^0$  and reward function  $R$  to calculate the optimal maneuver profile  $m_{ev}^{*,t}$ .*

Firstly, we make a **Reconstruction** for **Problem 1** since the SFM-based vehicle model is established:

#### Problem 1 Reconstruction:

Considering that SFM model generates force that is exerted on vehicle and causes the changing on vehicle trajectory, and the force is continues. Therefore, the optimal maneuver  $m_{ev}^*$  is regarded to be determined by initial system state  $\mathbb{S}^0$  and the optimal force set  $\vec{F}_{ev}^*$  is determined by related SFM parameters, the solution of  $m_{ev}^*$  could be transformed into the optimization of those parameters, which is written as  $\Phi_{ev}^*$ , in SFM-based vehicle model with the same constraints (68)-(74).

As the definition of original SFM-based model (96)-(98) and (105), there are 8 parameters that could be optimized which are:

- (1) Parameters  $A_{p2ev}, B_{p2ev}$  of function  $f_{exp}$  in force from pedestrian  $\vec{F}_{p2ev}^{i,t}$ .  $A_{p2ev}$  mainly provides the magnitude of  $\vec{F}_{p2ev}^{i,t}$  and  $B_{p2ev}$  indicates rate of decaying in distance;
- (2) Parameter  $\lambda_{p2ev}$  of function  $\mathbf{A}_{sin}$  in  $\vec{F}_{p2ev}^{i,t}$ , it mainly indicates rate of decaying in direction;
- (3) Parameter  $\kappa_{des2ev}$  of force from destination  $\vec{F}_{des2ev}^t$ , it provides the magnitude of  $F_{des2ev}^t$ ;
- (4) Parameter  $d_{ev}^{swi}$  of function  $\beta_{p2ev}^i$  in  $\vec{F}_{des2ev}^t$ , it determines the switch distance.
- (5) Parameters  $\omega_v, \omega_p$  and  $\vec{v}_{ref4ev}^t$  of force from destination  $\vec{F}_{des2ev}^t$ , which give the tracking weights and the reference velocity, respectively.

So, the initial **Problem 1** is transformed from directly calculating optimal maneuver  $m_{ev}^*$  to searching the optimal parameters series  $\Phi_{ev}^*$  for SFM-based vehicle model where  $\Phi_{ev}^*$  is defined as:

$$\Phi_{ev}^* = [A_{p2ev}^*, B_{p2ev}^*, \lambda_{p2ev}^*, \kappa_{des2ev}^*, d_{ev}^{swi,*}, \omega_v^*, \omega_p^*, \vec{v}_{ref4ev}^{t,*}] \quad (111)$$

In the following section, we will introduce methods of obtain  $\Phi_{ev}^*$ .

### 3.3 SFM-based solution for ego vehicle interacting with multi-pedestrians

For a better view, here we re-draw Figure 2.25 in this section.

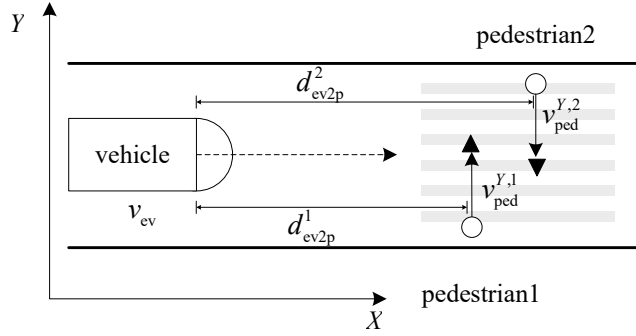


Figure 2.25 Case of multiple pedestrians

Firstly, we consider a simply interaction scenario between ego vehicle and multi-pedestrians, shown as Figure 2.25 in section 2.4.2. In the following section, we aim to solve the **reconstructed problem 1** and give a comparison of SFM-based CA strategy and MPC-based CA strategy when ego vehicle interacts with multi-pedestrians.

Initial setting is defined as following:

- (1) Vehicle initial speed  $v_{ev}^{ini}$  is  $6\text{ m/s}$  and the range of acceleration for vehicle is  $[-5\text{ m/s}^2 \quad 2.5\text{ m/s}^2]$ ;
- (2) The distance between vehicle and pedestrian 1  $d_{ev2ped}^1$  is  $20\text{ m}$  while the distance between vehicle and pedestrian 2  $d_{ev2p}^2$  is  $22\text{ m}$ ;
- (3) Vehicle mass  $m_{ev}$  is  $1700\text{ kg}$  while both pedestrians mass  $m_{ped}^1$  and  $m_{ped}^2$  are  $75\text{ kg}$ ;
- (4) Pedestrian 1 initial speed  $v_{ped}^{Y,1,ini}$  is  $1.2\text{ m/s}$  and Pedestrian 2 initial speed  $v_{ped}^{Y,2,ini}$  is  $1\text{ m/s}$ .

The range of acceleration for pedestrians is  $[-2.5\text{ m/s}^2 \quad 2.5\text{ m/s}^2]$ ;

- (5) Driveway is dry road with a good vision whose road friction coefficient  $\mu$  is  $0.8$ ;
- (6) The distance to collision point of pedestrian 1  $d_{ped2p}^1$  and pedestrian 2  $d_{ped2p}^2$  are both equal to  $4\text{ m}$ .

As we only consider the longitudinal speed of the ego vehicle in this section, the force from destination  $\vec{F}_{des2ev}^t$  (Equation (105)) is simplified as a longitudinal scalar:

$$F_{des2ev}^t = \beta_{p2ev} \cdot \kappa_{des2ev} \cdot \omega_v (v_{ev}^{x,t} - v_{ev}^{x,0}) \quad (112)$$

As shown in Figure 3.12, in SFM based vehicle model, the form of  $\beta_{des2ev}$  is defined as:

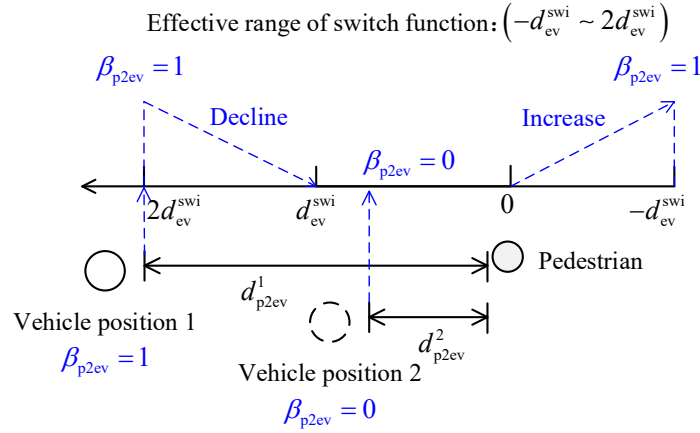


Figure 3.12 Switch function of  $\beta_{p2ev}^i$

The magnitude of  $\beta_{p2ev}$  is based on the distance between vehicle and the  $i^{\text{th}}$  pedestrian at time instant  $t$ , which is defined as

$$d_{p2ev}^{t,i,X} = X_{ped}^{t,i} - X_{ev}^t \quad (113)$$

where  $X_{ped}^{t,i}$  and  $X_{ev}^t$  are the  $X$ -axis coordinate of the  $i^{\text{th}}$  pedestrian and the ego vehicle, respectively.

And the definition of  $\beta_{p2ev}$  is as following:

- (1) If  $d_{p2ev}^{t,i,X} > 2d_{ev}^{swi}$  or  $d_{p2ev}^{t,i,X} \leq -d_{ev}^{swi}$ , then

$$\beta_{p2ev} = 1;$$

- (2) If  $2d_{ev}^{swi} \geq d_{p2ev}^{t,i,X} > d_{ev}^{swi}$ , then

$$\beta_{p2ev} = d_{p2ev}^{t,i,X} - d_{ev}^{swi} / d_{ev}^{swi} \quad (114)$$

- (3) If  $d_{ev}^{swi} \geq d_{p2ev}^{t,i,X} > 0$ , then

$$\beta_{p2ev} = 0;$$

- (4) If  $0 \geq d_{p2ev}^{t,i,X} > -d_{ev}^{swi}$ , then

$$\beta_{p2ev} = |d_{p2ev}^{t,i,X}| / d_{ev}^{swi} \quad (115)$$

The same as parameter  $d_{ped}^{swi}$  of pedestrian model,  $d_{ev}^{swi}$  allows vehicle to switch from mainly

focusing on reaching the destination to avoiding the collision with pedestrian. If  $\beta_{p2ev}^i$  is zero, it means the force from destination does not exist that the only force loaded on the vehicle comes from the pedestrian when ego vehicle gets too close to pedestrians.

Besides, considering that different road adhesion conditions will heavily affect the switch distance of vehicle, this parameter is adaptive with different road friction coefficient  $\mu$ :

$$d_{ev}^{adaSwi} = d_{ev}^{swi} / \mu \quad (116)$$

When the ego vehicle approaches a pedestrian,  $\beta_{p2ev}$  will decrease from 1 to 0 as the distance between the two interactors decreases. And when  $\beta_{p2ev}$  is equal to 0, that means the force from destination will not affect the movement of the vehicle as the  $F_{des2ev}^t$  is zero. Then only the force from pedestrians will affect the motion of ego vehicle.

Similarly, the total force from different pedestrian  $\vec{F}_{p2ev}^t$  is also simplified as a longitudinal scalar  $F_{p2ev}^t$  in this section. Besides, when calculating the total force from different pedestrians  $F_{p2ev}^t$ , for safety, it is defined as:

- (1) If the force from different pedestrians are in the same direction,

$$F_{p2ev}^t = \max F_{p2ev}^{t,i} \quad (117)$$

- (2) If the force from different pedestrians are in different direction,

$$F_{p2ev}^t = \min F_{p2ev}^{t,i} \quad (118)$$

which means the maximum deceleration force for ego vehicle will be selected in this case.

Since the form of  $\vec{F}_{p2ev}^t$  and  $\vec{F}_{des2ev}^t$  are all simplified as scalar, the solution  $\Phi_{ev}^*$  of **reconstructed problem 1** here is also simplified as:

$$\Phi_{ev}^{*,1} = [A_{p2ev}^*, B_{p2ev}^*, \lambda_{p2ev}^*, \kappa_{des2ev}^*, d_{ev}^{swi,*}] \quad (119)$$

The parameter  $\omega_v$  could be merged into  $\kappa_{des2ev}^*$  for reducing optimization consume and the  $\vec{v}_{ref4ev}^{t,*}$  is considered replacing by initial speed of the ego vehicle  $v_{ev}^{ini}$ .

### 3.3.1 Particle swarm optimization-based parameters calibration

As optimization problem **reconstructed problem 1** is highly non-convex, we consider using particle swarm optimization (PSO) to search solution. The PSO [66] is a random search algorithm based

global search algorithm that simulates natural biological activities and swarm intelligence. It is well suitable for finding the (near)-optimal solutions to complex systems because it has no special requirement for the continuity of the optimization problem. During parameters optimization in this study, simulated annealing (SA) and adaptive weights/learning rates are adopted based on basic PSO, hence possibly being benefit to overcoming the local minima problem.

Generally, we need to define a swarm of particles when using PSO to search optimal solution, such as:

$$\Theta_i = (\Theta_{i1}, \Theta_{i2}, \dots, \Theta_{iD}), i = 1, 2, \dots, N \quad (120)$$

where  $N$  is the total number of particles adopting for searching,  $D$  represents the dimension of optimization problem. For  $\Phi_{ev}^*$  in Equation (111),  $D$  is equal to 8.

For particles, they own different position  $X$  and speed  $v$  in each iteration:

$$X_i = (X_{i1}, X_{i2}, \dots, X_{iD}), i = 1, 2, \dots, N \quad (121)$$

$$v_i = (v_{i1}, v_{i2}, \dots, v_{iD}), i = 1, 2, \dots, N \quad (122)$$

The iterations of velocity and position are defined as:

$$v_i(k+1) = w \cdot v(k) + c_1 r_1 [pbest_i(k) - X_i(k)] + c_2 r_2 [gbest_i(k) - X_i(k)] \quad (123)$$

$$X_i(k+1) = X_i(k) + v_i(k+1) \quad (124)$$

where  $w$  is the inertia weight,  $c_1$  is individual learning rate and  $c_2$  is group learning rate.  $r_1, r_2 \in [0,1]$  represent a random number for increasing the randomness of search process.  $pbest_i(k)$  is the historical optimal position of particle  $i$  in the  $k$ -th iteration, that is, the optimal solution obtained by searching for the  $i$ -th particle (individual) after the  $k$ -th iteration.  $gbest_i(k)$  is the historical optimal position of the group in the  $k$ -th iteration, that is, the optimal solution in the entire particle group after the  $k$ -th iteration.

For **reconstructed problem 1** of section 3.3, the dimension  $D$  is 5 according to Equation (119). Therefore, each particle in swarm  $\Theta_i = (\Theta_{i1}, \Theta_{i2}, \dots, \Theta_{i5}), i = 1, 2, \dots, N$  with an initial random speed  $v_i = (v_{i1}, v_{i2}, \dots, v_{i5}), i = 1, 2, \dots, N$  will traversal the whole CA process. Then the performance of  $\Theta_i$  was evaluated by a loss function. And when iterations of position and speed of each particle is reached the set limit or the cost of loss function is acceptable, it is considered that the optimal set  $\Theta_i^{opt}$  is the solution set, shown as Figure 3.13.

In addition, lower bounds and upper bounds were added to ensure that in the process of calibration, the parameters do not go beyond unrealistic values, as shown in Table 3-1. The total number of particles

in the PSO was set to 64, which is sufficient for the calibration.

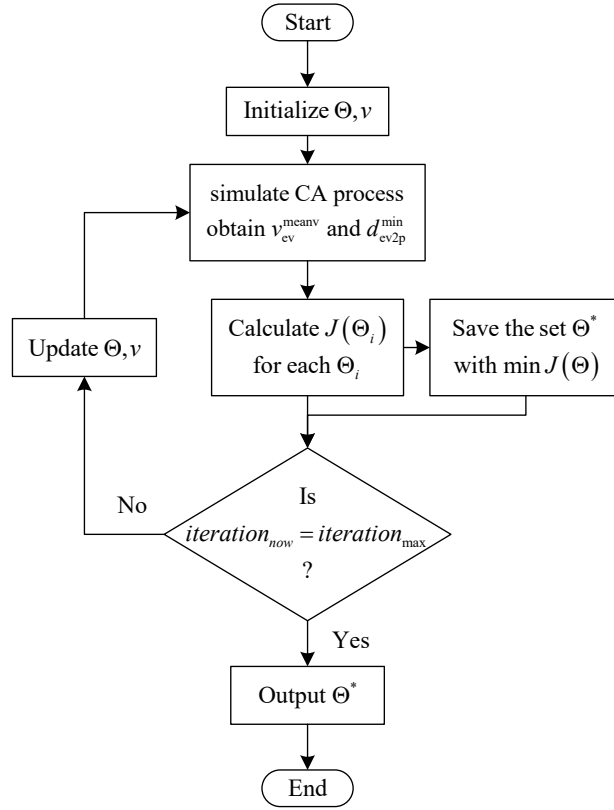


Figure 3.13 Optimization process of PSO

The loss function is defined as:

$$J(\theta_i) = Q^{PSO} \cdot \frac{1}{v_{ev}^{meanv,i}} + R^{PSO} \cdot \frac{1}{d_{ev2p}^{min,i}} \quad (125)$$

$$\text{where } \begin{cases} R^{PSO} = R^{PSO}, \text{ if } d_{ev2p}^{min,i} \geq \min D_{safe} \\ R^{PSO} = 100R^{PSO}, \text{ if } d_{ev2p}^{min,i} < \min D_{safe} \end{cases} \quad (126)$$

where  $v_{ev}^{meanv,i}$  is the mean speed of vehicle and  $d_{ev2p}^{min,i}$  is the minimum distance between vehicle and pedestrians during the whole CA process under the particular parameter set  $\Theta_i$ . This loss function requires ego vehicle passing pedestrians with less deceleration cost under promise of safe avoidance.

The  $R^{PSO}$  is a very small constant when the  $d_{ev2p}^{min,i}$  is bigger than  $\min D_{safe}$  at which time ego vehicle need a series of optimized parameter for pursuing higher passing speed. However, when  $d_{ev2p}^{min,i}$  is smaller than  $\min D_{safe}$ ,  $R^{PSO}$  will be extremely larger (actually the value of  $R^{PSO}$  at this time does

not have to be 100 times of original value, as long as it is large enough), the priority of being optimized parameter series is to ensuring that the minimum distance between ego vehicle and pedestrians is an acceptable safe distance.

### 3.3.2 Physical explanation of parameters optimization

The final optimized value of each parameter is also shown in Table 3-1.

The total iteration time is 500 times, the changes of values of parameters and loss with the iteration are shown in the Figure 3.14. The final value of optimized parameters of social force can be explained physically as following.

**Table 3-1 Range and optimized value of parameters**

Parameters	Range	Optimized value	Unit
$A_{p2ev}$	[0 5000]	1126.6347	$N$
$B_{p2ev}$	[0 1]	0.010920247	-
$\lambda_{p2ev}$	[0 1]	0.3541411	-
$\kappa_{des2ev}$	[2000 4000]	3203.0952	-
$d_{ev}^{swi}$	[8 20]	11.033603	$m$

For  $A_{p2ev}$  and  $B_{p2ev}$ , combined with the boundary of each parameter, the final values of these two parameters tend to be close to lower bounds, as shown in Figure 3.14 (a) and Figure 3.14 (b). The reasons for these results are explained as following. Considering Equation (93),(96) and (104), it indicates that the magnitude of  $F_{p2ev}^{i,t}$  is mainly provided by  $A_{p2ev}$ , and the  $B_{p2ev}$  mainly indicates rate of decaying in distance, the illustration of decaying function  $f_{exp}$  is shown as Fig. 14. When the other parameters are fixed, the only thing that affects the motion of the vehicle is the decaying function  $f_{exp}$ .

Considering about the form of loss function (the Equation (125)), there are two option for ego vehicle to meet the requirement of safely avoiding pedestrians while keeping a relative high passing speed, that are:

**Strategy 1:** a lager force magnitude when being close to pedestrian but a drastic decay amplitude,

shown as the red dotted line 1 in Figure 3.15(a);

**Strategy 2:** a small force magnitude when being close to pedestrian but a gentle decay amplitude, shown as the blue dotted line 2 in Figure 3.15(b).

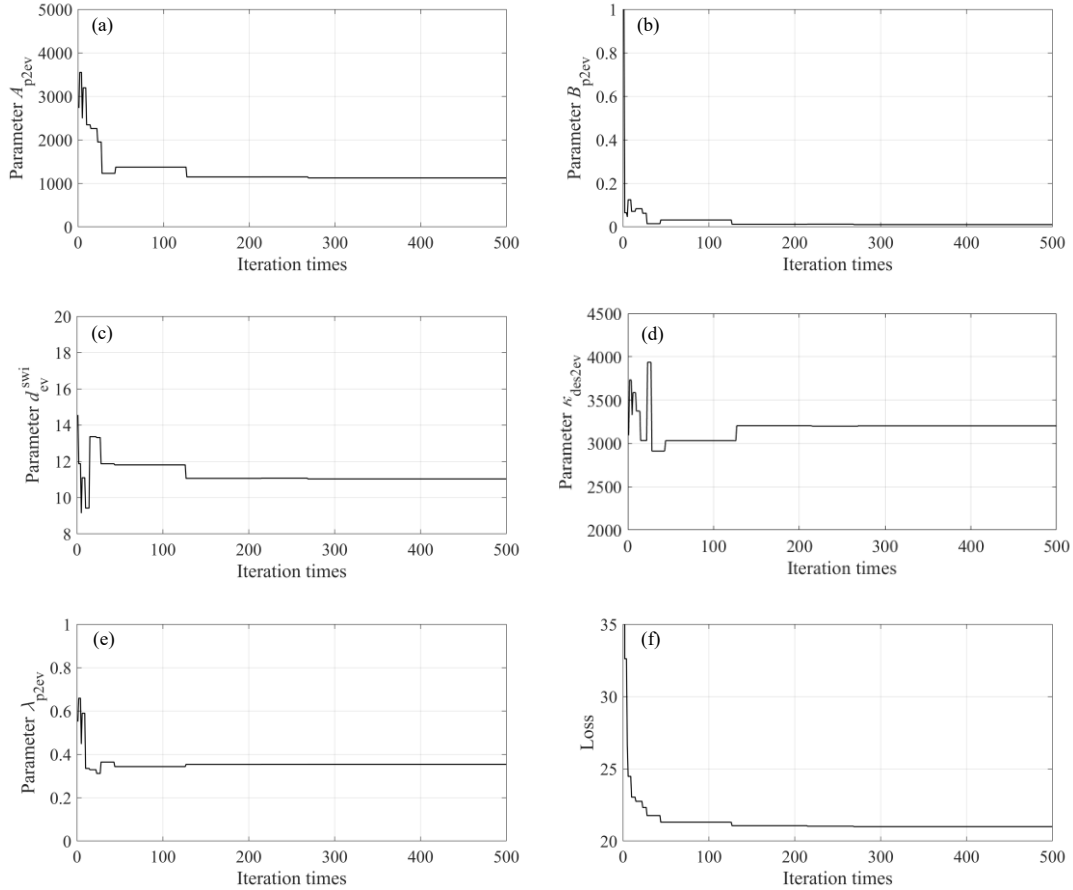


**Figure 3.14 Convergence process of SFM parameters: (a) Convergence process of  $A_{p2ev}$ ; (b) Convergence process of  $B_{p2ev}$ ; (c) Convergence process of  $\lambda_{p2ev}$ ; (d) Convergence process of  $\kappa_{des2ev}$ ; (e) Convergence process of  $d_{ev}^{swi}$ ; (f) Change of loss.**

However, considering the maximum limit of the deceleration for ego vehicle in populated traffic sections and passenger comfort, when the strategy 1 is chosen, it may lead to that the minimum distance between ego vehicle and pedestrian tend towards the danger zone.

When fixing other parameters and only  $A_{p2ev}$  and  $B_{p2ev}$  is took into consideration, a 3-D surface plot was made to illustrate the loss changes under different values of  $A_{p2ev}$  and  $B_{p2ev}$ , as shown in Figure 3.18(a). And Figure 3.18 (b) shows the value of these two parameters around the

minimum loss, which also confirms the above qualitative analysis.

For  $\lambda_{p2ev}$ , it is a parameter belong to anisotropy function  $A_{sin}$  and used to adjust the anisotropy characteristics.  $A_{sin}$  takes input as the interaction angle  $\phi_{p2ev}^{i,t}$  between the ego vehicle's moving direction and the direction to the target agent that is interacting with the ego vehicle. The output of anisotropy function is a scalar ranging from 0 to 1, representing how the influence attenuates as the angle increases [48].

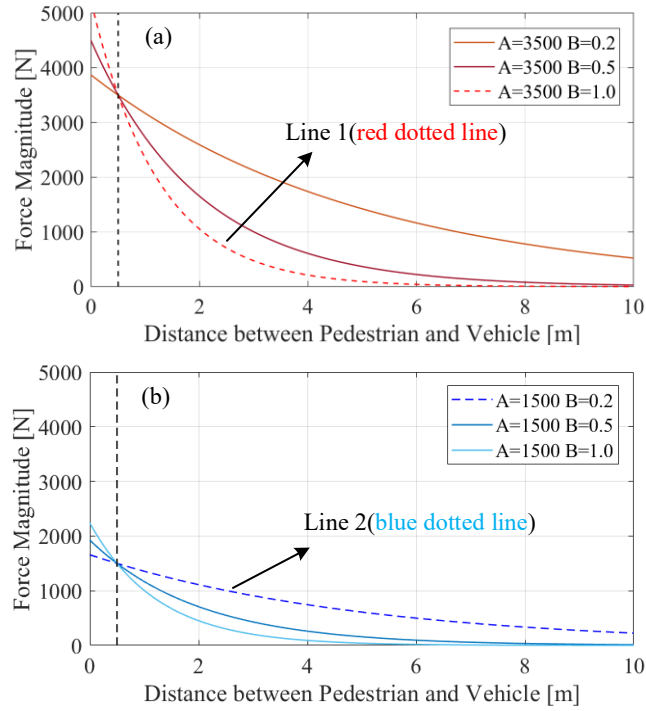


**Figure 3.15 Analysis of Parameters in Decaying Function: (a) Case of  $A_{p2ev} = 3500$ ; (b) Case of  $A_{p2ev} = 1500$**

In this type of anisotropy function, the severity of the decay increases as  $\lambda_{p2ev}$  decreases. When ego vehicle runs in the proposed scenario, as shown in Figure 2.25, the collected interaction angel between vehicle and pedestrian 1 ( $\phi_{p2ev}^{1,t}$ ) or vehicle and pedestrian 2 ( $\phi_{p2ev}^{2,t}$ ) in most time ( $> 97.7\%$  of total time) are in the range of  $(-1,1)$ , as shown in Figure 3.16.

Therefore, combining with the anisotropy value under different angle shown by Figure 3.17, the anisotropy value is close to 1 during the whole CA process, that results in the choice of  $\lambda_{p2ev}$  value

has no significant effect on  $F_{p2ev}^{i,t}$ . And this analysis can be verified by Figure 3.18 (c) and Figure 3.18 (d), when an optimized  $A_{p2ev}$  is determined, the influence of different value of  $\lambda_{p2ev}$  on  $F_{p2ev}^{i,t}$  is similar.

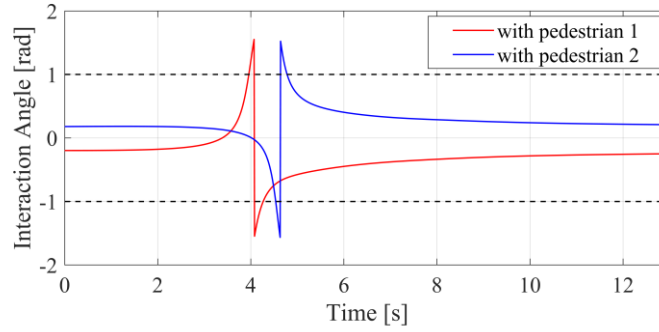


**Figure 3.16 Interaction angles between vehicle and pedestrians during the whole CA process**

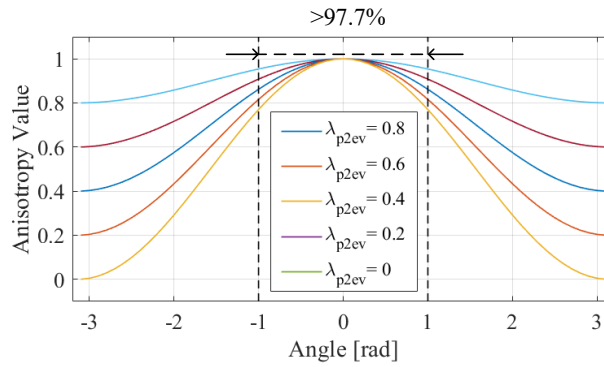


**Figure 3.17 Relation between anisotropy value and interaction angles under different  $\lambda_{p2ev}$**

For  $\kappa_{des2ev}$  and  $d_{ev}^{swi}$ , these parameters belong to the force from destination  $F_{des2ev}^t$  that this force is used to keep the vehicle tracking the reference speed, which is the initial speed (and also the maximum speed) throughout the CA process. Therefore, the  $F_{des2ev}^t$  can be considered as a driving force. When the ego vehicle expects to complete the CA process in a relative short time, it should keep this force in a relative high magnitude, which means choice of  $\kappa_{des2ev}$ , which mainly determines the magnitude of  $F_{des2ev}^t$ , should be relatively large.

Besides, according to the form of switch function  $\beta_{p2ev}^i$ ,  $d_{ev}^{swi}$  indicates the magnitude decaying distance of  $F_{des2ev}^t$ . When  $d_{ev}^{swi}$  owns a relative high value, the decaying of  $F_{des2ev}^t$  will happen sooner

which is not conducive to maintaining a high speed for ego vehicle. Therefore, the final value of  $d_{ev}^{swi}$  after optimization is close to lower bound. This qualitative analysis can be verified by Figure 3.18 (e) and Figure 3.18 (f).

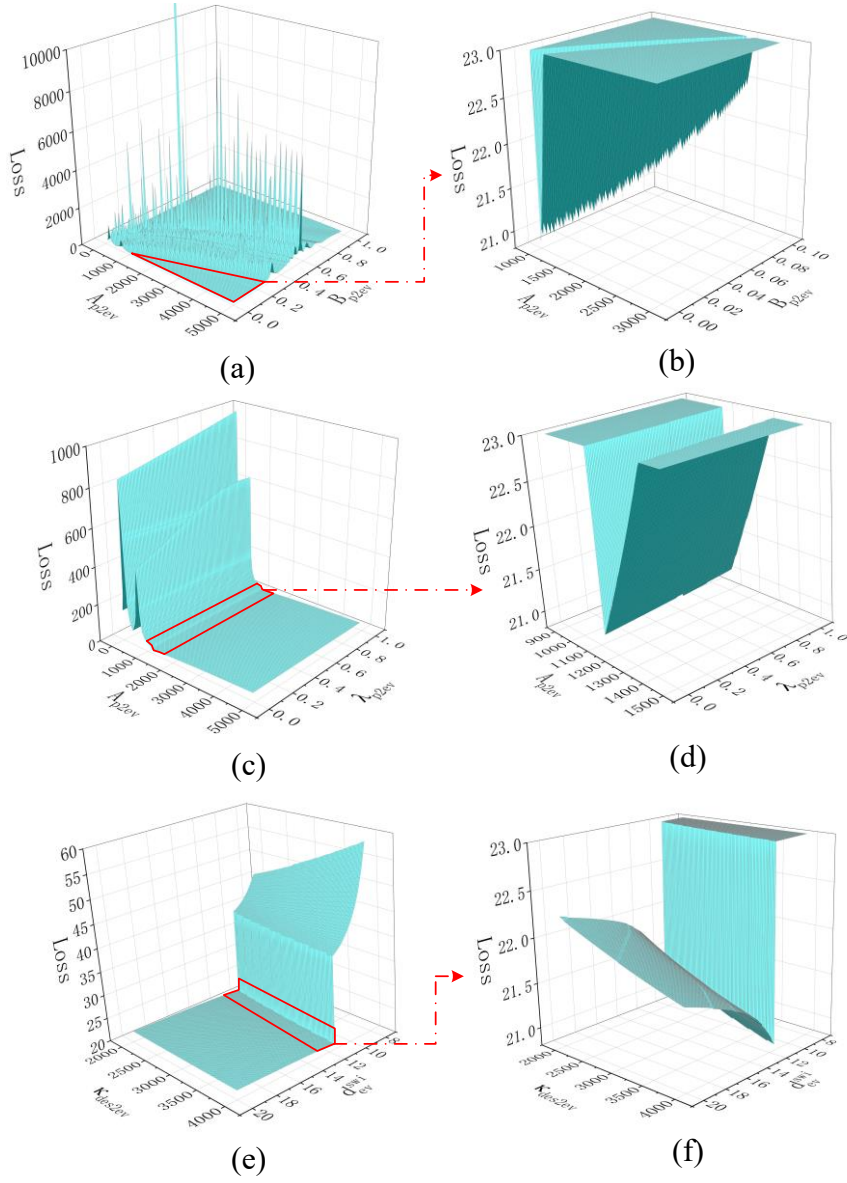


**Figure 3.18 Analysis of optimized value of SFM parameters (a) curved surface of loss when only considering  $A_{p2ev}$  and  $B_{p2ev}$ ; (b) local magnification of (a); (c) curved surface of loss when only considering  $A_{p2ev}$  and  $\lambda_{p2ev}$ ; (d) local magnification of (c); (e) curved surface of loss when only considering  $\kappa_{des2ev}$  and  $d_{ev}^{swi}$ ; (f) local magnification of (e)**

Besides, the comparison of vehicle acceleration profiles under optimized parameters of different

loss is shown as Figure 3.20(a). As the optimization iteration proceeds, the extreme value of the acceleration in the whole process is smaller, and its change tends to be more gradual. When the initial speed for each iteration remains the same, smaller and more gradual acceleration means smaller  $A_{p2ev}$  and  $B_{p2ev}$  (that can also be illustrated by Figure 3.18 (a) and Figure 3.18 (b)), which approaches a smaller loss and better performance as it is discussed before. Changes of vehicle speed and its moved distance from initial position are shown as Figure 3.20 (b) and Figure 3.20 (d), with more reasonable deceleration and acceleration provide by better optimized parameters, the mean speed over the whole CA process is larger. And as the comparison of minimum distance between ego vehicle and pedestrians shown by Figure 3.20 (c), final optimized parameters reach the best performance that ego vehicle spends less time in passing crowded intersections and closest distance between ego vehicle and pedestrians is minimum but acceptable.

The ego vehicle speed is set as relatively lager under urban crowded scenario when the initial distance between ego vehicle and 1<sup>st</sup> pedestrian is 20m. Actually, when the initial interaction distance or initial speed is changed, the optimized parameters will be different, shown as Table 3-2. When other settings are fixed and the only change is initial distance between vehicle and 1<sup>st</sup> pedestrian from 20m to 25m or initial speed of vehicle from 6 m/s to 5 m/s, the main change is the value of  $A_{p2ev}$ , which is reduced a lot compared to unchanged settings due to no drastic deceleration process is required.

And when considering more requirements of safety and real-time application, the recommended initial values of parameters for SFMC are list as Table 3-3 under the situation of the initial interaction distance is bigger than 15m and initial ego vehicle speed is smaller than 7 m/s.

**Table 3-2 Optimized value of parameters under different initial settings**

Parameters	Optimized values I	Optimized values II	Unit
	(The initial position is changed)	(The initial speed is changed)	
$A_{p2ev}$	185.946	271.439	$N$
$B_{p2ev}$	0.014	0.015	-
$\lambda_{p2ev}$	0.363	0.402	-
$\kappa_{des2ev}$	3106.788	3065.159	-
$d_{ev}^{swi}$	10.957	10.212	$m$

In Table 3-3, recommended values for some parameters are given as ranges. For  $B_{p2ev}$  and  $d_{ev}^{swi}$ , smaller values result in less passing time consume, however, their values should take larger values as the weight of safety rises. For  $\kappa_{des2ev}$ , its value and the value of the previous three parameters have the opposite effect and it will affect the re-acceleration performance of ego vehicle after passing pedestrians where a bigger value of  $\kappa_{des2ev}$  will brings more intense re-acceleration.

**Table 3-3 The recommended values of parameters**

Parameters	recommended value	Unit
$A_{p2ev}$	$f_A(d_{ev2p}^{ini}, v_{ev}^{ini})$	$N$
$B_{p2ev}$	0.01	-
$\lambda_{p2ev}$	0.4	-
$\kappa_{des2ev}$	3000 – 3200	-
$d_{ev}^{swi}$	10 – 12	$m$

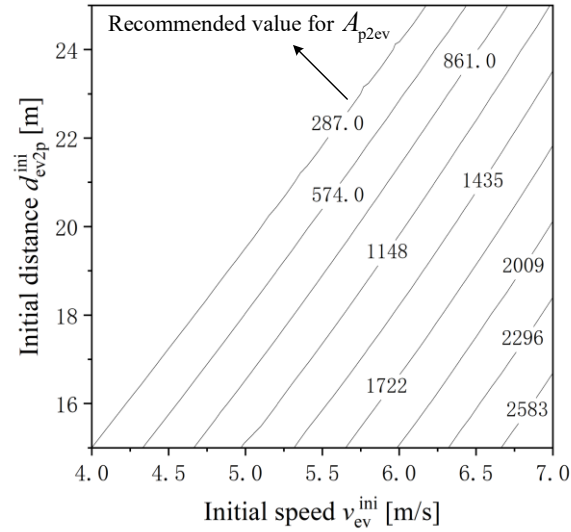


**Figure 3.19 Recommended value for  $A_{p2ev}$**

And for  $A_{p2ev}$ , this is the only parameters that is highly related to initial interaction distance  $d_{ev2p}^{ini}$  and initial speed  $v_{ev}^{ini}$  of ego vehicle. The recommended value  $f_A(d_{ev2p}^{ini}, v_{ev}^{ini})$  of  $A_{p2ev}$  under different  $d_{ev2p}^{ini}$  and  $v_{ev}^{ini}$  is given as a look-up-table when other parameters is fixed as recommended value and only  $A_{p2ev}$  is take into consideration, shown as Figure 3.19. Besides, if initial speed of ego

vehicle is smaller than  $4 \text{ m/s}$  and its initial distance to pedestrian is larger than  $16 \text{ m}$ , the recommended value for  $A_{p2ev}$  can be considered as a constant ( $= 287$ ), shown as the left above region in Figure 3.19.

In summary, with the decrease of  $d_{ev2p}^{\text{ini}}$  and the increase of  $v_{ev}^{\text{ini}}$ , the recommended  $A_{p2ev}$  should be larger to maintain a safe distance when passing pedestrians.

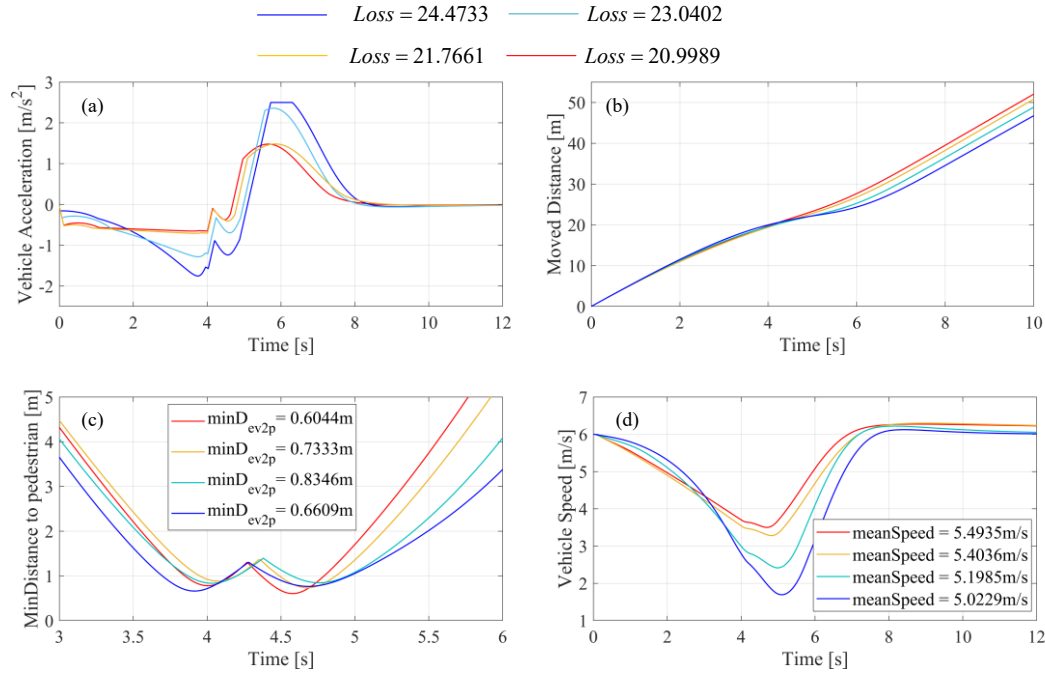


**Figure 3.20 Comparison under different loss (a) comparison of vehicle's acceleration; (b) comparison of vehicle's moved distance from initial position; (c) comparison of minimum distance between ego vehicle and pedestrians; (d) comparison of vehicle's longitudinal speed**

### 3.3.3 Comparison of simulation results between MPC and SFM

To verify and compare two different types of CA strategies, that are MPC based active strategy (in section 2.4) and SFM based passive strategy (in section 3.3-3.3.2), simulation based on MATLAB/SIMULINK is conducted. The sampling time is  $0.01\text{s}$ . The initial setting of the scenario is described in section 2.3. The simulation results for both MPC-based controller and SFM-based controller are exhibited in Figure 3.21. The minimum distances between ego vehicle and pedestrians are  $0.5866\text{m}$  of MPC and  $0.6044\text{m}$  of SFMC, which is similar to each other and both of them are

acceptable safe distance, as shown in Figure 3.21 (c). Besides, the mean passing speed of two strategies are  $4.84 \text{ m/s}$  and  $5.49 \text{ m/s}$ , respectively as shown in Figure 3.21 (d), which means both of them meet the need to reduce passing time consumption to a certain extent. So, from the simulation results, both strategies meet the initial design requirements that quickly passing pedestrians of unpredictable motion under promise of safety. Although this paper is not established to prove which strategy is better, some differences could be found from the simulation results and the reasons for difference occurs are analyzed as following.

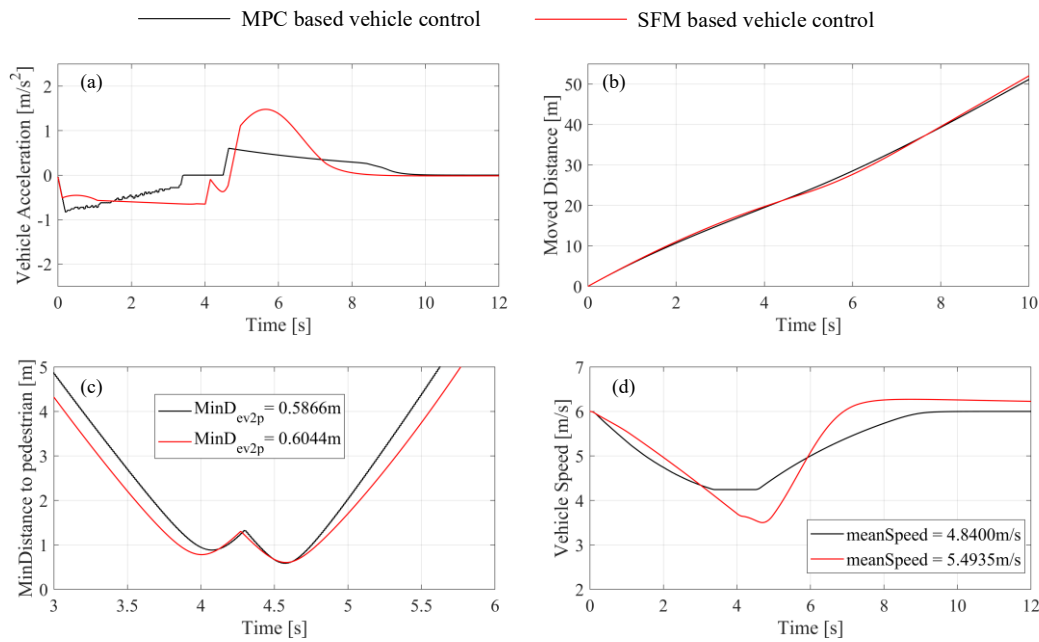


**Figure 3.21 Comparison of MPC and SFM (a) comparison of vehicle acceleration; (b) comparison of vehicle's moved distance from initial position; (c) comparison of minimum distance between ego vehicle and pedestrians; (d) comparison of vehicle's longitudinal speed**

For MPC based ego vehicle controller, a reference re-planning speed according to minimum safe distance is given at each simulation time. Due to the limited jerk, the deceleration will slowly increase at the beginning. And before passing pedestrians, because of the motion randomness of pedestrians, the vehicle's deceleration for current reference re-planning speed will be slightly changed until the minimum re-planning speed in the whole CA process is reached. In summary, ego vehicle with MPC will be required to decelerated to a minimum safe speed then keeps it unchanged. However, for SFM-

based ego vehicle controller (hereinafter referred to as SFMC), the force from pedestrians  $F_{p2ev}^{i,t}$  is always existed as a brake force before passing them. Therefore, the vehicle is required to continue decelerating by SFMC, as shown before the 5 seconds of Figure 3.21 (a) and Figure 3.21 (d).

After passed the pedestrians, the acceleration of MPC is smaller than that of SFMC because that MPC is mainly focus on approaching back to the initial speed with a small comfort acceleration but  $F_{p2ev}^{i,t}$  of SFMC is at a very large extent when it is close to pedestrian, which also result in the mean speed of SFMC is higher than that of MPC, as shown after the 5 seconds of Figure 3.21 (a) and Figure 3.21 (d).

The main difference between MPC and SFMC is in the process of generating the actual acceleration. For MPC, the actual acceleration is generated by solving the optimization problem of MPC predictive horizon in the lower layer by reference re-planning speed  $v_{ev}^{ref}$  from upper layer. The time consumed by this process depends on some factors likes the horizon length of predictive and control, the complexity of the vehicle dynamics model, etc. Besides, it also takes additional time to generate  $v_{ev}^{ref}$  in the upper layer. Although some tricks are used to calculate  $v_{ev}^{ref}$  faster, the time consumption is relatively lager compared to that of SFMC which just calculates the real acceleration by real-time force balance. And when considering the interaction of ego vehicle with more pedestrians, the time consumption will finally approach an unacceptable extent due to the ever-increasing computational complexity.

Besides, MPC will perform repeated optimization solutions for similar scenarios due to the inability to refer to past experience, which limits its application in environments with high real-time requirements. Although the same series of optimized parameters for SFMC based on one scenario may not reach optimal performance in the others, the recommended parameter values of SFM, as shown in Table 3-3, have been given in the way that the ego vehicle can avoid the pedestrians with a safe distance while maintaining a relative high passing speed. Calculating force which is based on the force balance of the ego vehicle and objects in real-time does not need high computation cost, which is more important for real application. Another advantage for passive algorithms like SFM, they rarely need the dynamic model of obstacles but just their current states, which is also benefit for reducing the computation.

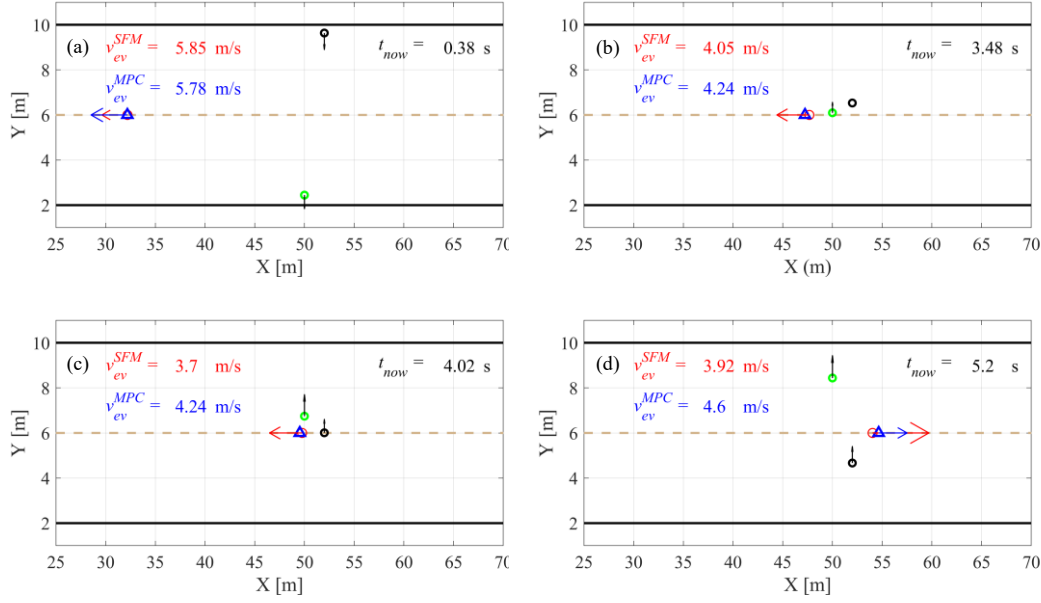


**Figure 3.22 Comparison of force exerting on pedestrians and vehicle's longitudinal acceleration under Strategies of MPC and SFM during the whole CA process (a) Relative positions between participants at  $t=0.38s$ ; (b) Relative positions between participants at  $t=3.48s$ ; (c) Relative positions between participants at  $t=4.02s$ ; (d) Relative positions between participants at  $t=5.2s$**

The comparison of acceleration difference between MPC and SFMC are clearly illustrated by Figure 3.22 (a)-(d), where the red circle is the SFMC based ego vehicle, blue triangle represents the MPC based vehicle, the green and black circles represent the 1<sup>st</sup> and the 2<sup>nd</sup> pedestrian, respectively. The arrows attaching to the pedestrians (ego vehicle) indicate the direction of total social force (converted to vehicle longitudinal acceleration) and the length of arrow indicates the magnitude of the force (the corresponding acceleration).

And the speed of MPC and SFMC under each time point is attached to the Figure 3.22. In the beginning, deceleration of MPC is larger, as shown in Figure 3.22 (a). Until the ego vehicle reaches the minimum safe speed, the MPC based ego vehicle will keep this speed before passing all the pedestrians, which is different with continuous deceleration of SFM based ego vehicle, as shown in Figure 3.22 (b) and Figure 3.22 (c). Finally, when passing all pedestrians, both MPC and SFMC will require ego vehicle re-acceleration, while the re-acceleration of SFMC is larger due to large force from pedestrian brought by a very short interaction distance between Ego vehicle and pedestrians, as shown in Figure 3.22 (d).

### 3.4 Adaptive parameters method for SFM

For a better view, here we re-draw Figure 3.2 in this section.

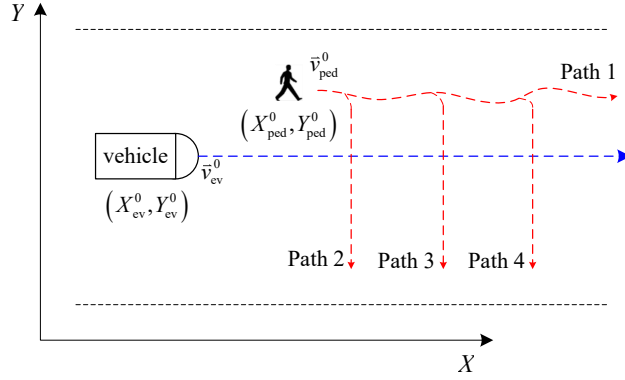


**Figure 3.2 Typical interaction scenario between vehicle and pedestrian**

In section 3.3, we discussed the ego vehicle interaction with pedestrian owns unpredictable speed. However, facing with pedestrian with unpredictable lateral motion, as shown in Figure 1.4, a fixed series of  $\Phi_{ev}^*$  maybe not enough for the all situations. In order to solve such case of problem, we proposed adaptive parameters for SFM-based vehicle model based on current interaction states of pedestrian and the ego vehicle.

For numerical modeling the scenario shown in Figure 3.2, the initial states of the ego vehicle and pedestrians are set as:

$$\delta_{ped}^0 = \delta_{ev}^0 = 0 rad \quad (127)$$

$$\begin{cases} v_{ped}^{x,0} = 1.2 m/s \\ v_{ped}^{y,0} = 0 m/s \end{cases} \quad (128)$$

$$a_{ped}^0 = a_{ev}^0 = 0 m/s^2 \quad (129)$$

$$D_{ev2p}^{Y,0} = Y_{ped}^0 - Y_{ev}^0 = 2m \quad (130)$$

where  $D_{ev2p}^{Y,0}$  is the  $Y$ -direction deviation distance between the ego vehicle and pedestrian at the initial time. The minimum safe distance, which is defined as  $\min D_{safe}$ , is set as  $1.5m$  in this section.

Considering the ego vehicle is approaching a pedestrian with stochastic moving, a  $0.5m$  offset is added to  $D_{ev2p}^{Y,0}$ . The  $X$ -direction deviation distance  $D_{ev2p}^{X,0}$  is unspecified, or in other words, it can be any reasonable value for ego vehicle to successfully complete the CA process. Namely, the previous state of the vehicle is supposed to be cruising with an initial velocity  $v_{ev}^0$ .

From the **Problem 1 Reconstruction** in section 3.2.4, it indicates we need to search a  $\Phi_{ev}^*$  that contains 8 parameters needs to be optimized. However, if the force from pedestrian  $\vec{F}_{p2ev}^t$  is equal to zero, the vehicle will keep the initial speed and operate no turning maneuver. It means the ego vehicle maintains the reference trajectory in this research, which results in the force from destination  $\vec{F}_{des2ev}^t$  will also be zero. And from the Physical explanation of parameters optimization in section 3.3.2, the decisive parameter that needs to be optimized is  $A_{p2ev}$ . Besides, we consider the lateral motion of the ego vehicle here, therefore, different from the modified  $\vec{F}_{des2ev}^t$  in section 3.3 (Equation (112)), the original form of  $\vec{F}_{des2ev}^t$  (Equation (105)) is taken into consideration. And for simplification, we only consider optimizing  $A_{p2ev}^*$  and  $\vec{v}_{ref4ev}^{t,*}$  in this section 3.4. Besides, due to the global reference path is a straight line from Figure 3.2, the reference speed in  $Y$ -axis  $v_{ref4ev}^{Y,t,*}$  is considered constant zero, which means the  $\Phi_{ev}^*$  is simplified as the following:

$$\Phi_{ev}^{*,2} = [A_{p2ev}^*, v_{ref4ev}^{X,t,*}] \quad (131)$$

while other parameters are set as defaults according to Table 3-3.

Besides, as the lateral motion of the ego vehicle is taken into consideration, the original total force for vehicle (Equation (103)) is modified as following:

$$\vec{F}_{ev}^t = \vec{F}_{p2ev}^t + \vec{F}_{des2ev}^t + \vec{F}_{brake}^t \quad (132)$$

The new added item  $\vec{F}_{brake}^t$  is used to provide a force that is generated by vehicle controller to indicate ego vehicle to operate optimal obstacle avoidance maneuvers, which is established as

$$\vec{F}_{brake}^t = f(Flag, D_{ev2p}^{X,t}) \quad (133)$$

where  $Flag$  is a Boolean using to judge whether the pedestrian is now crossing the road and  $D_{ev2p}^{X,t}$  is the  $X$ -direction distance between the pedestrian and the ego vehicle. This force is considered an artificially applied force. And this new added force contributes to controller parameter optimization [67].

### 3.4.1 Analysis of avoidance process

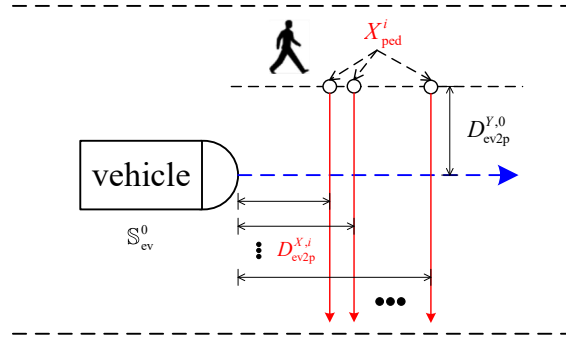


Figure 3.23 Random choices of pedestrian crossing road

The following part describes the optimal raw parameters of SFM-based vehicle model at various vehicle-pedestrian distances. Considering that the initial conditions (defined by Equation (127)-(130)) of the target scenario do not specify the initial X-direction vehicle-pedestrian distance  $D_{ev2p}^{X,0}$ . So, firstly, a PSO-based optimization is employed to determine the relation between  $\Phi_{ev}^{*,2}$  and various  $D_{ev2p}^{X,0}$ .

A test scenario is shown by Figure 3.23. Fixing the initial state  $S_{ev}^0$  of vehicle and the Y-direction deviation distance between the ego vehicle and the pedestrian  $D_{ev2p}^{Y,0}$ . When the pedestrian chooses different X-position (defined as  $X_{ped}^i$ ), to cross road, it leads to different  $D_{ev2p}^{X,i}$ . And this scenario simulates the sudden crossing of a pedestrian under varying  $D_{ev2p}^{X,0}$  when the vehicle is cruising.

Similarly, here we use PSO to optimize the  $\Phi_{ev}^{*,2}$ . And here the solution dimension for PSO is 2. Therefore, a new swarm  $\Theta_i^2 = (\Theta_{i1}^2, \Theta_{i2}^2), i = 1, 2, \dots, N$  with  $v_i^2 = (v_{i1}^2, v_{i2}^2), i = 1, 2, \dots, N$  is defined for PSO initialization to traversal the whole CA process. The performance of each particle  $\Theta_i^2$  is evaluated by a cost function. And when iterations of traversal are reached the upper limit or the cost of value function is acceptable, it is considered that the current set  $\Theta_i^2(k)$  is the solution set  $\Theta_i^{2,*}$ .

Lower bounds and upper bounds were added to  $A_{p2ev}^*$  and  $v_{ref4ev}^{X,t}$ , where  $A_{p2ev}^* \in [0, 6000]$  and  $v_{ref4ev}^{X,t} \in [0, 10]$  to ensure that in the process of calibration, the parameters are not set to unrealistic values. Additionally, the total number of particles in the PSO was set to 40 ( $N = 40$ ), which is sufficient for the calibration process.

The loss function is defined as

$$J(\theta_i^2) = q^{\text{PSO}} \cdot \frac{1}{v_{\text{ev}}^{\text{mean},i}} + r^{\text{PSO}} \cdot \frac{1}{d_{\text{ev2p}}^{\text{min},i}} + p^{\text{PSO}} \cdot d_{\text{ev2p}}^{\text{max},i} \quad (134)$$

where

$$\begin{cases} r^{\text{PSO}} = r^{\text{PSO}}, & \text{if } d_{\text{ev2p}}^{\text{min},i} \geq \min D_{\text{safe}} \\ r^{\text{PSO}} = L \cdot r^{\text{PSO}}, & \text{if } d_{\text{ev2p}}^{\text{min},i} < \min D_{\text{safe}} \end{cases} \quad (135)$$

$$d_{\text{ev2p}}^{\text{min},i} = \min\{d_{\text{ev2p}}^{i,t} | t \in (t_0, t_{\text{end}})\} \quad (136)$$

$$d_{\text{ev2p}}^{\text{max},i} = \max\{d_{\text{ev2p}}^{i,t} | t \in (t_0, t_{\text{end}})\} \quad (137)$$

This loss function aims for the ego vehicle to pass pedestrians with minimal steering and deceleration, ensuring a safe avoidance. The  $r^{\text{PSO}}$  is a very small constant when the  $d_{\text{ev2p}}^{\text{min},i}$  is larger than  $\min D_{\text{safe}}$ , which means the ego vehicle needs a series of optimized parameters to achieve a higher passing speed when the distance is deemed safe.  $L$  is a large constant that provides a sufficient cost that the ego vehicle maintains an acceptable, safe distance away from the pedestrian.

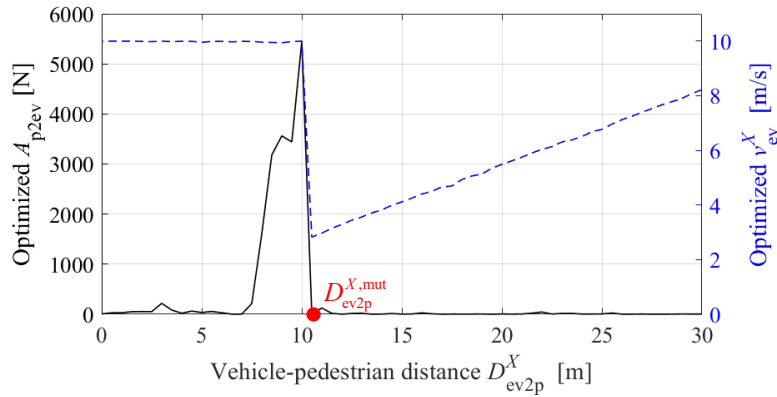


**Figure 3.24** The optimal  $A_{p2ev}$  and  $v_{\text{ref4ev}}^{X,t}$  under different  $D_{\text{ev2p}}^{X,i}$

Figure 3.24 shows the optimized value of  $A_{p2ev}$  and  $v_{\text{ref4ev}}^{X,t}$  under different  $D_{\text{ev2p}}^{X,i}$ . The maneuver of the ego vehicle in different  $D_{\text{ev2p}}^{X,i}$  can be obviously separated to two cases, as shown in Figure 3.25.

When the pedestrian is crossing the road and the vehicle-pedestrian distance is larger than a specific value, which is defined as mutation distance  $D_{\text{ev2p}}^{X,\text{mut}}$ , the ego vehicle will be required to decelerate and wait for the pedestrian passing firstly, as shown in Figure 3.25. However, when the

current interaction distance is extreme short ( $< D_{ev2p}^{X,mut}$ ), the ego vehicle tends to keep a relative higher speed and operate steering maneuver. Because in such case, the benefits of maintaining high-speed passing are greater than the cost caused by slight steering. This is easily explained when we associate the actions of human drivers in real situations. When drivers find a pedestrian is crossing road with a distance far from the vehicle, they generally tend to slow down and wait for pedestrian to cross road firstly. Conversely, when drives approach a pedestrian who does not have an unpredictable crossing intent, the drive tend to operate turning maneuver with a relative high speed to avoid potential dangers and complete the CA process in a short period of time.

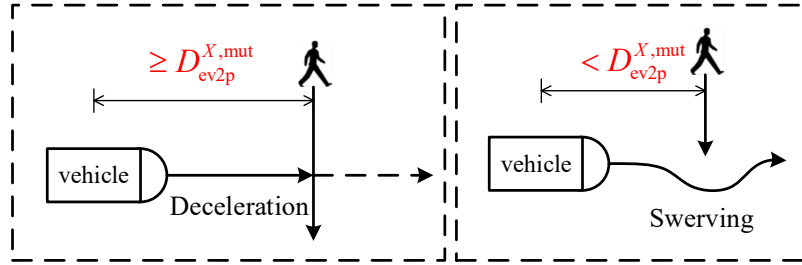


Figure 3.25 Two different avoidance maneuvers of ego vehicle

Based on the results from Figure 3.24, if it is assumed that a pedestrian is equally likely to cross the road in the future during the approaching process of the ego vehicle, the optimal strategy is to follow the optimal  $A_{p2ev}^*$  and  $v_{ref4ev}^{X,t,*}$  based on Figure 3.24. The  $A_{p2ev}^*$  and  $v_{ref4ev}^{X,t,*}$  piecewise polynomial fitted as:

$$v_{ref4ev}^{X,t,*} = f_{fit.v}(D_{ev2p}^X) \quad (138)$$

$$A_{p2ev}^* = f_{fit.A}(D_{ev2p}^X) \quad (139)$$

However, noticing there is mutation for both  $A_{p2ev}^*$  and  $v_{ref4ev}^{X,t,*}$  in mutation distance  $D_{ev2p}^{X,mut}$ . Forces can be mutated but not the velocity in the reality. Therefore, when  $D_{ev2p}^{X,t}$  is around  $D_{ev2p}^{X,mut}$ , which could also be roughly considered as the distance between these two interactors decreases from ‘long distance’ to ‘short distance’ in Figure 3.25, there are two choices for ego vehicle:

- (1) *Following strategy*: the ego vehicle keeps deceleration and following the pedestrian until the

pedestrian has crossed the road. However, if

$$-\delta_{\text{ped}}^{\text{thr}} \leq \delta_{\text{ped}}^t \leq \delta_{\text{ped}}^{\text{thr}}, t \in [t_0, \text{inf}) \quad (140)$$

which means pedestrian keeps walking straightly. However, when  $t_{\text{end}} = \text{inf}$ , the time consumption is unreasonable.

(2) *Overtaking strategy*: the ego vehicle keeps unchanged speed or accelerates to overtake the pedestrian. However, this approach is somewhat risky as it resembles a gambler's strategy. A sudden crossing caused by a careless pedestrian could result in an irreversible collision.

Based on the above analysis, the whole CA process is separated into two processes which are approaching process and yielding process, shown as Figure 3.26. For convenient, the switch distance here is the same as  $d_{\text{ev}}^{\text{swi}}$  in Equation (98).

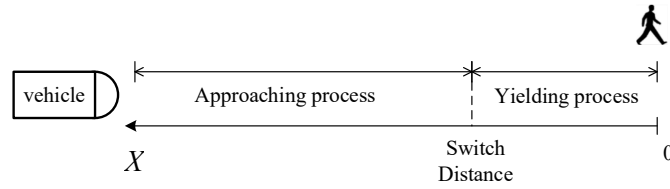


Figure 3.26 Segmentation of CA process

In approaching process, the ego vehicle will decelerate to a reference longitudinal speed:

$$v_{\text{ref4ev}}^{X,t} = v_{\text{ev}}^{X,*,t} = f_{\text{fit.v}}(D_{\text{ev2p}}^{X,t}) \quad (141)$$

Noticing that  $D_{\text{ev2p}}^{X,\text{mut}} < d_{\text{ev}}^{\text{swi}}$ , the mutation of velocity is avoided in approaching process. In other worlds, the *Following strategy* is adopted in approaching process.

In yielding process, the reference longitudinal speed keeps a constant which is the same as that of switch distance  $d_{\text{ev}}^{\text{swi}}$ :

$$v_{\text{ref4ev}}^{X,t}(D_{\text{ev2p}}^{X,t} \leq d_{\text{ev}}^{\text{swi}}) = v_{\text{ev}}^{X,*,\text{swi}} = f_{\text{fit.v}}(d_{\text{ev}}^{\text{swi}}) \quad (142)$$

If the pedestrian does not cross road, this constant speed  $v_{\text{ev}}^{X,*,\text{swi}}$  for the ego vehicle in yielding process helps to avoid the problem caused by *Following strategy*. However, when facing with danger caused by overtaking strategy, it is necessary to calculate a safe speed for the ego vehicle when the pedestrian suddenly crosses the road.

### 3.4.2 Two modes of Adaptive parameters method

1) *Proposed method 1 for yielding process*: In this method, it is assumed that the pedestrian is now crossing the road and will not yield to the ego vehicle, as shown in Figure 3.27. In other words, the pedestrian here is considered as a 'careless' individual that the force from the ego vehicle  $\vec{F}_{ev2p}^t$  will be ignored by the pedestrian.

The pedestrian is considered as a circle whose radius is the minimum safe distance  $\min D_{\text{safe}}$  with ego vehicle. Besides,  $S$  represents the  $X$ -direction distance between outlines of these two interactors, which is named safe vehicle-pedestrian distance in  $X$ -direction.

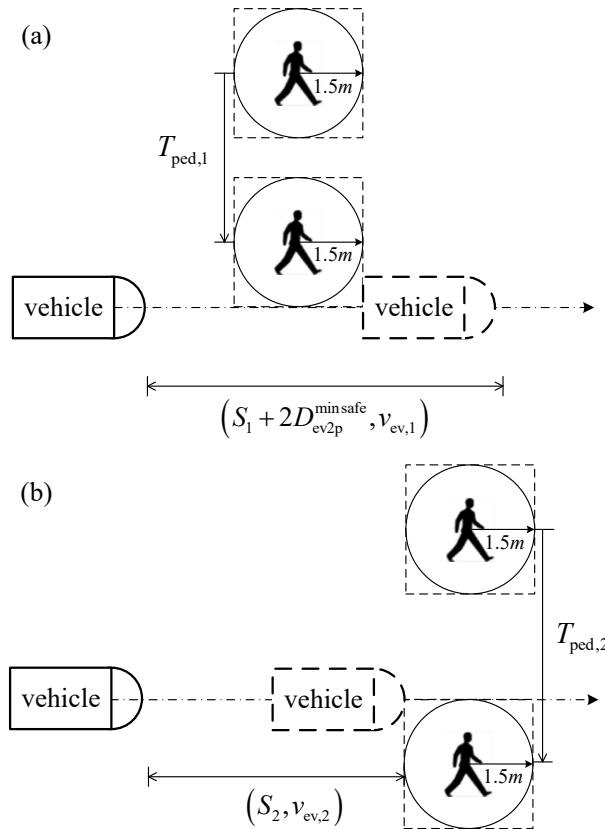


Figure 3.27 Boundary longitudinal speed for ego vehicle

Then, there are two case for the ego vehicle to yield the pedestrian without turning:

*Case 1*: the longitudinal speed of the ego vehicle is fast enough that it has already finished the CA process when the pedestrian reaches the collision point, as shown in Figure 3.27 (a);

*Case 2*: the longitudinal speed of ego vehicle is slow enough that the pedestrian has already passed

the ego vehicle when the ego vehicle reaches the collision point, as shown in Figure 3.27 (b).

According to the above analysis, the boundary longitudinal speed could be established as:

$$v_{ev,1} = \frac{S_1 + 2 \cdot \min D_{\text{safe}}}{T_{\text{ped},1}} \text{ or } v_{ev,2} = \frac{S_2}{T_{\text{ped},2}} \quad (143)$$

Where  $T_{\text{ped},1}$ ,  $T_{\text{ped},2}$  is the time to collision point (TTC) of the pedestrian in *case 1* and *case 2*, respectively.  $S_1$  and  $S_2$  are the moving distance of ego vehicle in *case 1* and *case 2*, respectively.  $v_{ev,1}$  is the lower boundary of longitudinal speed in *case 1*, and  $v_{ev,2}$  is the upper boundary of *case 2*, as shown by Figure 3.28.

As the definition of  $S$ ,

$$S^t = D_{\text{ev}2\text{p}}^t - \min D_{\text{safe}} \quad (144)$$

When the pedestrian starts crossing the road in current  $D_{\text{ev}2\text{p}}^t$ , the maximum safe speed  $v_{\text{max}}^S$  is less than the current speed  $v_{\text{ev}}^{X,t}$  as we consider that acceleration is unreasonable. The ego vehicle needs to decelerate to keep the average longitudinal speed no larger than  $v_{\text{max}}^S$ . Here we assume acceleration is counter-intuitive for simplification. The following function is established to obtain  $a_{\text{ev}}^{X,t,*}$ :

$$v_0 t_1 - \frac{1}{2} a t_1^2 + v_{t_1} (t - t_1) = S \quad (145)$$

$$v_{t_1} = v_0 - a t_1 \quad (146)$$

the  $v_{\text{ev}}^{X,t}$ ,  $S^t$  and  $a_{\text{ev}}^{X,t,*}$  is rewritten as  $v_0$ ,  $S$  and  $a$  for simplification,  $t_1$  is the deceleration time,  $v_{t_1}$  is the final speed after deceleration and  $t$  is the time when  $S = 0$ . As the current initial longitudinal speed is relatively small, the effect of jerk of acceleration could be ignored so that it is not under take into consideration for simplification.

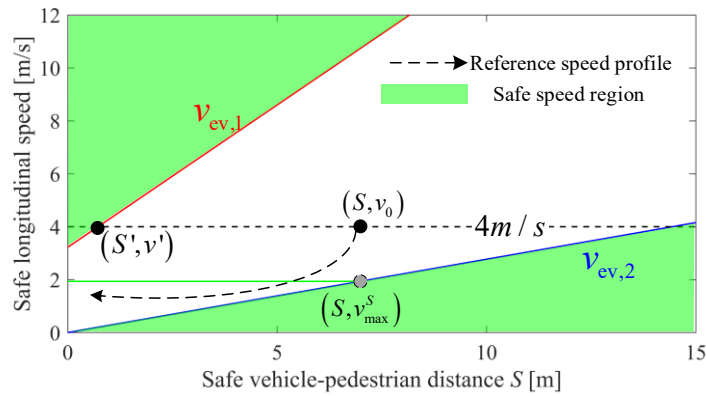


Figure 3.28 Safe longitudinal speed for ego vehicle

For pedestrian comfort, a minimum deceleration  $a$  is required for ego vehicle:

$$\begin{aligned} \min a &= \frac{S-v_0t}{\frac{1}{2}t_1^2-tt_1} \\ \text{s.t. } v_{t_1} &\geq 0 \\ 0 &\leq t_1 \leq t \end{aligned} \quad (147)$$

For obtaining minimum  $a$ , the derivation of  $a$  is

$$a' = \frac{(v_0t-S)(t_1-t)}{\left(\frac{1}{2}t_1^2-tt_1\right)^2} \quad (148)$$

And in this equation,

$$(t_1 - t) \leq 0 \quad (149)$$

$$v_0t - S = v_0t - v_{\max}^S t > 0 \quad (150)$$

Therefore,

$$(v_0t - S)(t_1 - t) \leq 0 \quad (151)$$

which means  $a$  is a non-increasing function.

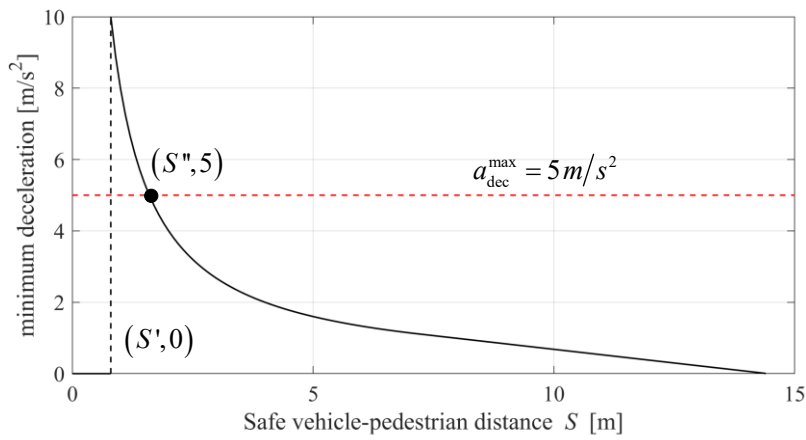


**Figure 3.29 Optimal deceleration under different safe distance**

Besides, about the limitation factors, the first limitation is  $v_{t_1} \geq 0$ , which can be transformed into

$a \leq \frac{v_0}{t_1}$ , and combining with definition of  $\min a$  (Equation (147)), we can get:

$$\frac{S-v_0t}{\frac{1}{2}t_1^2-tt_1} \leq \frac{v_0}{t_1} \quad (152)$$

and Equation (152) can be simplified as  $t_1 \leq \frac{2S}{v_0}$ .

As  $t = \frac{S}{v_{\max}^S}$ , the second limitation  $0 \leq t_1 \leq t$  can be rewritten as  $0 \leq t_1 \leq \frac{S}{v_{\max}^S}$ .

So, the limitation factors are final equal to the following form:

$$0 \leq t_1 \leq \min\left(\frac{2S}{v_0}, \frac{S}{v_{\max}^S}\right) \quad (153)$$

Considering  $a$  is a non-increasing function, we finally get:

$$a = \min a \text{ when } t_1 = \min\left(\frac{2S}{v_0}, \frac{S}{v_{\max}^S}\right) \quad (154)$$

And the relation between the optimal deceleration and safe vehicle-pedestrian distance  $S$  is shown by Figure 3.29.

From Figure 3.28, when  $S < S'$ ,  $v_0 > v_{\text{ev}}^1$  always holds, therefore:

$$\min a(S < S') = 0 \quad (155)$$

Besides, as the maximum deceleration speed  $a_{\text{dec}}^{\max}$  is set as  $5 \text{ m/s}^2$ ,

$$\min a(S \in (S', S'')) > a_{\text{dec}}^{\max} \quad (156)$$

which means if pedestrian chooses to cross road in this range of distance, deceleration for ego vehicle cannot meet the target of avoidance for ego vehicle. The turning is necessary in this case.

The final optimal  $a_{\text{ev}}^{X,t,*}$  is established as:

$$a_{\text{ev}}^{X,t,*} = \begin{cases} 0, & 0 \leq S < S'' \\ \min a, & S \geq S'' \end{cases} \quad (157)$$

The reason of  $a_{\text{ev}}^{X,t,*} = 0, S \in [S', S'')$  is that the force  $\vec{F}_{\text{p2ev}}$  also owns function of decelerating the ego vehicle. So, when calculating the optimal  $A_{\text{p2ev}}^*$  in the range of  $S \in [S', S'')$ , the  $a_{\text{ev}}^{X,t,*}$  is set to zero for simplification.

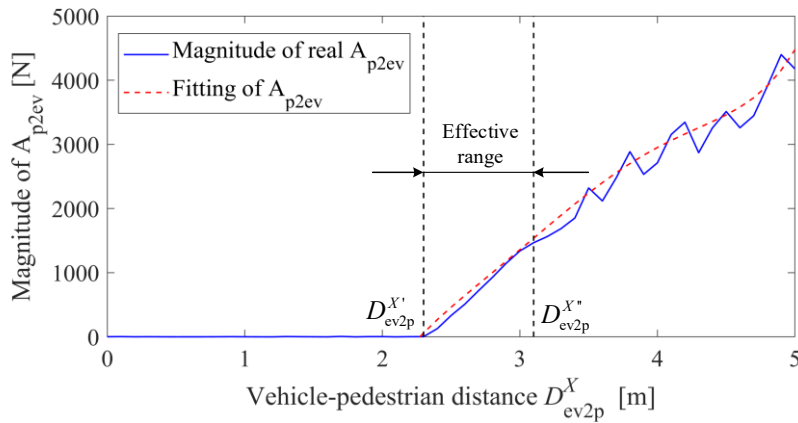


Figure 3.30 Optimal  $A_{\text{p2ev}}^*$  under different vehicle-pedestrian distance

The optimal  $A_{p2ev}^*$  in SFM-based vehicle model is obtained by balancing the yield speed and deviation distance by PSO with the same loss function Equation (134). And the results are shown in Figure 3.30.

As the turning option for ego vehicle is the only choice when the deceleration is larger than the upper limited, the effective range for  $A_{p2ev}^*$  is when the relative distance belongs to  $(D_{ev2p}^{X'}, D_{ev2p}^{X'')}$ , where:

$$\begin{cases} D_{ev2p}^{X'} = S' + \min D_{safe} \\ D_{ev2p}^{X''} = S'' + \min D_{safe} \end{cases} \quad (158)$$

And a fifth order polynomial is used to fit the optimized  $A_{p2ev}^*$ ,

$$A_{p2ev}^* = f_{fit.A}(D_{ev2p}^X) \cdot Flag, D_{ev2p}^X \in [D_{ev2p}^{X'}, D_{ev2p}^{X''}] \quad (159)$$

as the red dot line that is shown in Figure 3.30, where  $Flag$  is a Boolean that  $Flag = 1$  (or  $Flag = 0$ ) means the pedestrian is (or is not) crossing road now, respectively.

Besides, the optimal deceleration should be transformed into a brake force (Equation (133)) in SFM-based vehicle model, which is defined as:

$$\vec{F}_{brake}^{t,*} = \begin{cases} 0, D_{ev2p}^{X,t} > d_{ev}^{swi} \\ (a_{ev}^{X,t,*} \cdot mass_{ev} - \vec{F}_{des2ev}^t) \cdot Flag, D_{ev2p}^{X,t} \leq d_{ev}^{swi} \end{cases} \quad (160)$$

where  $mass_{ev}$  is the mass of the ego vehicle. Because the calculated  $a_{dec}^*$  is the final optimal deceleration of the ego vehicle during the yielding process, the effect of destination force  $\vec{F}_{des2ev}^t$  should be excluded.

2) *Proposed method 2 for yielding process:* In *method 1*, a consideration was given to a selfish pedestrian who will not yield to the oncoming vehicle during road crossing. When the interaction between the two participants is considered in the yielding process, the optimal operation will be different for ego vehicle. In other words, the pedestrian here is consider as a 'careful' individual that the force from the ego vehicle  $\vec{F}_{ev2p}^t$  will not be ignored by the pedestrian.

The operation of approaching process for the ego vehicle in this method is the same as *method 1*. In yielding process, if considering  $\vec{F}_{ev2p}^t$ , the solution of  $a_{ev}^{X,t,*}$  will be highly complicated. So, it is transformed into directly search an optimal series of  $\vec{F}_{brake}^{t,*}$  by PSO. The cost function is the same as

Equation (134). The solution here owns two dimensions, and the particle swarm is defined as

$$\Phi_{ev}^{*,3} = [A_{p2ev}^*, \vec{F}_{brake}^{t,*}] \quad (161)$$

Similarly, lower bounds and upper bounds are added to  $\Phi_{ev}^{*,3}$ :

$$\begin{cases} A_{p2ev}^i \in [0, 3000] \\ \vec{F}_{brake}^{t,i} \in [0, 4000] \end{cases} \quad (162)$$

The boundaries are used to ensure that the parameters do not exceed unrealistic values during the calibration process. Besides, the total number of particles in the PSO is set to 40, which is sufficient for the calibration.

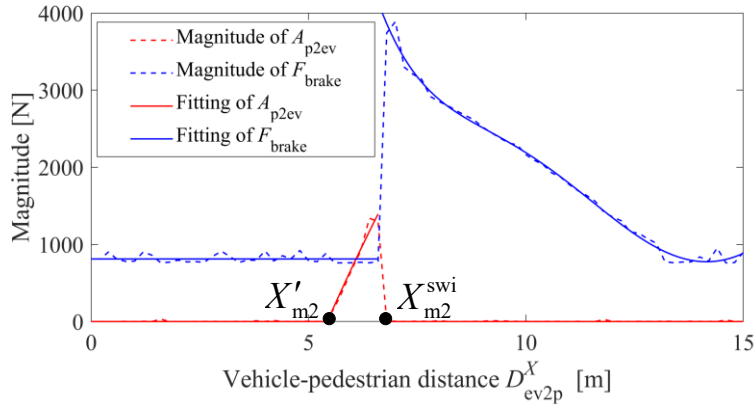


**Figure 3.31 Optimal  $\vec{F}_{brake}^{t,*}$  and  $A_{p2ev}^*$  under different vehicle-pedestrian distance**

The optimized  $\vec{F}_{brake}^{t,*}$  and  $A_{p2ev}^*$  under different interaction distance  $D_{ev2p}^X$  is shown in Figure 3.31.

The fitting of  $\vec{F}_{brake}^{t,*}$  and  $A_{p2ev}^*$  is written as:

$$A_{p2ev}^{t,*} = \begin{cases} f'_{fit.A}(D_{ev2p}^{X,t}) \cdot Flag, D_{ev2p}^{X,t} \in [X'_{m2}, X_{m2}^{swi}] \\ 0, D_{ev2p}^{X,t} \notin [X'_{m2}, X_{m2}^{swi}] \end{cases} \quad (163)$$

$$\vec{F}_{brake}^{t,*} = \begin{cases} f_{fit.F}(D_{ev2p}^{X,t}) \cdot Flag, D_{ev2p}^{X,t} \in [X_{m2}^{swi}, d_{ev}^{swi}] \\ C_F, D_{ev2p}^{X,t} \in [0, X_{m2}^{swi}] \end{cases} \quad (164)$$

where  $X_{m2}^{swi}$  is a certain distance that when  $D_{ev2p}^{X,t} \geq X_{m2}^{swi}$ , ego vehicle is only required to deceleration.

$C_F$  is a constant used to balance the force  $\vec{F}_{brake}^{t,*}$ .

The control logic given by *method 2* is similar to that of *method 1*. Firstly, the ego vehicle is only required to deceleration if  $D_{ev2p}^{X,t}$  is larger than  $X_{m2}^{swi}$ . Besides, when  $D_{ev2p}^{X,t} \in [X_{m2}', X_{m2}^{swi}]$ , the optimal  $A_{p2ev}^*$  now is not equal to zero which means turning is the optimal operation choice for the ego vehicle in current stage.

Here, the  $X_{m2}'$  is larger than  $D_{ev2p}^{X''}$  in Figure 3.31 because that the pedestrian is set to actively avoid the ego vehicle in *method 2*. So, even if  $D_{ev2p}^{X,t} \in [D_{ev2p}^{X'}, D_{ev2p}^{X''}]$ , the ego vehicle does not need to turn for maintaining  $d_{ev2p} \geq \min D_{safe}$  due to the active yielding of the pedestrian.

### 3.4.3 Simulation results

The control flow of simulation is shown in Figure 3.32, which is as following:

- (1) Based on current state information of the ego vehicle  $S_{ev}^t$  and the pedestrian  $S_{ped}^t$  generate interacting force  $\vec{F}_{ev2p}^t$  and  $\vec{F}_{p2ev}^t$ .
- (2) Based on current  $D_{ev2p}^{X,t}$  and the pedestrian moving mode, calculate  $A_{p2ev}^{t,*}$  and  $\vec{F}_{brake}^{t,*}$  according to Equation (159) and Equation(160) or (Equation (163) and Equation (164));
- (3) Generate  $v_{ev}^{ref,t+1}$  and  $a_{ev}^{x,ref,t+1}$  for next time step  $t + 1$  according to mass point vehicle model Equation (106)-(109);
- (4) Generate corresponding steering wheel angle  $\delta_{ev}^{t+1}$  and pedal opening  $p_{ev}^{t+1}$  by PID for T3R bench.

To verify the reliability of the algorithm under uncertain pedestrian motion, a sequence of discrete times intervals for the pedestrian crossing the road was established at 0.1 second intervals, which is defined as:

$$t_{ped}^{cro} = k \cdot t_s, k \in N^+, t_s = 0.1s \quad (165)$$

And, if  $t \geq t_{ped}^{cro}$ , the pedestrian will operate crossing road maneuver. The crossing road decision is not known in advance by ego vehicle. The results *method 1* and *method 2* is given by Figure 3.33.

From the results, it is obvious that *method 2* is a more aggressive strategy due to the active avoidance of the pedestrian, as demonstrated in Figure 3.33(d). In Figure 3.33 (d), the number of times the vehicle's minimum longitudinal speed under method 1 equals zero is much higher than that of

*method 2*, meaning that *method 1* requires the ego vehicle to decelerate and wait for the pedestrian to pass in most cases while *method 2* tends to requires the ego vehicle to avoid the pedestrian with turning maneuver under a relative higher speed.

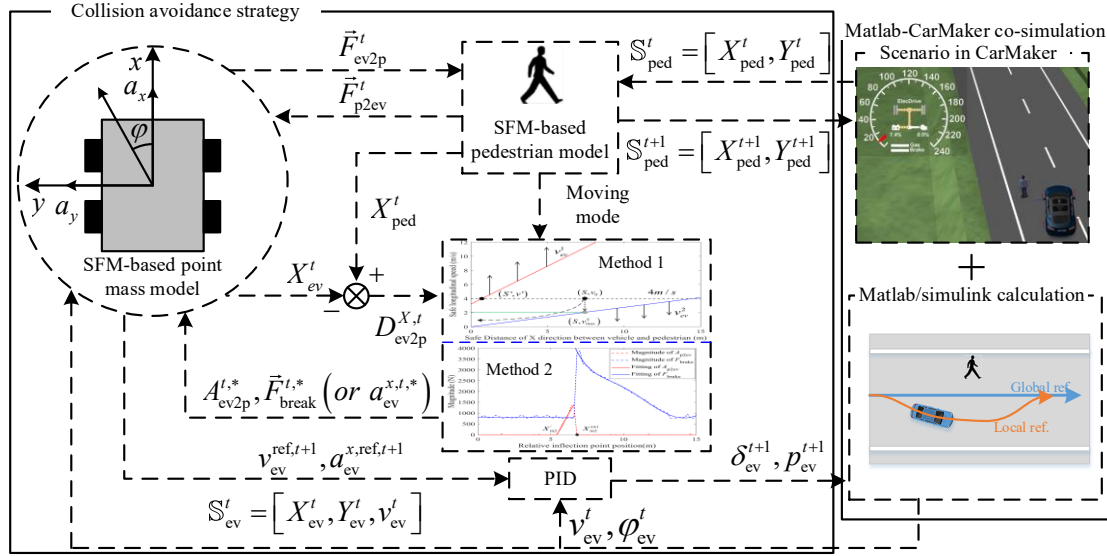


Figure 3.32 Control flow

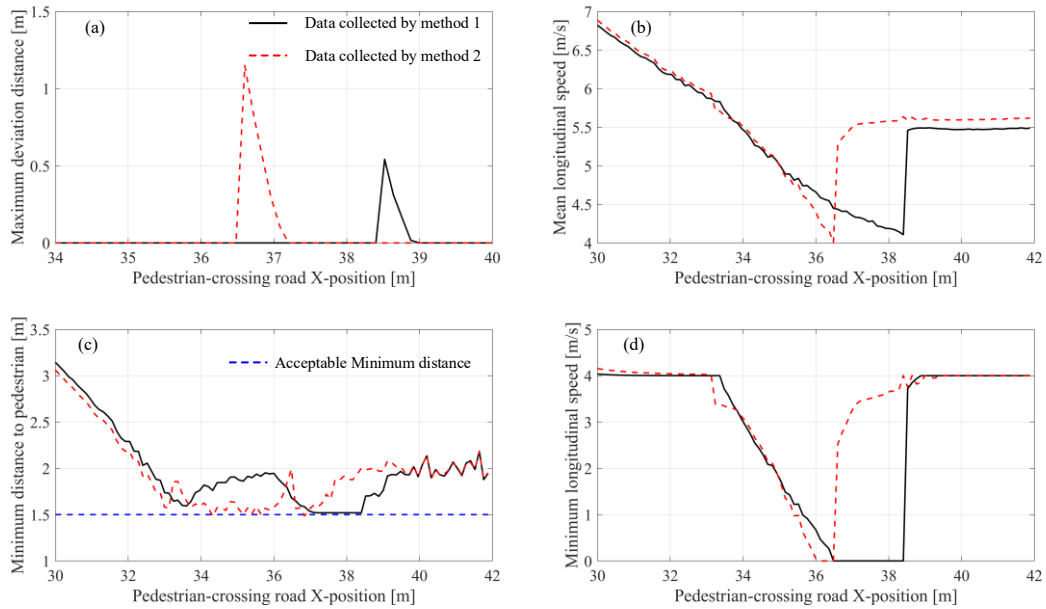


Figure 3.33 Results of method 1 and 2 under successive pedestrian-crossing road X-position:(a) Maximum deviation distance from reference path of ego vehicle;(b) Mean longitudinal speed of ego vehicle;(c) Minimum distance between ego vehicle and pedestrian;(d) Minimum longitudinal speed of ego vehicle.

Although the more aggressive strategy of *method 2* results in a higher mean longitudinal speed, it also causes a larger maximum deviation distance from the reference path, which are shown by Figure 3.33 (b) and Figure 3.33 (a). Besides, both *method 1* and *method 2* ensure that the ego vehicle safely avoids the pedestrian, as the minimum distance between them is larger than  $1.5m$  which is set as the minimum safety distance, as shown in Figure 3.33(c).

### 3.5 SFM-based solution for ego vehicle interacting with bike

In some countries in southeast Asia, electric bikes are more and more involved in the interaction of traffic flow due to its convenience and quickness [3]. Users of this type of transportation blur the line between vehicles and bicycles, as both can often move freely in the same space. Facing with these kind of traffic sections, car drivers need to carefully assess the collision risk although driving speed is relatively low. Moreover, in such areas, the moving priority of bicycles is usually not very high, which means vehicles usually do not need to come to a complete stop to wait for bicycles to pass. So, taking into account the need for vehicle drivers to save commute time or to quickly pass through similar areas, drivers or control agents need to balance of keeping relative higher velocity and ensuring proper safety distance during avoidance process.

Therefore, during driving in non-signalized areas, this section also considers adopting SFM-based strategy to instruct the ego vehicle for collision avoidance (CA) with moving bicycles in real time. And the comparison of SFM-based strategy and MPC-based strategy is obtained. The results show the effectiveness of SFM-based collision avoidance strategy which provide a reference for the future research of CA strategy in shared space or mixed traffic flow.

#### 3.5.1 Scenario modeling

This section addresses the typical driving scenario illustrated in Figure 3.34, where the ego vehicle moves forward in the same direction as a bicycle. In Figure 3.34, the Cartesian coordinates that belong to the earth-fixed coordinate are defined by  $X$  and  $Y$ , respectively. Superscript  $b$  represents the bicycle while  $ev$  is the abbreviation of ego vehicle.  $v$  represents the longitudinal speed and  $\theta$  is the yaw angle of the bicycle with respect to the forward direction of the road  $X$ . Generally, mostly the vehicle will

choose to stop and wait when they encounter bicycles turning. However, considering the congested sections with no traffic lights or other indications, drivers generally tend to yield with low speed to pass through that it requires that ego vehicle avoids the collision with the bicycle by balancing the safety, comfort with less time consumption.

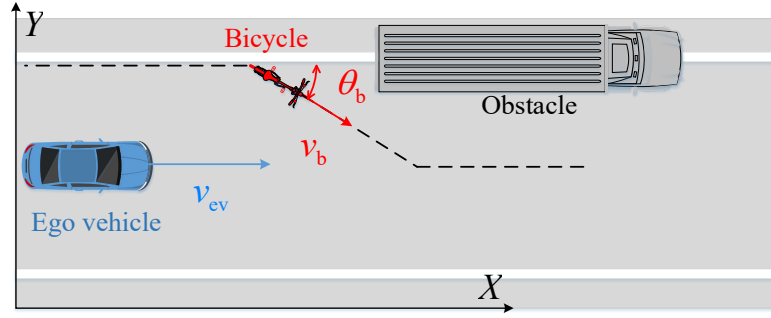


Figure 3.34 Simulation scenario

In order to accurately model this scene mathematically, initial setting is defined as following:

- (1) Vehicle initial speed  $v_{ev}^{ini}$  is  $30\text{ km/h}$  and the range of acceleration for vehicle is  $[-5\text{ m/s}^2 \quad 5\text{ m/s}^2]$ ;
- (2) Bicycle keeps a constant longitudinal speed of  $10\text{ km/h}$ , and the trajectory of bicycle follows a given profile for calculation convenience;
- (3) The length of parked vehicle is  $7\text{ m}$ , and the mass of ego vehicle is set as  $1700\text{ kg}$ ;
- (4) Driveway is dry road with a good vision whose road friction coefficient  $\mu$  is  $0.8$ .

### 3.5.2 Modified SFM-based Vehicle Model

As a new item (bicycle) is added into the interaction system and there is no pedestrian left, the original SFM-based total force  $\vec{F}_{ev}^t$  (Equation (103)) is modified as following:

$$\vec{F}_{ev}^t = \vec{F}_{b2ev}^t + \vec{F}_{des2ev}^t + \vec{F}_{pv2ev}^t + \vec{F}_{brake}^t \quad (166)$$

The force from pedestrian  $\vec{F}_{p2ev}^t$  is ignored. The new added force  $\vec{F}_{pv2ev}^t$  represents the force from the parking vehicle and  $\vec{F}_{b2ev}^t$  is the force from the moving bicycle.  $\vec{F}_{brake}^t$  is an artificial force which is adopted to obtain a better performance for SFM, it owns the same form described by Equation (133).

The force  $\vec{F}_{b2ev}^t$  is defined as:

$$\vec{F}_{b2ev}^t = f_{\exp}(d_{b2ev}^t, A_{b2ev}, B_{b2ev})A_{\sin}(\phi_{b2ev}^t, \lambda_{b2ev}) \quad (167)$$

Actually, the definition of  $\vec{F}_{b2ev}^t$  is the same with that of  $\vec{F}_{p2ev}^t$ , the details of each item in  $\vec{F}_{b2ev}^t$  are explained by Equation (96) and Equation (97). Besides, the definition of  $\vec{F}_{des2ev}^t$  is the same with Equation (105).

And in this section, the effectiveness of  $\vec{F}_{des2ev}^t$  can be illustrated by Figure 3.35, that it mainly requires ego vehicle to follow the global reference.

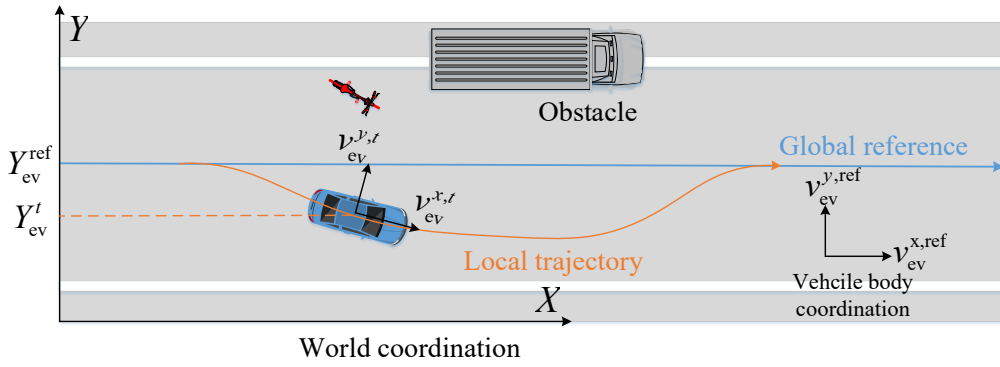


Figure 3.35 Effectiveness of  $\vec{F}_{des2ev}^t$ : requiring ego vehicle to follow the global reference

### 3.5.3 PSO-based parameters optimization

In the PSO calibration process, the particular parameter set  $\theta$  that needs to be optimized contains 6 parameters which means the solution of PSO is 6-dimensional:

- (1) Parameters  $A_{b2ev}$  and  $B_{b2ev}$  of function  $f_{\exp}$ ;
- (2) Parameter  $\lambda_{b2ev}$  of function  $A_{\sin}$ ;
- (3) Parameter  $\kappa_{des2ev}$  of force  $\vec{F}_{des2ev}^t$ ;
- (4) Parameter  $d_{ev}^{swi}$  of function  $\beta_{des2ev}$ ;
- (5) Force  $\vec{F}_{brake}^t$ .

Each particle in swarm  $\theta_i^4 = (\theta_{i1}^4, \theta_{i2}^4, \dots, \theta_{i6}^4), i = 1, 2, \dots, N$  with an initial random speed  $v_i^4 = (v_{i1}^4, v_{i2}^4, \dots, v_{i6}^4), i = 1, 2, \dots, N$  will traversal the whole CA process. Then the performance of  $\theta_i$  was evaluated by a cost function, then the performance of  $\theta_i^4$  was evaluated by a cost function Equation (168). And when iterations of position and speed of each particle is reached the set limit or the cost of loss function is acceptable, it is considered that the optimal set  $\theta_i^{opt}$  is the solution set.

In addition, lower bounds and upper bounds were added to ensure that in the process of calibration, the parameters do not go beyond unrealistic values, as shown in Table 3-4. The total number of particles in the PSO was set to 30, which is sufficient for the calibration.

Table 3-4 Range and optimized value of parameters

Parameters	Range	Optimized value	Unit
$A_{p2ev}$	[0 6000]	4094.16	$N$
$B_{p2ev}$	[0 1]	5.4e-5	-
$\lambda_{p2ev}$	[0 1]	0.13680475	-
$\kappa_{des2ev}$	[2000 4000]	661.6054	$N$
$d_{ev}^{swi}$	[0 20]	1.07	$m$
$\vec{F}_{break}^t$	[0 1000]	289.5765	$N$

The cost function is defined as follows:

$$J(\theta_i) = q \cdot \frac{1}{v_{ev}^{meanv,i}} + r \cdot \frac{1}{d_{b2ev}^{min,i}} + p \cdot d_{ref2ev}^{max,i} \quad (168)$$

$$\text{where } \begin{cases} r = r, \text{ if } d_{b2ev}^{min,i} \geq \min D_{safe} \\ r = 100r, \text{ if } d_{b2ev}^{min,i} < \min D_{safe} \end{cases}$$

where  $v_{ev}^{meanv,i}$  is the mean speed of vehicle,  $d_{b2ev}^{min,i}$  is the minimum distance between vehicle and bicycle and  $d_{ref2ev}^{max,i}$  is the deviation distance between ego vehicle and reference path during the whole CA process under the particular parameter set  $\theta_i$ .  $q, r, p$  are the weight of each cost. The  $r$  is a very small constant when the  $d_{b2ev}^{min,i}$  is bigger than the minimum safe distance ( $\min D_{safe}$ ) between the ego vehicle and the bicycle at which time ego vehicle need a series of optimized parameter for pursuing higher passing speed. However, when  $d_{b2ev}^{min,i}$  is smaller than  $\min D_{safe}$ ,  $r$  will be extremely larger (actually the value of  $r$  at this time does not have to be 100 times of original value, as long as it is large enough), the priority of being optimized parameter series is to ensuring that the minimum distance between the ego vehicle and the bicycle is an acceptable safe distance.

This cost function requires ego vehicle passing pedestrians with less deceleration cost under

promise of safe avoidance and slight steering.

### 3.5.4 Simulation Results

To verify the proposed SFM-based CA strategies, a comparison simulation with MPC-based controller is conducted in Matlab/Simulink. Figure 3.36 shows the simulation results.

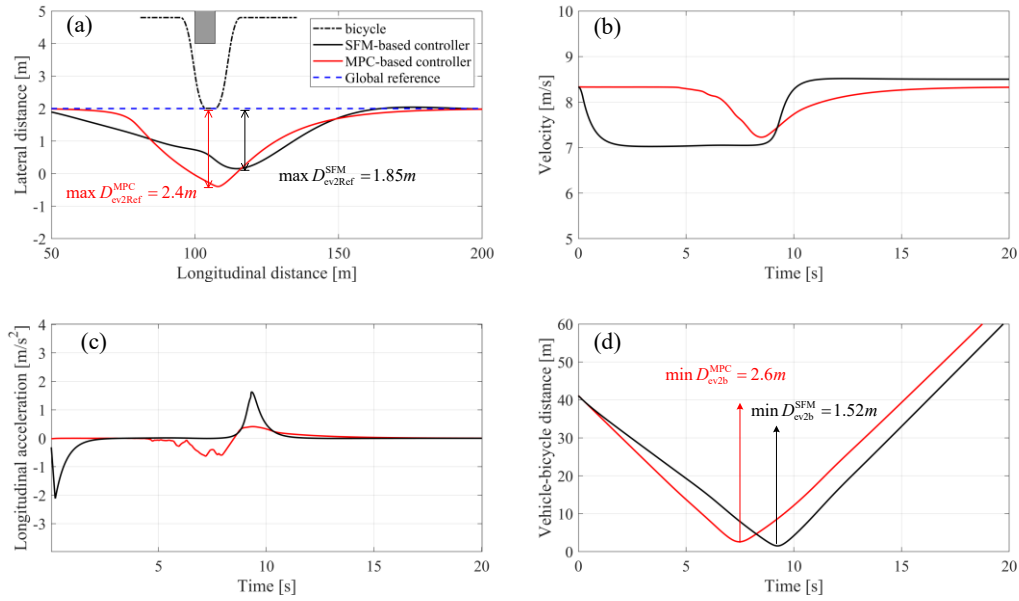


**Figure 3.36** Simulation results: (a). Trajectories of the bicycle, SFM-based ego vehicle and MPC-based ego vehicle; (b). Comparison of velocity; (c). Comparison of longitudinal acceleration; (d). Comparison of vehicle-bicycle distance

Figure 3.36 (a) shows the lateral deviation of SFM-based strategy (1.85m) is less than that of MPC-based strategy (2.40m), which indicates the motion of SFM-based ego vehicle is more stable. The small fluctuations of longitudinal acceleration of SFM-based strategy in Figure 3.36 (c) also proved this. Although the mean longitudinal velocity of SFM (7.85m/s) is less than that of MPC (8.12m/s), which is calculated from Figure 3.36(b), the difference is negligible. Besides, Figure 3.36(d) shows that the minimum distance between the bicycle and the ego vehicle of SFM (1.52m) and of MPC (2.6m) both meet security requirement.

The computation times of SFM-based method and MPC-based method are plotted in Figure 3.37. When the parameters in SFM are well-calibrated, the ego vehicle avoid the bicycle by the real time force balance decided by their current relative position. So, it is not necessary for SFM-based strategy

to obtain the optimal longitudinal speed and steering wheel angle by solve a non-linear problem at each time step like MPC, which greatly reduces computation time and gives insight that SFM-based method is promising for real-time application.

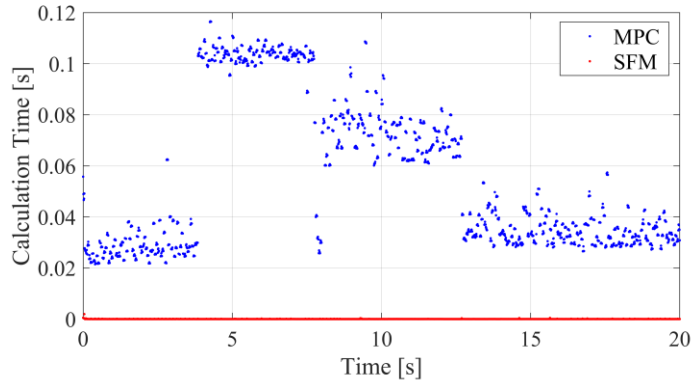


Figure 3.37 Comparison of calculation time in MPC and SFM

### 3.6 Existing Problems of SFM

For SFM-based vehicle model, the calibration process of its parameters is in offline. And in online, SFM just needs to make some simple numerical calculations which brings the real-time application potential to SFM-based CA strategy. However, the offline calibration also brings some problems.

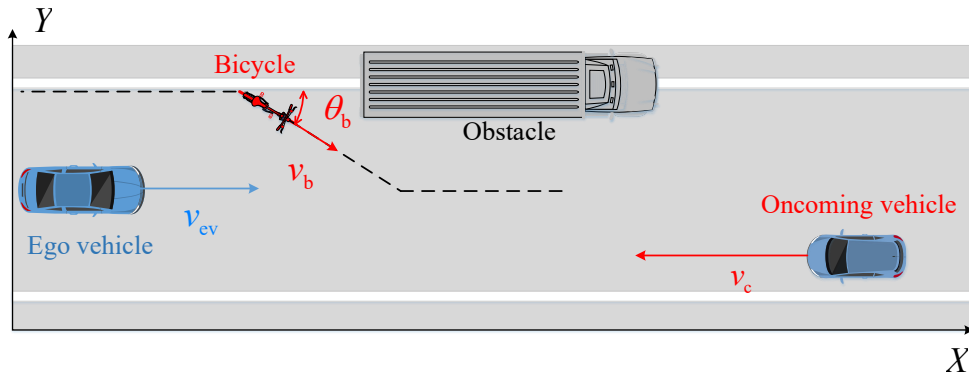


Figure 3.38 Interaction scenario among multiple traffic objects: ego vehicle, bicycle, parking vehicle and oncoming vehicle

A new scenario is constructed illustrate these issues. The Figure 3.38 shows an interaction scenario of ego vehicle and multiple traffic objects. This scenario is similar with that of Figure 3.34 in where

only an additional oncoming vehicle is added. This scenario is established to illustrate that when the scene is different, it may be necessary to re-optimize parameters to achieve better control effects.

The PSO algorithm is also adopted for calibrating the optimal parameters in this scenario. And the optimized parameters are list in Table 3-5. Table 3-5 shows the Comparison of optimized parameters in Section 3.5.3 and this section. Although, there is no big change for most parameters, the magnitude of  $\kappa_{\text{des2ev}}$  and  $d_{\text{ev}}^{\text{swi}}$  is increased sharply.

**Table 3-5 Comparison of optimized parameters in Section 3.5.3 and this section**

Parameters	Range	Optimized	Optimized	Unit
		value in Section 3.5.3	value in this section	
$A_{\text{p2ev}}$	[0 6000]	4094.16	5764.94	$N$
$B_{\text{p2ev}}$	[0 1]	5.4e-5	0.03898	-
$\lambda_{\text{p2ev}}$	[0 1]	0.13680475	0.0025	-
$\kappa_{\text{des2ev}}$	[2000 4000]	661.6054	2363.4	$N$
$d_{\text{ev}}^{\text{swi}}$	[0 20]	1.07	14.49	$m$
$\vec{F}_{\text{break}}^t$	[0 1000]	289.5765	225.23	$N$

The comparison results between original parameters and re-optimized parameters are shown in Figure 3.39. From the results, it is obvious that the ego vehicle's trajectory with re-optimized parameters fluctuates less than that of original parameters, which is shown in Figure 3.39(a). And the Figure 3.39(c) shows the longitudinal acceleration of ego vehicle with re-optimized parameters is smoother, which means the average speed of this case is higher, that ego vehicle can pass the collision-prone area more quickly. Besides, the Figure 3.39(d) shows the minimum distance between ego vehicle and obstacles, the minimum distance in the case of re-optimized parameters is 1.52m while the minimum distance in the case of original parameters is 1.55m. The minimum distance in both cases is larger than a minimum safe distance, which is 1.5m. Therefore, the requirement of safety for both the original parameters and the re-optimized parameters is promised.

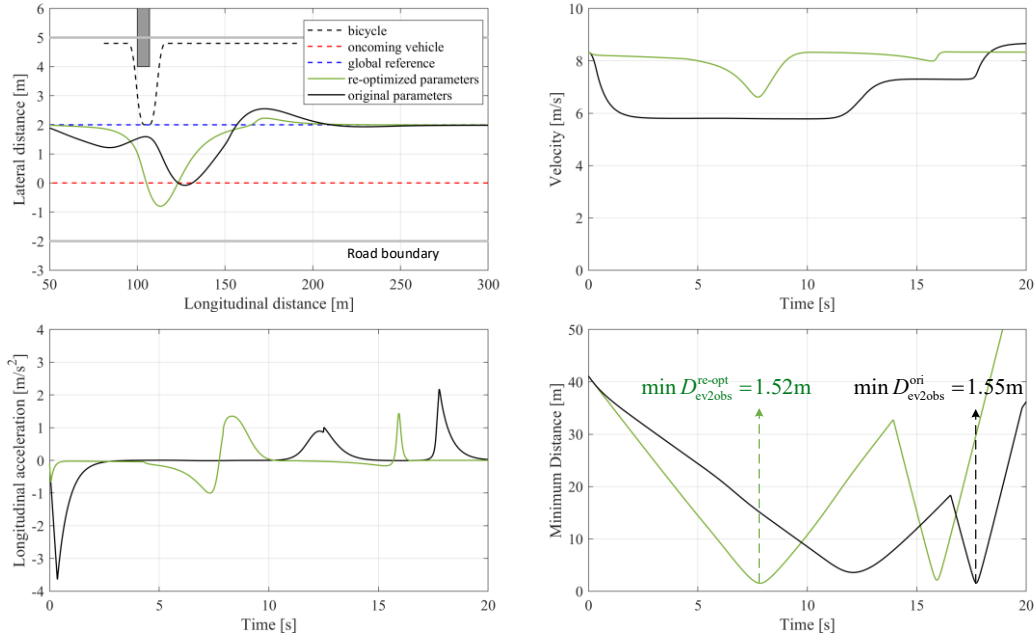


**Figure 3.39 Comparison of control effect when adopting original parameters and re-optimized parameters: (a). Comparison of trajectories; (b). Comparison of velocity; (c). Comparison of longitudinal acceleration; (d). Comparison of vehicle-obstacles distance**

The comparison simulation shows the limitations of the SFM-based CA strategy that, although a series of optimized parameters are able to help vehicle avoid obstacles under promise of safety, quickness and comfort in a specific scenario, such as the optimized parameter in Table 3-4 for scenario shown in Figure 3.34, the control effect will become worse when facing to a new CA scenario. A re-optimization for original parameters may need to carry out for better control effect. To address this problem, it may be necessary to improve the functions of virtual forces from different objects or add new virtual forces with different meanings. Besides, combining SFM with other control methods, such as combining SFM with rule-based control or combining SFM with MPC, may bring higher scalability for SFM.

In addition, SFM needs precisely model of ego vehicle and other traffic participants, and in different scenario, the parameters of SFM are different. Though it provides a quick solution of CA problem compared to that of MPC because it is unnecessary for SFM to make prediction, the real application of SFM still needs further research due to its limits such as model mismatch and the accuracy of parameter calibration for both SFM-based pedestrian and vehicle models.

Besides, that the force balance is calculated only based on the relative position of the vehicle and obstacles at the current moment and there is no requirement for SFM-based strategy to predict the dynamics of the future interactive system between vehicle and obstacles improve the real-time performance, this brings difficulty in parameter calibration especially when the ego vehicle faces with multiple obstacles as well as the control effect is not as good as MPC in some cases due to the loss of prediction.

The strange or extreme behaviors of other traffic objects that may threaten the safety of the ego vehicle should also be considered, such as pedestrian behaves in strange way: accelerating suddenly or changing direction immediately. It is necessary to calculate a range of pedestrian's speed or pedestrian's motion angle that defines which range is safe or which range is dangerous (actually it is also related to the ego vehicle's own speed and motion angle). A possible way is improving the functions of virtual forces from different objects or add new virtual forces with different meanings, such as combining the risk potential field with SFM that defines an additional force from risk potential field to help ego vehicle address the dangerous behavior from other traffic objects.

### 3.7 Neural Approximate Feedback Network

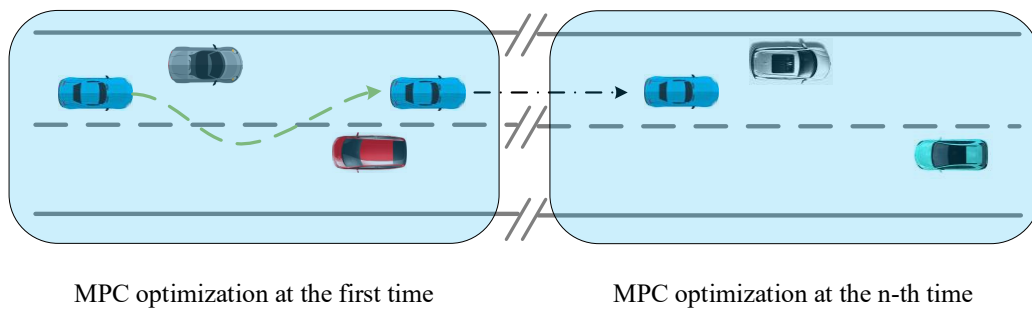


**Figure 3.40 MPC repeatedly search solutions in similar scenarios**

The MPC-based method proposed in section 2.3 shows good results when indicating ego vehicle to avoid the collision. However, MPC performs rolling optimization at every time step, and its optimization performance depends on the length of the time step and the length of the prediction time horizon. Although shorter time step and shorter prediction time horizon bring more precise solution, the

time required to solve will increase significantly. MPC-based method is suitable for slow dynamic processes and condition with low real-time requirements, is still unable to be applied in real-time high-speed vehicle dynamic control due to its numerous calculations. And other shortcomings for MPC is that its inability of referring to past experience and will iteratively search the optimal solution for similar scenarios, shown in Figure 3.40 , that also limits its real-time application.

For the shortcomings of the above algorithms, we propose a method whose architecture is based on artificial neural networks (ANN) named neural approximate feedback network (NAFC). The training data for NAFC comes from a well-calibrated MPC controller that the input data used for training is a series of states of MPC-based ego vehicle and the input data used for training is the optimal output from MPC corresponding to the current state. And comparing to human drivers, the output from MPC, which avoids data fluctuation and noise caused by the instability of human drivers' output, is beneficial for training process. And a well-trained NAFC is able to control vehicle avoiding collision in real time.

### 3.7.1 Application scenario

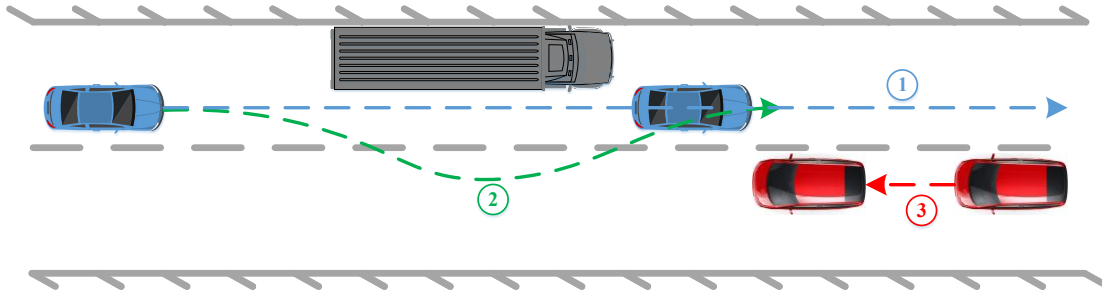


**Figure 2.2: Scenario of collision avoidance overtaking a parked vehicle and yielding an oncoming vehicle.**

In order to show an intuitive comparison between the MPC-based controller and NAFC-based controller, the target scenario designed for NAFC is the same with that of MPC, shown as Figure 2.2. And for a better view, we re-draw Figure 2.2 here.

Similarly, we give some initial state and limits here for a more reasonable motion for vehicles under crowd urban traffic situation. In the proposed typical urban traffic scenario, shown as Figure 3.41, the vehicle A yielding to stationary and moving obstacles is the ego vehicle controlled by the algorithm.

The vehicle B is a parked vehicle that represents a stationary obstacle while the vehicle C is an oncoming vehicle that represents the moving obstacle.

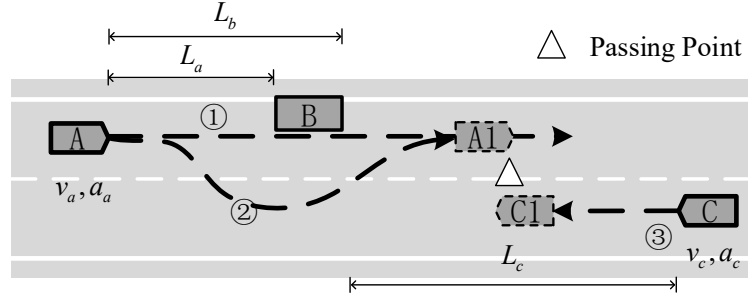


Figure 3.41 Simulation scenario modelling for NAFC

The dotted line 3 is the trajectory of the oncoming vehicle and the dotted line 1 is the initial reference trajectory (also known as the global reference trajectory) of the ego vehicle. Due to the existence of the parking vehicle and oncoming vehicle, the ego vehicle needs to alternate the local trajectory planning (shown as the dotted line 2) at this stage. The triangle represents the passing position of vehicle A and vehicle C. We consider that:

(1)  $L_a, L_b$  are global fixed parameters for the scenario, that means the initial relative position of the ego vehicle and the parked vehicle are not changed in any simulation;

(2)  $L_c$  is treated as a local invariant, that means the initial relative position of the ego vehicle and the parked vehicle will only be changed as the initial condition of a simulation;

(3)  $0 \text{ m/s} \leq v_a \leq 15 \text{ m/s}$ ,  $10 \text{ m/s} \leq v_c \leq 15 \text{ m/s}$ ;

(4)  $-3 \text{ m/s}^2 \leq a_a \leq 1 \text{ m/s}^2$ ,  $-3 \text{ m/s}^2 \leq a_c \leq 1 \text{ m/s}^2$

When considering safety factor, a minimum safe passing distance  $D_{safety}$  is set as an indicating threshold, as shown in Fig. 2, which is a distance between the passing position and the front side of the parked vehicle. It is considered that if the passing position is too close to parked vehicle, it's an unsafety overtaking maneuver that is banned.

PET is an indicator that is used to estimate the criticality of a certain traffic situation. It has been defined as the elapsed time between the front of the lead vehicle passing a point on the roadway and the front of the following vehicle passing the same point [56]. This research adopts PET as a safety indicator for behavior re-planning due to the variability of the oncoming vehicle's speed. When  $D_{safety}$  is set as

20m. And the equivalent PET is defined as:

$$PET = \frac{D_{safety}}{v_a} + \frac{D_{safety}}{v_c} \quad (169)$$

And in this paper, different  $L_c$  is adopted to obtain different PET to instruct the behavior re-planning.

So, if keeping constant speed or after accelerating, ego vehicle's passing position with oncoming vehicle is enough far away from parked vehicle, like at point 2 shown in Figure 3.42, then deceleration is unnecessary. Otherwise, the re-behavior of deceleration will be activated that Ego vehicle needs to decelerate until oncoming vehicle finishes overtaking parked vehicle.

As this section is a further study of MPC controller proposed in section 2.3, more detailed reasons and processes of re-planning the speed and the local trajectory can be found in section 2.3.

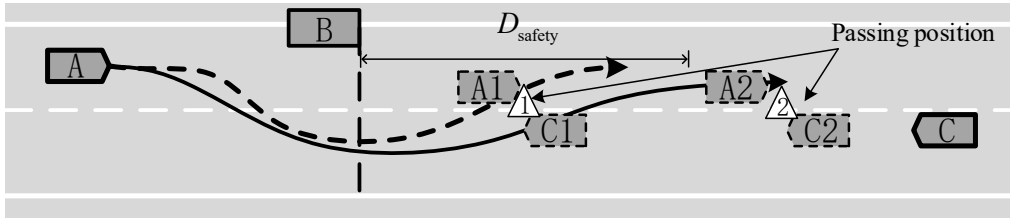


Figure 3.42 Different passing position

### 3.7.2 Training data collection

The normal ANN need large trial data and iteration epochs to update weights and biases of the network[68, 69], shown as Figure 3.43.

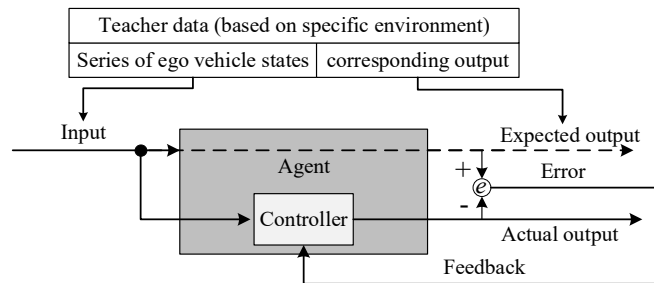
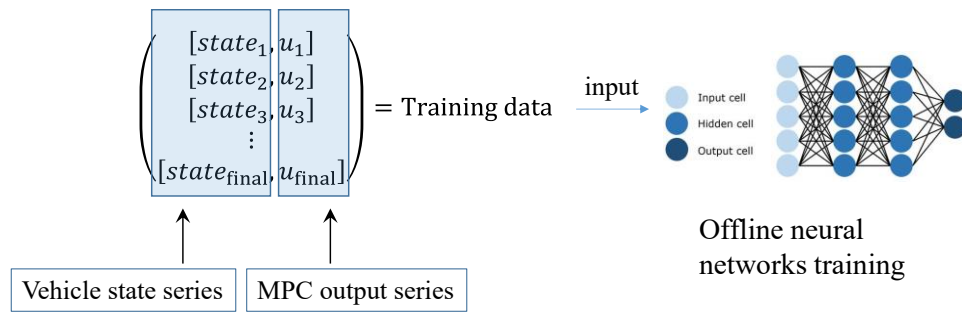


Figure 3.43 Training Process Overview of Neural Network

The training data, which is also known as teacher data[70], if collected from human driver, will be deeply affected by driving style of different individuals. The output of the same human driver in the same scene will also vary over time on the other hand.

However, if the training data is from MPC, the instability and noise of the data set can be controlled to a minimum as the output of MPC is highly consistent at the same collision avoidance scenario. Although MPC is hardly used in real scenario, it can be used for data collection based on simulation or hardware-in-loop, which is very convenient for specific scenarios. The process of data collection is shown in Figure 3.44.



**Figure 3.44 Data collection and training process for NAFC**

A two layers model predictive control (TL-MPC) architecture (we proposed in section 2.3) is used to collect the data. The data contains trajectory re-planning layer and tracking layer. The trajectory re-planning layer outputs the local reference path and the acceleration for next time step based on current relative position of the ego vehicle and obstacles. And the re-planned path is given by discrete points in the prediction time horizon. And a fifth-order polynomial is adopted as the fitting curve. The tracking layer outputs steering wheel angle based on the current state of ego vehicle and the relative position of the ego vehicle and local reference path.

With different initial speed and position of ego vehicle controlled by MPC, the state's series of the whole CA process and the corresponding output, acceleration and steering wheel angle, are collected for NAFC training process.

### 3.7.3 Structure of NAFC

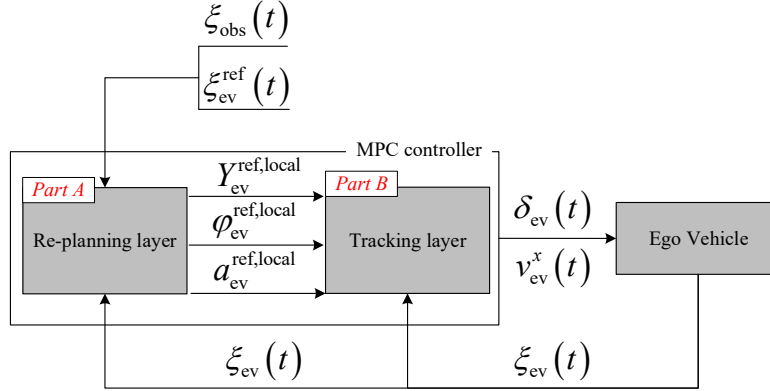


Figure 3.45 Structure of MPC-based controller in section 2.3

We aim to use NAFC as a quick solution method for MPC-based controller proposed in section 2.3. The structure of MPC-based controller is shown as Figure 3.45.

For NAFC-based controller, we aim to use neural networks to replace both the re-planning layer (*part A* in Figure 3.45) and tracking layer (*part B* in Figure 3.45).

NAFC is established to approximate the optimal output of the MPC controller while the input of ego vehicle is the same. The two layers of MPC will be both replaced after the NAFC is well-trained, shown as Figure 3.46, re-planning layer of MPC is replaced by re-planning fitting layer of NAFC and tracking layer of MPC is replaced by tracking fitting layer of NAFC, shown as *part A* and *part B* in Figure 3.46. The NAFC in re-planning layer is a fully connected neural networks containing one hidden layer with 10 neurons, its output is the acceleration  $\ddot{x}$  and its input contains  $\dot{x}$ , yaw angle  $\phi$ , yaw angle change rate  $\dot{\phi}$  and the coordinate  $(X, Y)$  belonging to world axis frame and the information of obstacles. The  $X_{\text{obs}}$  represents the  $X$ -axis coordination of oncoming vehicle. And the  $D_{\text{ev2obs}}^x$  represents the relative distance between ego vehicle and oncoming vehicle in  $X$ -axis direction. NAFC in tracking layer is also a fully connected neural networks containing two hidden layers that each owns 20 neurons, its output is the steering wheel angle  $\delta_f$  and its input is similar to that of NAFC in re-planning layer except lacks of yaw angle change rate  $\dot{\phi}$  and  $X_{\text{OnC}}$ . And the output of re-planning layer and tracking layer are the reference longitudinal speed  $v_{\text{ev}}^x$  of the ego vehicle and the reference steering wheel angle  $\delta_f$  of the ego vehicle, respectively.

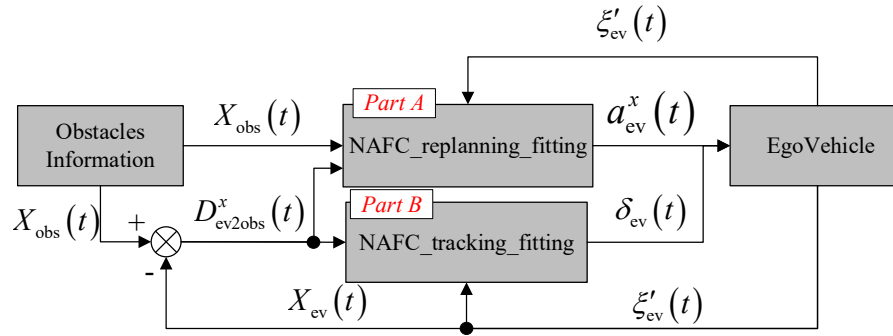


Figure 3.46 NAFC Control Flow

Therefore, the total control flow can be summarized as:

- (1) Based on current states of ego vehicle, parking vehicle and oncoming vehicle, the speed re-planning layer will generate a reference acceleration by NAFC;
- (2) The steering wheel angle is generated in tracking layer by NAFC based on current states of all objects under interaction;
- (3) The reference acceleration and steering wheel angle will be processed by a PID module then input to CarSim module;
- (4) With the ego vehicle's state output from CarSim, NAFC will calculate the optimal control output for next time step.

### 3.7.4 Simulation results for NAFC

To verify the effectiveness of the obstacle avoidance strategy based on NAFC which is trained by the data collected from MPC controller, CarSim-MATLAB co-simulation is conducted. The vehicle used in the simulation is based on the front wheel driving C-class hatchback model in Carsim software. The sample time is 0.01 s. The three cases are based on different PET, which is established as Equation (169), will be discussed in this section. Therefore, to get different PET, we assume that the distance between the ego vehicle and parked vehicle is a constant while the initial position of the oncoming vehicle is variable. At the same time, the initial speed of the ego vehicle is set as 11 m/s in all three simulations.

The Figure 3.47 gives a comparison of ego vehicle's longitudinal speed under different cases. The case that ego vehicle needs to accelerate is shown in Figure 3.47 (a), and the cases of constant speed and

deceleration are shown as Figure 3.47 (b) and Figure 3.47 (c), respectively. It is illustrated that the ego vehicle controlled by NAFC can successfully complete the re-planning of longitudinal acceleration.

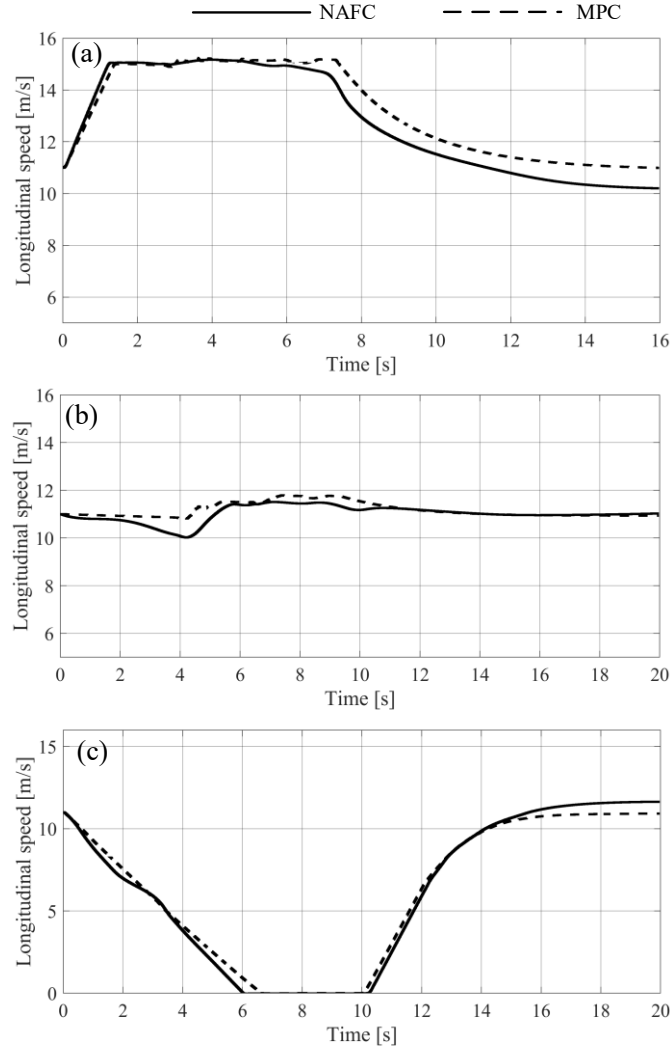


**Figure 3.47 Comparison of the planned longitudinal velocity between NAFC and MPC (case a: case of acceleration, case b: case of constant speed, case c: case of deceleration)**

The trajectory comparison under each case is also established in Figure 3.48. Under various cases of that ego vehicle keeps constant speed and ego vehicle need to accelerate, the trajectories of the two controllers are almost coincident. In deceleration case, the ego vehicle controlled by NAFC owns less steering. However, the oncoming vehicle has already passed ego vehicle in this case, which means the re-acceleration of ego vehicle will not interact with oncoming vehicle. So, the steering of NAFC under deceleration case is also safe.

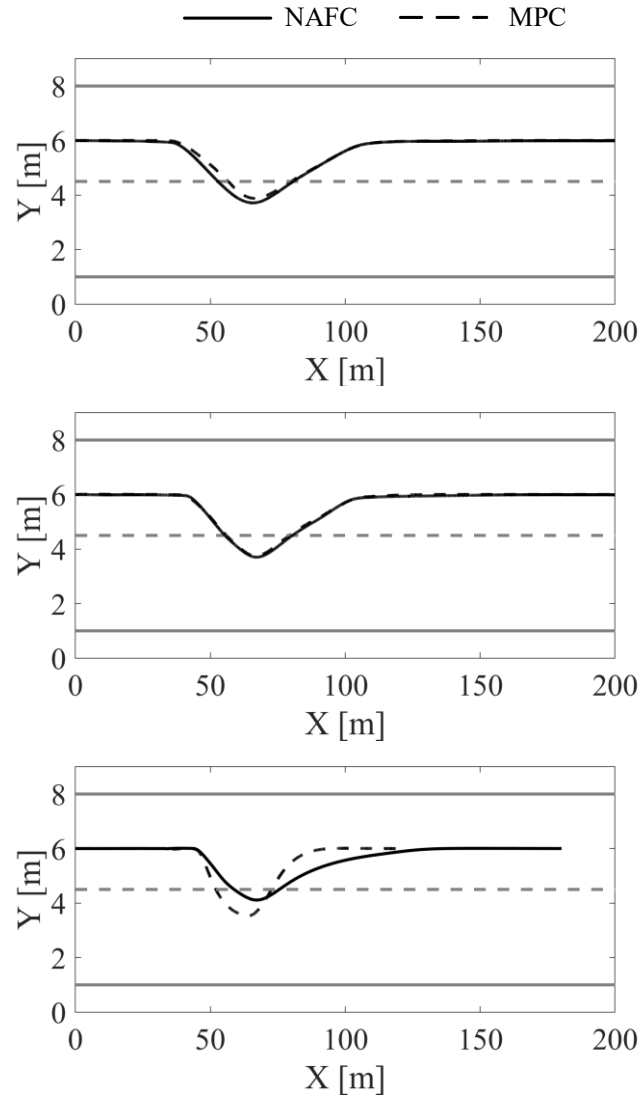


**Figure 3.48 Comparison of the trajectories between NAFC and MPC**  
 (case a: case of acceleration, case b: case of constant speed, case c: case of deceleration)

The Figure 3.49 gives a comparison of ego vehicle's steer wheel angle under different cases. The case that ego vehicle needs to accelerate is shown in Figure 3.49 (a), and the cases of constant speed and deceleration are shown as Figure 3.49 (b) and Figure 3.49 (c), respectively. In all three cases, NAFC's control output for steer wheel angle is more stable because it's actually a fitting to MPC output based on the current states of all interacting objects. So, there is more comfort that ego vehicle controlled by NAFC will provide.

Besides, the minimum distance between the ego vehicle based on NAFC and obstacles in the whole CA process are given to compared with that of MPC, shown as Table 3-6. Since the ego vehicle model is considered as a mass point and ignored the information of body size, the obstacles should be expanded.

At the same time, the obstacle needs to be segmented according to a certain resolution to prevent the vehicles passing through the obstacle when its size is too large, shown as Figure 3.50.

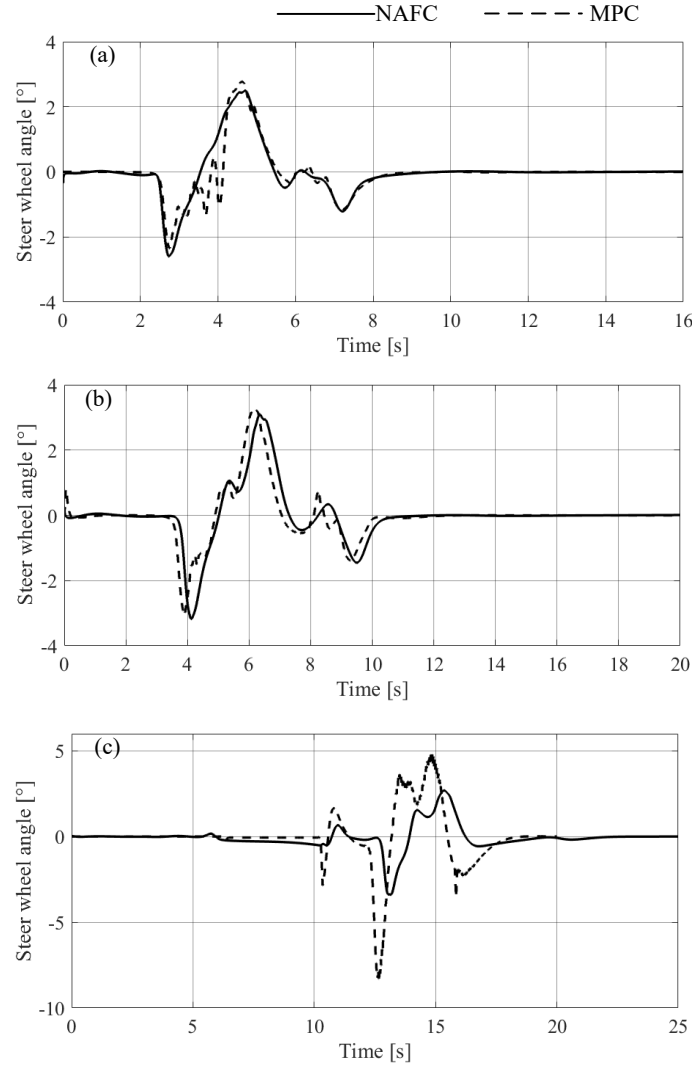


**Figure 3.49 Comparison of steering wheel angle between NAFC and MPC**

**(case a: case of acceleration, case b: case of constant speed, case c: case of deceleration)**

Compared with MPC, NAFC maintains a large safe distance in the cases of constant speed and acceleration. In deceleration case, ego vehicle controlled by NAFC has a smaller minimum distance, however it is acceptable due to the relatively narrow road width under crowded urban condition.

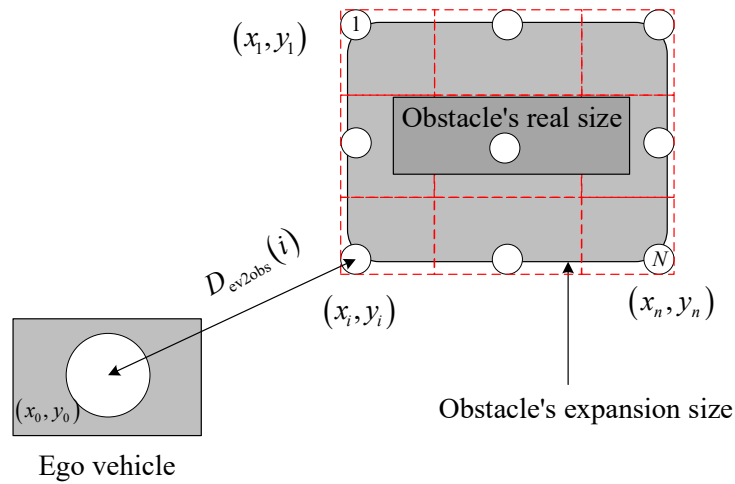


Figure 3.50 Obstacle Expansion

Table 3-6 Minimum distance

Cases	MPC	NAFC	
(a) deceleration case	0.5	0.28	$m$
(b) constant speed case	0.24	0.46	$m$
(c) acceleration case	0.52	0.70	$m$

### 3.7.5 Existing Problems of NAFC

Different with MPC-based or SFM-based control, NAFC is a type of model free control. And similar with deep learning, complexity of neural network makes it considered as "black boxes" and makes it challenge to understand and interpret their decisions. And in this section, the proposed NAFC-based controller is simply trained by the data provide by MPC, although the control effect is satisfactory, whether the generalization of the NAFC can be guaranteed when the scene has deviations still needs to be further discussed. This question can also be attributed to whether the proposed NAFC controller is prone to overfitting, where it performs well on training data but poorly on unseen data.

Besides, although the MPC-based controller is used for data collection for training NAFC which brings convenience in data collection, training and deploying deep learning models still require significant computational resources, limiting it accessibility in resource-constrained environments.

### 3.8 Summary of this chapter

Firstly, the Markov process was adopted to simplify the vehicle-pedestrian interaction system and the rationality of the simplification was illustrated by real driving data.

Then, the following works are completed in this chapter:

(1) Considering about the individual difference among pedestrians and the nuances of different shared space (like different road friction coefficient or visibility), the precise motion prediction of pedestrians is difficult to achieve, the uncertainties of pedestrian motion are defined as:

- The SFM-based pedestrians' longitudinal dynamic model is modified with Gaussian based random noise;
- The time point at which a pedestrian crosses the road is a random value that the vehicle controller does not know in advance.

And collision probability estimation of CA process when considering pedestrian motion randomness is discussed in detail;

(2) Considering the interaction between pedestrians and ego vehicle, a modified SFM-based vehicle dynamic model is proposed as passive CA strategy. The key parameters of SFM-based vehicle model are optimized, and the final values are explained physically in details;

(3) Comparison between controller of MPC and SFM is given, and advantages and shortcomings of the two strategies are discussed, which provide a reference for the future research of CA strategy in shared space or mixed traffic flow;

(4) Considering one series of optimized parameter is not enough for all CA situations especially when pedestrians motion owns uncertainty, a novel SFM-based adaptive parameters method to help ego vehicle make avoidance without motion prediction of pedestrian, just by the force balance.

(5) The SFM-based CA strategy is also adopted in a wider scenario of vehicle-bicycle interaction. And the comparison of SFM-based strategy and MPC-based strategy is obtained. The results show the effectiveness of SFM-based collision avoidance strategy which provide a reference for the future research of CA strategy in shared space or mixed traffic flow.

(6) Considering the drawback of ANN that it requires a large trial and long training process to obtain the results and the drawback of MPC that though its real-time application is not very

satisfactory. A method whose architecture is based on ANN named NAFC is proposed as a fast solver of MPC.

Besides, the issues raised by the two (SFM-based and NAFC-based) control strategies are also discussed, giving some prospects for future research accessing to CA problems.

## **Chapter4   SFM-based driver assistance system**

### **4.1 Preface**

The Section 3.3 to 3.5 presents a validation of the Structure-from-Motion (SFM)-based Collision Avoidance (CA) strategies designed for fully automated vehicles. Within the context of this chapter, we have successfully established and validated an SFM-based driver assistance system using a Hardware-in-Loop (HIL) testing approach. This validation process involved a collaborative integration of Matlab/Simulink, IPG CarMaker, and the T3R test bench, which collectively replicated real-world driving scenarios.

The results of our experiments unequivocally demonstrate the effectiveness of the SFM-based driver assistance system. Particularly, it exhibits remarkable capabilities in navigating shared spaces and navigating narrow road conditions within residential areas. One of its noteworthy functionalities is its ability to assist drivers in avoiding pedestrians with unpredictable motion, thus significantly enhancing safety in these complex driving environments.

### **4.2 Design of SFM-based driver assistance system**

This section introduces a non-autonomous driving experiment. Here, the proposed SFM-based CA controller serves as a driver assistance system, aiding the driver in achieving swift and secure pedestrian avoidance in narrow shared-space traffic conditions, especially when pedestrians exhibit unpredictable movements.

In this section, considering that it is not a suitable choice to compete with the driver for vehicle control when avoiding obstacles at low speed on a narrow road section, the SFM-based system serves as a driver assistance system that is intentionally decoupled from the vehicle's lateral and longitudinal controls. In other words, it does not vie for control over the steering wheel, accelerator, or brake pedals with the driver. Instead, this assistance system offers the driver a visual representation of a secure area or a safe trajectory to guide their interaction with a pedestrian.

Ongoing research is being conducted into visual assistance systems aimed at enhancing the driver's

overall experience. In reference to [71], they introduced a virtual risk field, which takes into account the vehicle's current speed and the longitudinal distance between the pedestrian and the ego vehicle. This system guides the driver in the manner of an experienced driver when dealing with sudden pedestrian movements, shown as Figure 4.1. The red field symbolizes the danger zone for the ego vehicle based on its current interaction state with the pedestrian. In contrast, the blue field serves as a safe zone, offering guidance to the driver to preemptively select a path to evade unexpected pedestrian movements.

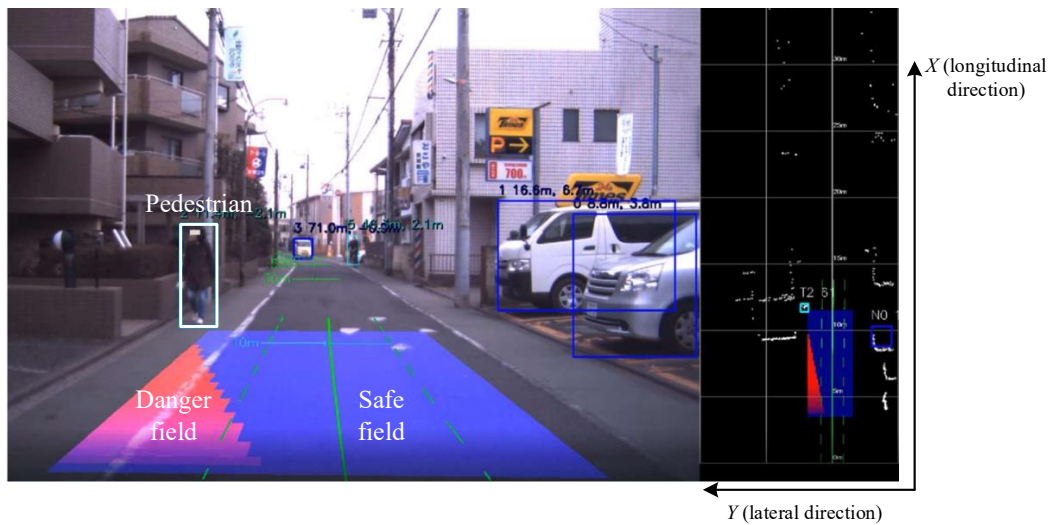


**Figure 4.1 Risk estimation system for pedestrian passing sideways[71]**

#### 4.2.1 Test process for SFM-based driving assistant system

In the context of an SFM-based assistant system, its primary role does not involve direct engagement in vehicle longitudinal and lateral control. Instead, it serves to generate a reference path for the driver, enabling them to safely and efficiently navigate past obstacles. This reference path is derived from the real-time data provided by the vehicle-pedestrian interaction system and the meticulously calibrated SFM-based vehicle/pedestrian parameters.

In Figure 4.4, the bench test process for the SFM-based assistant system is executed through the following stages:

- (1) Initialization of test scenario: The process commences with the initialization of a test scenario,

which is managed by IPG CarMaker module. This step involves configuring the initial settings for the ego vehicle and pedestrian by Matlab/Simulink module.

(2) Driver input integration: Subsequently, the driver's inputs, including steering wheel angle and acceleration/brake commands, are transmitted to the IPG CarMaker module in the host computer. This communication is achieved through the utilization of a steering controller and pedals.

(3) Vehicle state update: Within the IPG CarMaker module, the vehicle's states are dynamically updated to reflect the inputs from the driver. These updated states are then forwarded to the Matlab/Simulink module for further analysis.

(4) Local reference path generation: Leveraging the current state of the vehicle-pedestrian interaction system, a local reference path for the driver is synthesized. This path is derived from well-calibrated SFM-based vehicle and pedestrian models, and it spans a specified prediction horizon. This task is accomplished within the Matlab/Simulink module.

(5) Pedestrian position renewal: The position of the pedestrian is subject to periodic renewal through the vehicle-pedestrian interaction system and some initial settings, which operates within the Matlab/Simulink module.

(6) Data exchange: The local reference path, along with the refreshed pedestrian position, as generated by the Matlab/Simulink module, is transmitted to the IPG CarMaker module in the form of discrete data points.

(7) Scenario display: The refreshed scenario, now synthesized by the IPG CarMaker module, is visually displayed on a monitor. This display serves to influence and modify the behavior of the driver.

(8) Iterative process: Steps (2) through (7) are repeated iteratively until the vehicle completes its traversal of the intersection segment, thereby concluding the bench test process.

This methodology delineates the comprehensive procedure used to conduct bench testing for the SFM-based assistant system. It encompasses the orchestration of vehicle, driver, and pedestrian interactions, facilitating the assessment of the system's performance in a controlled environment.

Furthermore, with regard to the initial settings for both the ego vehicle and pedestrian within the scope of step (1), the Matlab/Simulink module assumes responsibility for configuring these parameters. Specifically, the initial settings pertain to the initial speed and initial position of both the ego vehicle and the pedestrian.

Additionally, within the context of step (5), the process of renewing the pedestrian's position is not solely contingent on external forces exerted by the vehicle. Rather, it is a multifaceted operation influenced by a confluence of factors, including the impact of forces emanating from the pedestrian's intended destination. As part of the validation process for the SFM-based assistance system, a randomized crossing-road-choice time for the pedestrian is introduced within initial setting of the pedestrian. This temporal element plays a crucial role in assessing the system's performance and the dynamics of pedestrian behavior.

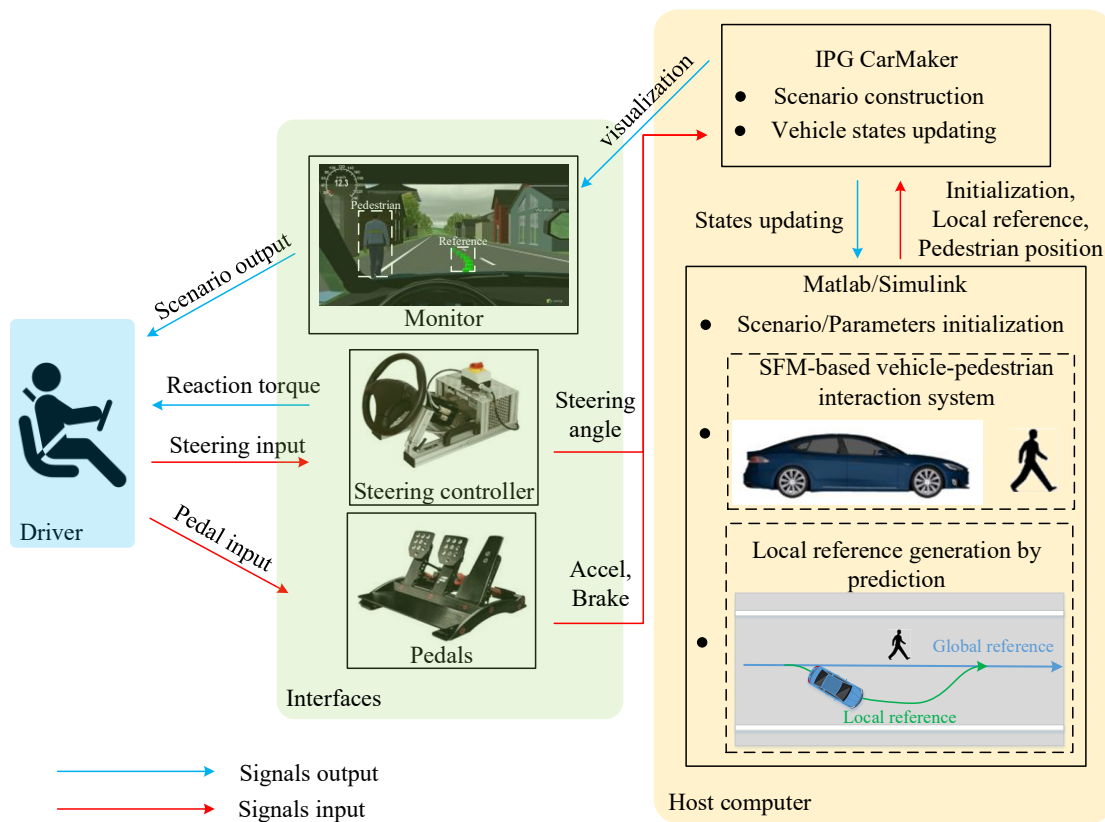


**Figure 4.2 Overview of bench test process**

Moreover, it is essential to acknowledge that generating a reference speed for the driver while they are actively controlling the vehicle can be considered an impractical endeavor unless the vehicle speed is not controlled by the driver. As a result, the SFM-based driver assistance system is designed to generate solely a local reference path for the driver. This dynamically computed reference path is then visually presented in real-time through cutting-edge virtual imaging technology, similar with the danger/safe field illustrated in Figure 4.1.

The generation of this local reference path is contingent upon an intricate interplay of factors, which encompass the current state of the vehicle-pedestrian interaction system. Additionally, this process incorporates various constraints, namely vehicle motion constraints, pedestrian motion constraints, and load boundaries constraints, all of which collectively contribute to shaping the driver's navigational reference in complex and ever-changing scenarios.

#### **4.2.2 Local reference path generation**

As the parameters of SFM-based pedestrian have been carried out in long-term research [45, 46, 48], in this thesis, we focus on the calibrated parameters of SFM-based pedestrians as presented in [48] and consider them suitable for predicting pedestrian behavior to a reasonable degree of accuracy, despite minor deviations.

Simultaneously, the prediction module for local reference generation draws insights from the principles of MPC, specifically the well-established concept known as "Moving Horizon Control," the comprehensive details of which are expounded upon in section 2.2. This adaptation is necessitated by the presence of external disturbances and potential incongruities between the actual dynamics and the prediction generated by the SFM-based vehicle-pedestrian interaction system.

Rather than attempting to predict the entire trajectory of the interaction system throughout the entirety of the CA process, the assistant system focuses exclusively on predicting the system states within a defined prediction horizon. We formulate and provide the driver with a local reference path, rooted in these temporary prediction states. In the subsequent time step, leveraging the newly observed states of the vehicle-pedestrian interaction system, we iteratively generate a fresh local reference path. This iterative process is strategically employed to minimize the impact of any disparities between the predicted values and the actual system state values on the projected trajectory. In doing so, we enhance the overall precision and efficacy of our predictive capabilities.

Noticing that the time of pedestrian crossing road is set random which means it could not be precisely predicted in prediction horizon, therefore in the prediction process, the pedestrian is considered remaining the same walking direction as the start of prediction. If the prediction pedestrian trajectory through the whole CA process is given just based on the initial vehicle-pedestrian states, it will become a path that contains slight jitter (some random motion is added to SFM-based pedestrian

model according to Equation (95)) but remains in the initial walking direction, which results in the local reference path for driver remains along the global reference. This is obviously unreasonable that collisions are more likely to occur when pedestrians swerve. This also explains why the predicted trajectory should be updated at each time step.

Simultaneously, it is important to note that the SFM-based driver assistance system exclusively generates a local reference path for the driver, omitting the provision of a reference speed. The SFM-based Collision Avoidance (CA) strategy utilized in the Hardware-in-Loop (HIL) test bench within this section adheres to the principles of the Proposed Method 2, as outlined in Section 3.4.2. Specifically, the approach involves the direct computation of  $\Phi_{ev}^{*,3} = [A_{p2ev}^*, \vec{F}_{brake}^{t,*}]$  from Equation (163) and Equation (164) based on Figure 3.31, which yields the optimal vehicle longitudinal acceleration, denoted as  $a_{ev}^{X,t}$ , and the lateral acceleration, denoted as  $a_{ev}^{Y,t}$ .

Subsequently, with the utilization of the SFM-based vehicle model (formulated in Equations (104), (105) and (132)) the mass point vehicle model (formulated in Equations (106)-(109)), the system calculates the positions of the vehicle at various time intervals within the prediction horizon. These positions are defined in the geodetic coordinate system and are instrumental in establishing a sequence of points, which collectively form a local reference path that extends into the future. This reference path is constructed based on the real-time dynamics of the vehicle-pedestrian interaction system, thereby ensuring optimal navigation and collision avoidance in upcoming scenarios.

Considering the target scenario is low-speed vehicle-pedestrian interaction and the online prediction is just numerical operations based on well-calibrated parameters of SFM-based interaction model, the computational consumption is not large compared to that of MPC. Therefore, the generation of local reference path is based on real-time vehicle-pedestrian states in every time step. The corresponding settings in local reference generation are as following:

- (1) The length of prediction horizon is set as 4s, which means the generated reference is in the following 4s based on the current vehicle-pedestrian states;
- (2) Time step in the prediction horizon is set as 0.05s, which means 80 temporary reference points (4/0.05) with equal time intervals of 0.05s will be generated;
- (3) Output reference points are set as 10, which means the visual reference points in screen is 10 with equal time intervals of 0.4s (4s/10).

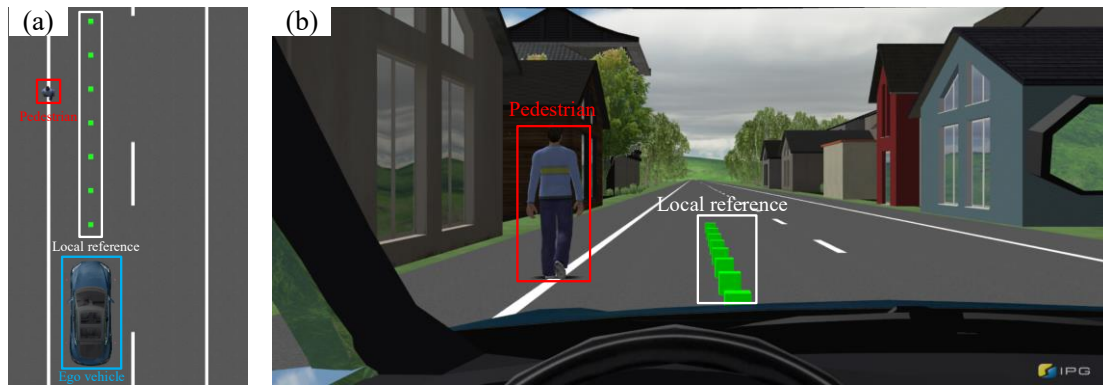


**Figure 4.3 Local reference path generation for the driver: (a) bird's eye view; (b) driver's eye view**

Figure 4.3 depicts the local reference path as observed from both a bird's-eye view and a driver's perspective. This reference trajectory is primarily employed to enhance the driver's decision-making process in the present context of vehicle-pedestrian interaction states. In general, strict adherence to this local reference trajectory is not a prerequisite for the driver. Besides, the global reference path will not be displayed to prevent causing disturbance to the driver.

### 4.3 T3R simulator

Figure 4.4 shows the view of test Hardware-in-the loop (HIL) bench.

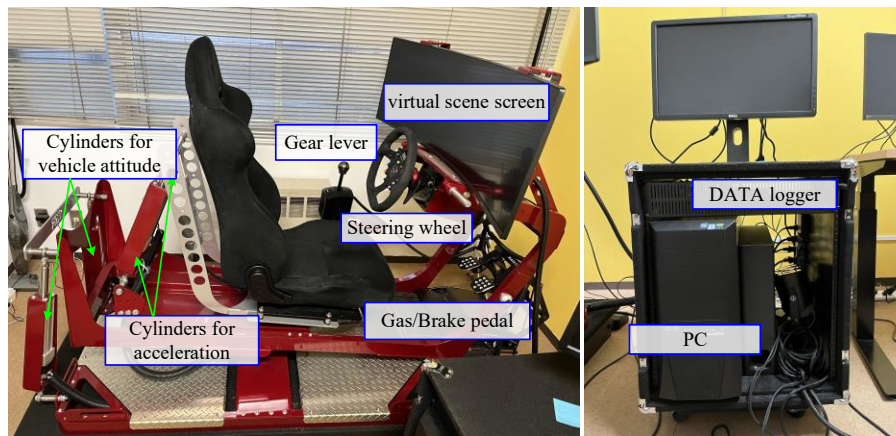


**Figure 4.4 View of test bench**

This section utilizes a 4-axis motion stage provided by IROC to validate the proposed SFM-based driving assistant system. Vibrations, rotations, accelerations, and jerks are induced using a system

comprising four cylinders: two of them control the pitch angle, modulated by the gas and brake pedals, while the remaining two cylinders manage the roll angle through manipulation of the steering wheel. The host computer interfaces seamlessly with Matlab/Simulink and Carmaker, enabling it to receive signals pertaining to pedal input and steering wheel angle.

In conjunction with Figure 4.2, the driver actively engages with a virtual vehicle within the IPG CarMaker environment by utilizing a steering controller and manipulating the acceleration and brake pedals. As a result of these driver inputs, the IPG CarMaker module generates and updates the vehicle's dynamic states. Simultaneously, the status of pedestrian entities, as generated by the Matlab/Simulink module, is integrated into the overall simulation.

The combined information, which encompasses both the updated vehicle states and the pedestrian status, is displayed in real-time on the screen. This visual representation provides a comprehensive overview of the dynamic interplay between the ego vehicle and pedestrians.

Furthermore, a local reference path is superimposed onto the screen, offering a visual indicator of the driver's intended behavior and trajectory. This reference path serves as a critical component for assisting the driver's actions within the simulated environment.

To further enrich the driver's experience and assist in the determination of their current driving behavior, the T3R system takes into account actual driving sensations, including the vehicle's front and rear body inclinations resulting from acceleration and deceleration. Additionally, the system considers the vehicle's roll angle caused by steering maneuvers. These physical sensations provide valuable feedback to the driver, aiding them in making informed decisions and judgments regarding their driving behavior within the simulated scenario. In addition, these tangible, real-time driving sensations play a pivotal role in substantiating the efficacy and impact of the SFM-based driver assistance system.

## **4.4 Application of SFM-based driver assistance system in T3R**

### **4.4.1 Pedestrian avoidance assistance**

In Figure 4.5, we provide a comprehensive overview that encompasses various key components. These components include the driver, the T3R test bench, which is equipped with a steering wheel and acceleration/brake pedals, as well as the screen display depicting the virtual scenario. Figure 4.5 (a)

showcases the initial phase where the ego vehicle approaches the pedestrian. In Figure 4.5 (b), we observe the driver's response as he steers the vehicle to overtake the pedestrian, who exhibits sudden crossing behavior. This response is guided by the local reference path generated by an SFM-based driver assistance system, demonstrating the real-time decision-making process. Continuing in Figure 4.5 (c), we witness the transition phase as the vehicle navigates back to the global reference road lane after successfully avoiding the pedestrian. Finally, Figure 4.5 (d) captures the ego vehicle's full reintegration into the global reference road lane, signifying the completion of the collision avoidance process.

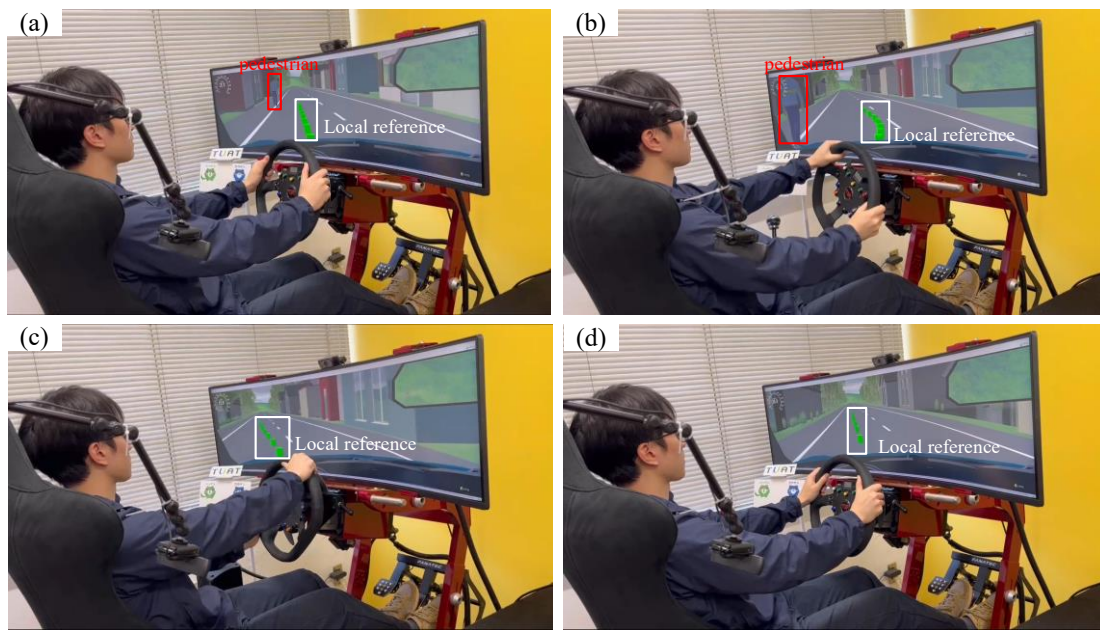


**Figure 4.5 Overall perspective of T3R HIL test for SFM-based pedestrian avoidance assistance system:**

**(a) Vehicle approaches pedestrian while cruising; (b) Driver avoids the crossing-road pedestrian according to local reference path; (c) Driver returns to global reference path after avoidance; (d) CA process is over and the vehicle returns to cruising state**

Figure 4.6 complements Figure 4.5 by offering bird's eye and driver's eye perspectives captured during different phases of the collision avoidance process, corresponding to the setup detailed in Figure 4.5.

In the initial state of the ego vehicle, while cruising, the local reference path aligns with the straight lane of the road, mirroring the global reference path, as depicted in Figure 4.6 (a)-1. When a pedestrian

does not attempt to cross the road, other vehicles can safely pass at reduced speeds. However, if the pedestrian is detected in the act of crossing the road, the driver assistance system, utilizing the SFM-based vehicle and pedestrian model, generates a local reference path contingent upon the current interaction dynamics between the vehicle and the pedestrian. This is illustrated in Figure 4.6 (b)-1.



**Figure 4.6 Bird's eye view and driver's eye view of T3R HIL test for SFM-based pedestrian avoidance assistance system((\*)-1 denotes bird's eye view and (\*)-2 denotes driver's eye view): (a) Vehicle approaches pedestrian while cruising; (b) Driver avoids the crossing-road pedestrian according to local reference path; (c) Driver returns to global reference path after avoidance; (d) CA process is over and the vehicle returns to cruising state**

The resultant local reference path is virtually projected onto the front window of the vehicle, providing a potential solution for the driver to evade a pedestrian who makes sudden movements, as illustrated in Figure 4.6 (b)-2. Subsequently, Figure 4.6 (c) and (d) chronicle the process by which the vehicle returns to its initial cruising state, guided by the local reference trajectory after successfully avoiding the pedestrian.

#### 4.4.2 Lane keeping assistance

Similar with Figure 4.5, in Figure 4.7, an overall perspective of T3R HIL test for SFM-based lane keeping assistance system is given. When the vehicle is leaving its lane, the local reference path is not a straight line anymore, it is an arc pointing to the global reference trajectory generated by force of

destination, denoted as  $\vec{F}_{des2ev}^t$  (refer to Equation (105)), with the real-time vehicle position.

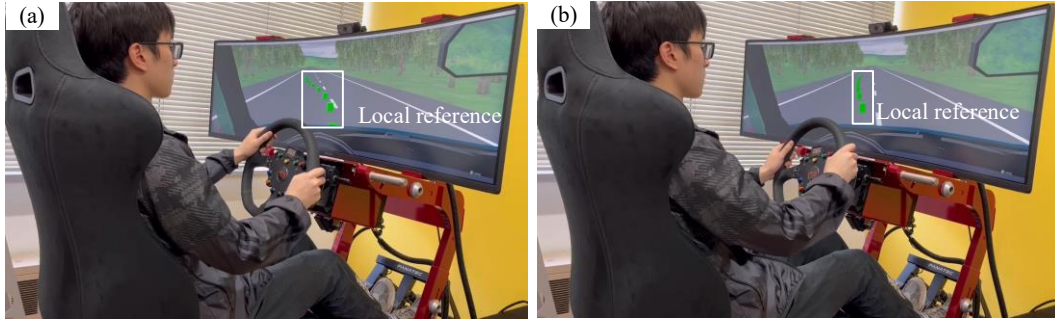


**Figure 4.7 Overall perspective of T3R HIL test for SFM-based lane keeping assistance system: (a) Vehicle leaves lane; (b) Lane back into alignment**

This dynamic adjustment serves as a visual reminder to the driver, signaling the need to return to the correct lane, as illustrated in Figure 4.7 (a). Subsequently, the driver can opt to follow the local reference path to re-establish proper lane alignment as illustrated in Figure 4.7 (b). Figure 4.8(a) and Figure 4.8 (b) shows bird's eye view and driver's eye view of T3R HIL test for SFM-based lane keeping assistance system which correspond to that of Figure 4.5.

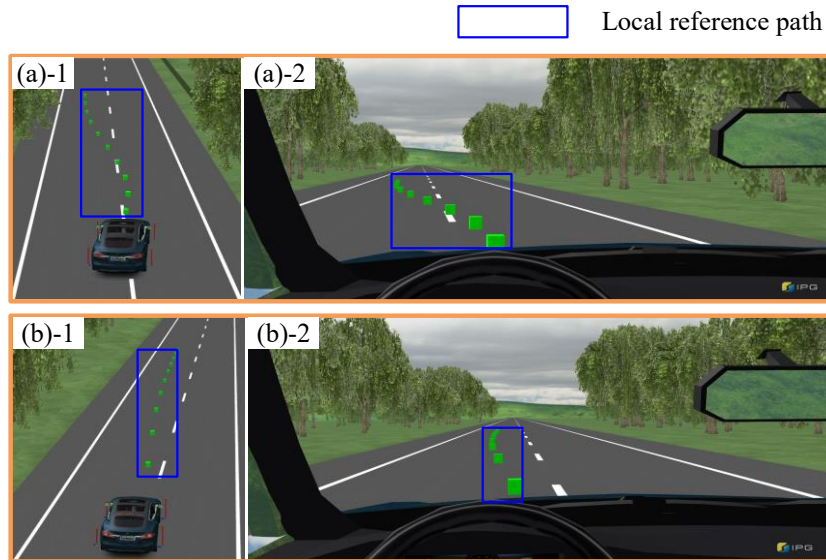


**Figure 4.8 Bird's eye view and driver's eye view of T3R HIL test for SFM-based lane keeping assistance system((\*)-1 denotes bird's eye view and (\*)-2 denotes driver's eye view): (a) Vehicle leaves lane; (b) Lane back into alignment**

### 4.4.3 Experimental comparison

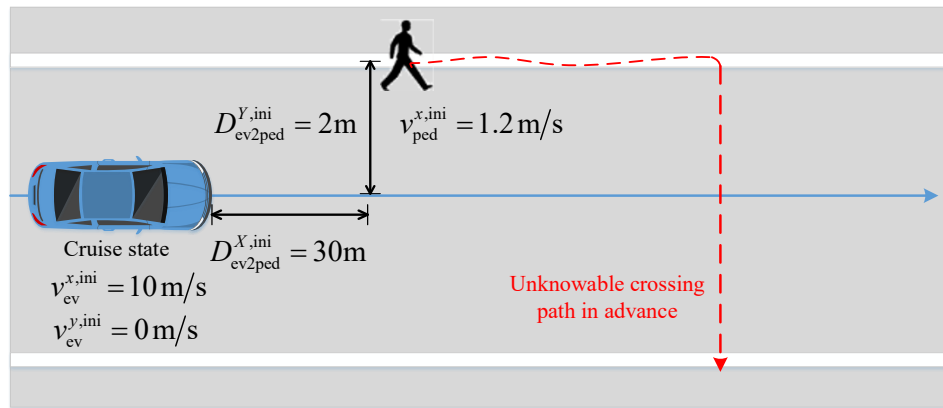


**Figure 4.9 Test scenario**

To verify the effectiveness of the SFM-based driving assistance system, a comparison experiment is established. The test scenario is similar with Figure 3.2, and the initial setting of the scenario is shown as Figure 4.9:

The ego vehicle is considered cruising state with an initial longitudinal speed of 10 m/s. The initial distance between ego vehicle and the pedestrian at  $Y$ -axis is 30 m and the lateral distance between these two objects is 2 m. The initial speed of pedestrian is set as 1.2 m/s. For drivers, the crossing road time (or the future motion) of the pedestrian is unknowable in advance.

Five experienced drivers were invited to complete the experiment while each person was asked to complete the experiment twice: once with driver assistance system and once without driver assistance system.

The experiment result is shown as Figure 4.10. From Figure 4.10 (b), in the avoidance process (blue area  $A$ ), drivers operate slighter steering with help of SFM-based driver assistance system (average of steering wheel angle in pedestrian avoidance process is -1.08 degree) than that of without SFM-based driver assistance system (average of front wheel angle in pedestrian avoidance process is -1.97 degree). And after overtaking the pedestrian, drivers will make a quicker and smoother lane back into alignment with SFM-based driver assistance system (average of front wheel angle in Lane back into alignment process is 0.52 degree) than that of without SFM-based driver assistance system (average of front wheel

angle in Lane back into alignment process is 1.44 degree).

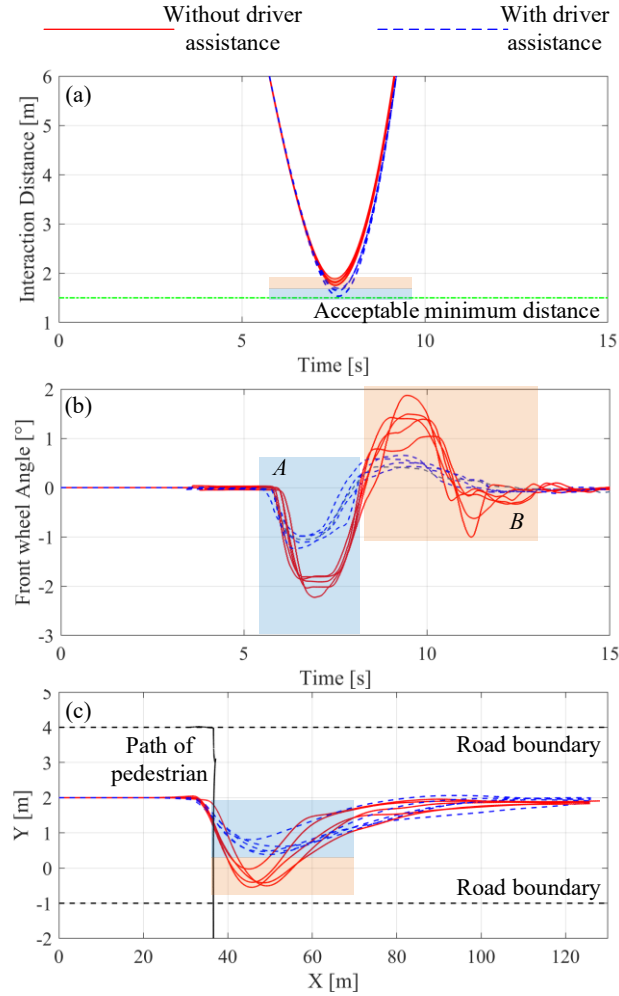


**Figure 4.10 Comparison of driver overtaking pedestrian with/without SFM-based driver assistance system: (a) comparison of distance between vehicle and pedestrian;(b) comparison of front wheel angle;(c) comparison of vehicle trajectory**

Besides, slighter steering brings smoother collision avoidance trajectory, shown as Figure 4.10 (c), the average maximum deviation in  $Y$ -axis with SFM-based driver assistance system is 1.45 m while the average maximum deviation in  $Y$ -axis without SFM-based driver assistance system is 2.38 m. Although the smoother trajectories may bring smaller distance between vehicle and pedestrian, the minimum distance between vehicle and pedestrian, shown in Figure 4.10 (a), is 1.53 m which is larger than the defined minimum safe distance (1.5m).

Therefore, the comparison experiments demonstrate that, even for experienced drivers, SFM-based

driver assistance system can help them better deal with pedestrians suddenly crossing the road in narrow road situations.

## **4.5 Summary of this chapter**

In this chapter, we present the HIL bench test of a driver assistance system based on SFM. Utilizing accurately calibrated SFM-based vehicle and pedestrian parameters, a local reference path is generated in real-time, reflecting the dynamic states of the vehicle-pedestrian interaction system. This path is then visually projected onto the vehicle's front window, serving as a valuable reference for the driver. Additionally, we explore the applicability of the SFM-based driver assistance system in lane keeping assistance. Our findings reveal that the SFM-based driver assistance system exhibits a high level of effectiveness, as demonstrated by the results obtained in Figure 4.5 to Figure 4.8. Besides, a comparison experiment based on five experienced drivers with/without SFM-based driver assistance system is conducted to examine the feasibility of the proposed driver assistance system in guiding drivers to safe path. The results show drivers with SFM-based driver assistance system can approach a smoother steering while safely avoid the suddenly crossing pedestrian.

## Chapter5 Conclusion

### 5.1 Summary of this thesis

Taking into account the traffic accidents with the largest number of fatalities (which are accidents of vehicle-pedestrian interaction and vehicle-vehicle interaction referring to Figure 1.1 and Figure 1.2 ) and focusing on the gaps of current research, this research gives feasible solutions for the following purposes illustrated in section 1.4.1(for a better view, the purposes of this thesis are re-wrote here) by designing MPC-based passive CA strategies, SFM-based active CA strategies and NAFC-based active CA strategy.

*The purposes of this thesis:*

- (1) An appropriate solution of CA problem in the case related to unpredictable motion of obstacles.*
- (2) Defining a mathematical model that can be interpreted physically of the interaction system between the ego vehicle and the pedestrian.*
- (3) Proposing CA algorithms with real time application potential.*

Chapter2 mainly gives solutions of *purpose (1)*, based on a normal urban driving scenario with interaction between vehicles, section 2.3 established MPC-based an effective vehicle motion control strategy for automated vehicles which contains TL-MPC and BR-PET to realize the function of both lane-keeping and collision avoidance. The difficulty of solving this motion planning problem is how to deal with the unpredictable or uncertain future speed of oncoming vehicle and to control the speed of an autonomous vehicle in the whole process. Firstly, the BR-PET is proposed to solve the problem of oncoming vehicle's unpredictable speed. Then, based on TL-MPC system, the vehicle's speed and steering wheel angle are controlled in real time, so that both trajectory re-planning and tracking are realized. Finally, the proposed control system is verified by co-simulations of MATLAB/Simulink and CarSim. The obtained simulation results showed that under three different cases, BR-PET successfully re-plans a collision-free movement of the vehicle while the TL-MPC ensures trajectory re-planning and tracking performance under the premise of a safe collision avoidance. Besides, the MPC-based CA strategy considering vehicle-pedestrian interaction system is also adopted in section 2.4, it is combined with the collision probability estimation when there is unpredict in pedestrian motion to re-plan the

## Conclusion

longitudinal speed for ego vehicle.

Chapter3 illustrates SFM-based vehicle-pedestrian interaction model in details which mainly focuses on *purpose (2)*, parameters of the SFM-based vehicle model are optimized by PSO and the reasons of achieving such final values are explained physically in detail in section 3.3.1, and the recommended initial values of SFM for different initial states of ego vehicle are determined, which could provide useful findings for further study. And based on the proposed vehicle-pedestrian interaction model, SFM-based CA strategies are proposed to address *purpose (1)*. The control results of MPC-based and SFM-based strategy is established by MATLAB simulation. The control effect of MPC and SFM is similar with each other when only two pedestrians are taken into consideration. These two controllers both achieve the goal of keeping safe distance and fast passing. Considering that MPC-based controller needs to predict motion of every pedestrian, so, when the number of participants rises, the computation cost and time for MPC controller may become unacceptable while this issue does not affect SFM once the parameters are well-calibrated (shown as Figure 3.37 in section 3.5.4). Thus, as SFM-based method is with two parts: offline parameter calibration and online simple numerical operations, it owns satisfactory real-time performance that *purpose (3)* is also reached when SFM-based strategy is adopted.

Besides, in order to apply SFM-based strategy extensively in different cases especially in the scenario of vehicle-pedestrian interaction, a novel SFM-based adaptive parameters CA method is proposed in section 3.4 to achieve *purpose (1)*. This method eliminates the dangers caused by inaccurate predictions from various environments or individuals' differences in pedestrians. By considering pedestrians with two different motion modes ("careless" or "careful"), the SFM-based adaptive parameters CA method was evaluated in a test bench, and the superior results showed that the proposed method helped the ego vehicle maneuver safely, quickly, and with a slight turning yielding to randomly crossing pedestrians.

Also, in order to achieve *purpose (1)* and illustrate that adopting the SFM-based strategy in CA can achieve *purpose (3)*, this research proposed another SFM-based strategy to deal with the interaction between vehicle and bicycle in section 3.5. The control results of MPC-based strategy and SFM-based strategy is established by MATLAB simulation to validate the effectiveness of SFM-based method. The vehicle controlled by SFM owns more motion stability. These two strategies both achieve the goal of

keeping safe distance and fast passing. However, the comparison of calculation time (shown as shown as Figure 3.37 in section 3.5.4) reveals the advantage of SFM-based strategy in real-time application.

And in order to achieve *purpose (3)*, another method based on a normal urban driving scenario, an effective vehicle motion control strategy for automated vehicles which named NAFC to realize the function of both lane-keeping and collision avoidance is proposed in section 3.7. And its control effect is verified by simulations. The advantages of NAFC are summarized that training data is collected from MPC that avoid large trial and iteration epochs of normal ANN training process causing by the instability and noise of the human driver data set and NAFC rarely needs the dynamic model of obstacles but just their current states, which is benefit for reducing computation.

And this thesis delves into the integration of SFM-based control strategies not only within the domain of fully autonomous vehicles but also within the context of a driver assistance system tailored to address the challenges posed by pedestrians with unpredictable motion on narrow roads. The envisaged driver assistance system, designed to alleviate these challenges, has been embraced and rigorously assessed within the T3R Hardware-in-the-Loop (HIL) test bench is established in Chapter4. The core mechanism of this system involves the real-time generation of a localized reference path, which is predicated on the dynamic states governing the interaction between the vehicle and pedestrians. This path is then seamlessly projected onto the front windshield, providing the driver with a virtual representation of the environment. Through this visual aid, the driver is empowered to navigate and respond to the intricate interplay of factors associated with pedestrian movements in narrow road settings. The empirical results stemming from the HIL tests examined the feasibility of the SFM-based driver assistance system in guiding drivers to safe path. This substantiates its potential to enhance safety and performance, ultimately contributing to the broader mission of advancing road safety and vehicular intelligence.

Furthermore, for the proposed NAFC-based controller, although its generalization needs to be further discussed, when facing with highly repetitive scenes, such as autonomous shuttles and delivery services, this method owns potential to increase the convenience of mobility used for such autonomous vehicles. At the same time, in this regard, well calibrated SFM parameters for such autonomous vehicles can also bring convenience with low cost computing power.

## 5.2 Future work

According to the remaining existing problem for the proposed MPC-based, SFM-based and NAFC-based which is given in section 2.5, section 3.6 and section 3.7.5, the future work can focus on the following aspects:

(1) Collision avoidance strategies design under extreme adhesion or at relative high-speed conditions. More issues such as considering vehicle stability and passenger comfort could also be taken into account in future;

(2) It's necessary to consider more complicated situations, such as stochastic number of pedestrians or unknown initial states of pedestrians, and adding prediction function to SFM for ego vehicle obtaining more competency and carefulness about safety is also worth considering.

(3) Although an adaptive parameter function is added to SFM-based vehicle model to deal with the unpredictable motion of obstacles and improve the generalizability of the controller. A more complex scenario, with multiple pedestrians and vehicles should be designed to verify the reliability of proposed method taking into account the interaction between pedestrians and vehicles. In section 3.4, pedestrians were simply classified as 'careless' or 'careful'. A more reasonable classification or identification for pedestrians, should be adopted, such as combining pedestrian-aware risk assessment or image recognition. Besides, a mass point vehicle model was used for simplification in proposed SFM-based strategies. However, the vehicle shape should be carefully considered, particularly in interacting with moving pedestrian in a low-speed scenario.

(4) Although the SFM-based driver assistance system is validated by T3R HIL test bench in the Chapter4, validation in real vehicle should be conducted. And for the SFM-based CA strategy adopted in fully automated vehicle, real vehicle testing needs to be completed in future work as well.

## Reference

1. *Regarding the occurrence of traffic accidents in 2022*. 2023; Available from: <https://www.npa.go.jp/bureau/traffic/bunseki/nenkan/050302R04nenkan.pdf>.
2. Saito, Y., et al., *Effectiveness of a driver assistance system with deceleration control and brake hold functions in stop sign intersection scenarios*. IEEE Transactions on Intelligent Transportation Systems, 2021. **23**(7): p. 8747-8758.
3. Qu, Z.-w., et al., *Modeling electric bike-car mixed flow via social force model*. Advances in Mechanical Engineering, 2017. **9**(9): p. 1687814017719641.
4. Hamilton-Baillie, B., *Towards shared space*. Urban Design International, 2008. **13**(2): p. 130-138.
5. Dimmer, C., *Re imagining public space: The vicissitudes of Japan's privately owned public spaces*, in *Urban Spaces in Japan*. 2012, Routledge. p. 74-105.
6. Anvari, B., et al., *Modelling shared space users via rule based social force model*. Transportation Research Part C: Emerging Technologies, 2015. **51**: p. 83-103.
7. Shearer, D., *Shared spaces in New Zealand urban areas*. 2011, University of Otago.
8. Hajiloo, R., et al., *Integrated steering and differential braking for emergency collision avoidance in autonomous vehicles*. IEEE Transactions on Intelligent Transportation Systems, 2020. **22**(5): p. 3167-3178.
9. Cheng, S., et al., *Longitudinal collision avoidance and lateral stability adaptive control system based on MPC of autonomous vehicles*. IEEE Transactions on Intelligent Transportation Systems, 2019. **21**(6): p. 2376-2385.
10. Nilsson, J., A.C. Ödblom, and J. Fredriksson, *Worst case analysis of automotive collision avoidance systems*. IEEE Transactions on Vehicular Technology, 2015. **65**(4): p. 1899-1911.
11. Thrun, S., et al., *Stanley: The robot that won the DARPA Grand Challenge*. Journal of field Robotics, 2006. **23**(9): p. 661-692.
12. Urmson, C., et al., *Autonomous driving in urban environments: Boss and the urban challenge*. Journal of field Robotics, 2008. **25**(8): p. 425-466.
13. Paden, B., et al., *A survey of motion planning and control techniques for self driving urban vehicles*. IEEE Transactions on intelligent vehicles, 2016. **1**(1): p. 33-55.
14. International, S., *Taxonomy and definitions for terms related to driving automation systems for on road motor vehicles*. SAE Int., 2018. **4970**(724): p. 1-5.
15. Anderson, J.M., et al., *Autonomous vehicle technology: A guide for policymakers*. 2014: Rand Corporation.
16. Fagnant, D.J. and K. Kockelman, *Preparing a nation for autonomous vehicles: opportunities, barriers and policy recommendations*. Transportation Research Part A: Policy and Practice, 2015. **77**: p. 167-181.
17. Guanetti, J., Y. Kim, and F. Borrelli, *Control of connected and automated vehicles: State of the art and future challenges*. Annual reviews in control, 2018. **45**: p. 18-40.
18. Bimbrow, K. *Autonomous cars: Past, present and future a review of the*

*developments in the last century, the present scenario and the expected future of autonomous vehicle technology.* in *2015 12th international conference on informatics in control, automation and robotics (ICINCO)*. 2015. IEEE.

19. Adnan, N., et al., *How trust can drive forward the user acceptance to the technology? In vehicle technology for autonomous vehicle.* Transportation research part A: policy and practice, 2018. **118**: p. 819-836.

20. Bansal, P. and K.M. Kockelman, *Forecasting Americans' long term adoption of connected and autonomous vehicle technologies.* Transportation Research Part A: Policy and Practice, 2017. **95**: p. 49-63.

21. Divakarla, K.P., et al., *A review of autonomous vehicle technology landscape.* International Journal of Electric and Hybrid Vehicles, 2019. **11**(4): p. 320-345.

22. Isermann, R., R. Mannale, and K. Schmitt, *Collision avoidance systems PRORETA: Situation analysis and intervention control.* Control Engineering Practice, 2012. **20**(11): p. 1236-1246.

23. Shen, X., et al., *Cooperative comfortable driving at signalized intersections for connected and automated vehicles.* IEEE Robotics and Automation Letters, 2020. **5**(4): p. 6247-6254.

24. Saito, Y. and P. Raksincharoensak. *Risk predictive shared deceleration control: Its functionality and effectiveness of an early intervention support.* in *2016 IEEE intelligent vehicles symposium (IV)*. 2016. IEEE.

25. Lefevre, S., A. Carvalho, and F. Borrelli, *A learning based framework for velocity control in autonomous driving.* IEEE Transactions on Automation Science and Engineering, 2015. **13**(1): p. 32-42.

26. Raksincharoensak, P., T. Hasegawa, and M. Nagai, *Motion planning and control of autonomous driving intelligence system based on risk potential optimization framework.* International Journal of Automotive Engineering, 2016. **7**(AVEC14): p. 53-60.

27. Falcone, P., et al., *Predictive active steering control for autonomous vehicle systems.* IEEE Transactions on control systems technology, 2007. **15**(3): p. 566-580.

28. Wang, T.-C. and T.-J. Lin, *Unmanned vehicle obstacle detection and avoidance using danger zone approach.* Transactions of the Canadian Society for Mechanical Engineering, 2013. **37**(3): p. 529-538.

29. Gray, A., et al. *Integrated threat assessment and control design for roadway departure avoidance.* in *2012 15th International IEEE Conference on Intelligent Transportation Systems*. 2012. IEEE.

30. Cheng, S., et al., *Virtual fluid flow model based lane keeping integrated with collision avoidance control system design for autonomous vehicles.* IEEE Transactions on Intelligent Transportation Systems, 2020. **22**(10): p. 6232-6241.

31. Balachandran, A., et al., *Predictive haptic feedback for obstacle avoidance based on model predictive control.* IEEE Transactions on Automation Science and Engineering, 2015. **13**(1): p. 26-31.

32. ElHamamsy, A., F. Aghili, and A. Aghdam, *Connectivity Preservation and Collision Avoidance in Multi Agent Systems using Model Predictive Control.* IEEE Transactions on Network Science and Engineering, 2023.

33. Ammour, M., R. Orjuela, and M. Basset, *A MPC Combined Decision Making and*

*Trajectory Planning for Autonomous Vehicle Collision Avoidance*. IEEE Transactions on Intelligent Transportation Systems, 2022. **23**(12): p. 24805-24817.

34. Duguleana, M., et al., *Obstacle avoidance of redundant manipulators using neural networks based reinforcement learning*. Robotics and Computer-Integrated Manufacturing, 2012. **28**(2): p. 132-146.

35. Huang, Y., *Intelligent technique for robot path planning using artificial neural network and adaptive ant colony optimization*. Journal of Convergence Information Technology, 2012. **7**(9): p. 246-252.

36. Chakravarthy, A. and D. Ghose, *Generalization of the collision cone approach for motion safety in 3 D environments*. Autonomous Robots, 2012. **32**: p. 243-266.

37. Balch, T. and R.C. Arkin, *Behavior based formation control for multirobot teams*. IEEE transactions on robotics and automation, 1998. **14**(6): p. 926-939.

38. Rasouli, A. and J.K. Tsotsos, *Autonomous vehicles that interact with pedestrians: A survey of theory and practice*. IEEE transactions on intelligent transportation systems, 2019. **21**(3): p. 900-918.

39. Keller, C.G. and D.M. Gavrila, *Will the pedestrian cross? a study on pedestrian path prediction*. IEEE Transactions on Intelligent Transportation Systems, 2013. **15**(2): p. 494-506.

40. Schneider, S. and K. Bengler, *Virtually the same? Analysing pedestrian behaviour by means of virtual reality*. Transportation research part F: traffic psychology and behaviour, 2020. **68**: p. 231-256.

41. Shen, X. and P. Raksincharoensak, *Pedestrian aware statistical risk assessment*. IEEE Transactions on Intelligent Transportation Systems, 2021. **23**(7): p. 7910-7918.

42. Shen, X. and P. Raksincharoensak, *Statistical models of near accident event and pedestrian behavior at non signalized intersections*. Journal of applied statistics, 2022. **49**(15): p. 4028-4048.

43. Feng, J., et al., *Active collision avoidance strategy considering motion uncertainty of the pedestrian*. IEEE transactions on intelligent transportation systems, 2020. **23**(4): p. 3543-3555.

44. Saleh, K., M. Hossny, and S. Nahavandi, *Intent prediction of pedestrians via motion trajectories using stacked recurrent neural networks*. IEEE Transactions on Intelligent Vehicles, 2018. **3**(4): p. 414-424.

45. Helbing, D. and P. Molnar, *Social force model for pedestrian dynamics*. Physical review E, 1995. **51**(5): p. 4282.

46. Kretz, T., J. Lohmiller, and P. Sukennik, *Some indications on how to calibrate the social force model of pedestrian dynamics*. Transportation research record, 2018. **2672**(20): p. 228-238.

47. Dias, C., et al., *Calibrating a social force based model for simulating personal mobility vehicles and pedestrian mixed traffic*. Simulation Modelling Practice and Theory, 2018. **87**: p. 395-411.

48. Yang, D., Ü. Özgüner, and K. Redmill, *A social force based pedestrian motion model considering multi pedestrian interaction with a vehicle*. ACM Transactions on Spatial Algorithms and Systems (TSAS), 2020. **6**(2): p. 1-27.

49. Yuan, H., X. Sun, and T. Gordon, *Unified decision making and control for highway collision avoidance using active front steer and individual wheel torque control*. Vehicle system

dynamics, 2019. **57**(8): p. 1188-1205.

50. Yang, D. and Ü. Özgüner, *Combining Social Force Model with Model Predictive Control for Vehicle's Longitudinal Speed Regulation in Pedestrian Dense Scenarios*. arXiv preprint arXiv:1907.05178, 2019.

51. Rawlings, J.B., *Tutorial overview of model predictive control*. IEEE control systems magazine, 2000. **20**(3): p. 38-52.

52. Morari, M. and J.H. Lee, *Model predictive control: past, present and future*. Computers & chemical engineering, 1999. **23**(4-5): p. 667-682.

53. Holkar, K. and L.M. Waghmare, *An overview of model predictive control*. International Journal of control and automation, 2010. **3**(4): p. 47-63.

54. Kouvaritakis, B. and M. Cannon, *Model predictive control*. Switzerland: Springer International Publishing, 2016. **38**.

55. Lefèvre, S., D. Vasquez, and C. Laugier, *A survey on motion prediction and risk assessment for intelligent vehicles*. ROBOMECH journal, 2014. **1**(1): p. 1-14.

56. Vogel, K., *A comparison of headway and time to collision as safety indicators*. Accident analysis & prevention, 2003. **35**(3): p. 427-433.

57. Falcone, P., *Nonlinear model predictive control for autonomous vehicles*. 2007.

58. Gong, J., Y. Jiang, and W. Xu, *Model predictive control for self driving vehicles*. Beijing Institute of Technology Press: Beijing, China, 2014.

59. Bertram, J., P. Wei, and J. Zambreno, *A fast Markov decision process based algorithm for collision avoidance in urban air mobility*. IEEE transactions on intelligent transportation systems, 2022. **23**(9): p. 15420-15433.

60. Abhishek, M.B., M. Mandjes, and R.N. NEZ-QUEIJA, *Congestion analysis of unsignalized intersections: the impact of impatience and Markov platooning*. arXiv preprint arXiv:1802.06732, 2018.

61. Shin, J. and M. Sunwoo, *Vehicle speed prediction using a Markov chain with speed constraints*. IEEE Transactions on Intelligent Transportation Systems, 2018. **20**(9): p. 3201-3211.

62. Mao, C., et al., *Analysis and prediction of pedestrians' violation behavior at the intersection based on a Markov chain*. Sustainability, 2021. **13**(10): p. 5690.

63. Stoica, P. and R.L. Moses, *Spectral analysis of signals*. Vol. 452. 2005: Pearson Prentice Hall Upper Saddle River, NJ.

64. Bellman, R., *Dynamic programming*. Science, 1966. **153**(3731): p. 34-37.

65. Yang, D., Ü. Özgüner, and K. Redmill. *Social force based microscopic modeling of vehicle crowd interaction*. in *2018 IEEE Intelligent Vehicles Symposium (IV)*. 2018. IEEE.

66. Kennedy, J. and R. Eberhart. *Particle swarm optimization*. in *Proceedings of ICNN'95 international conference on neural networks*. 1995. IEEE.

67. Gao, Y., et al., *Modified social force model based on predictive collision avoidance considering degree of competitiveness*. Fire technology, 2017. **53**: p. 331-351.

68. Wang, S.-C. and S.-C. Wang, *Artificial neural network*. Interdisciplinary computing in java programming, 2003: p. 81-100.

69. Wu, Y.-c. and J.-w. Feng, *Development and application of artificial neural network*. Wireless Personal Communications, 2018. **102**: p. 1645-1656.

70. Abiodun, O.I., et al., *State of the art in artificial neural network applications: A*

survey. Heliyon, 2018. **4**(11).

71. Shimizu, T. and P. Raksincharoensak. *Motion planning via optimization of risk quantified by collision velocity accompanied with AEB activation*. in *2017 IEEE International Conference on Vehicular Electronics and Safety (ICVES)*. 2017. IEEE.

## Acknowledgment

Through this thesis, I would like to express my most sincere gratitude to all the people who have given care, support and help during my study abroad career.

First of all, I would like to sincerely thank my supervisor, Professor Pongsathorn Raksincharoensak. Throughout the entire process of my study abroad, my supervisor gave me selfless care and superb guidance. His outstanding academic attainments, enthusiasm for scientific research, and patient guidance to students have always been my strong support on my academic path. I really appreciate his guidance, which has enabled me to continuously break through myself academically and gain some academic achievements.

In addition, I would like to sincerely thank Prof. Kamada, Prof. Mouri, Prof. Tagawa and Asst. Prof. Maeda for their careful review of my research work and their pertinent suggestions. Under their comments, my research has become more in-depth and systematic.

At the same time, I would like to sincerely thank the Mr. Shen Xun, Mr. Zhang Xingguo, Mr. Wang Wei, Mr. Yohei Fujinami. Their valuable opinions during my doctoral study are the driving force for me to continuously improve my research work and make me clearer about the direction and depth of the research.

And I would like to express my sincere appreciation to my family for the continuous support on my study.

As I am about to leave school, I would like to express my deepest gratitude to all the people who have helped me during my study abroad career. It was their support that made it possible for me to successfully complete my PhD studies. I hope our future will still have a wonderful intersection.

Finally, I would like to take this thesis to express my most sincere respect and gratitude to you.

My sincerest thanks,

Yan Zhang

## Achievement

### Journal Papers

1. Zhang Yan, Xun Shen, and Pongsathorn Raksincharoensak. 2021. "Automated Vehicle's Overtaking Maneuver with Yielding to Oncoming Vehicles in Urban Area Based on Model Predictive Control" Applied Sciences 11, no. 19: 9003. <https://doi.org/10.3390/app11199003> (Chapter 2)
2. Zhang Yan, Xun Shen, and Pongsathorn Raksincharoensak. "Study on Collision Avoidance Strategies Based on Social Force Model Considering Stochastic Motion of Pedestrians in Mixed Traffic Scenario." Journal of Robotics and Mechatronics 35.2 (2023): 240-254. (Chapter 2 and Chapter 3)
3. Y. Zhang, X. Zhang, Y. Fujinami and P. Raksincharoensak, "Social Force Model-Based Adaptive Parameters Collision Avoidance Method Considering Motion Uncertainty of the Pedestrian," in IEEE Access, vol. 12, pp. 794-809, 2024, doi: 10.1109/ACCESS.2023.3347779. (Chapter 3)
4. X. Shen, Y. Zhang, X. Zhang, P. Raksincharoensak and K. Hashimoto, "Robust Optimal Braking Policy for Avoiding Collision With Front Bicycle," in IEEE Open Journal of Intelligent Transportation Systems, doi: 10.1109/OJITS.2023.3335397 (Chapter 3)

### International Proceedings

1. YAN ZHANG, Xun Shen, Pongsathorn Raksincharoensak, "Decision Making and Motion Control for Automated Collision Avoidance Based on Neural Approximate Approach" Proceedings of 15th International Symposium on Advanced Vehicle Control (AVEC'22), Kanagawa Institute of Technology, 2022.9.12-15. No. Th2C-04. (Chapter 3)
2. Zhang Yan, Xun Shen, and Pongsathorn Raksincharoensak: "Social Force Model-based Strategy for Avoiding Collision with Front Bicycle", FAST-zero'23, 2023. (Chapter 3)